Different Rheologies

Figure 5.7-1: Elastic and plastic rheologies.

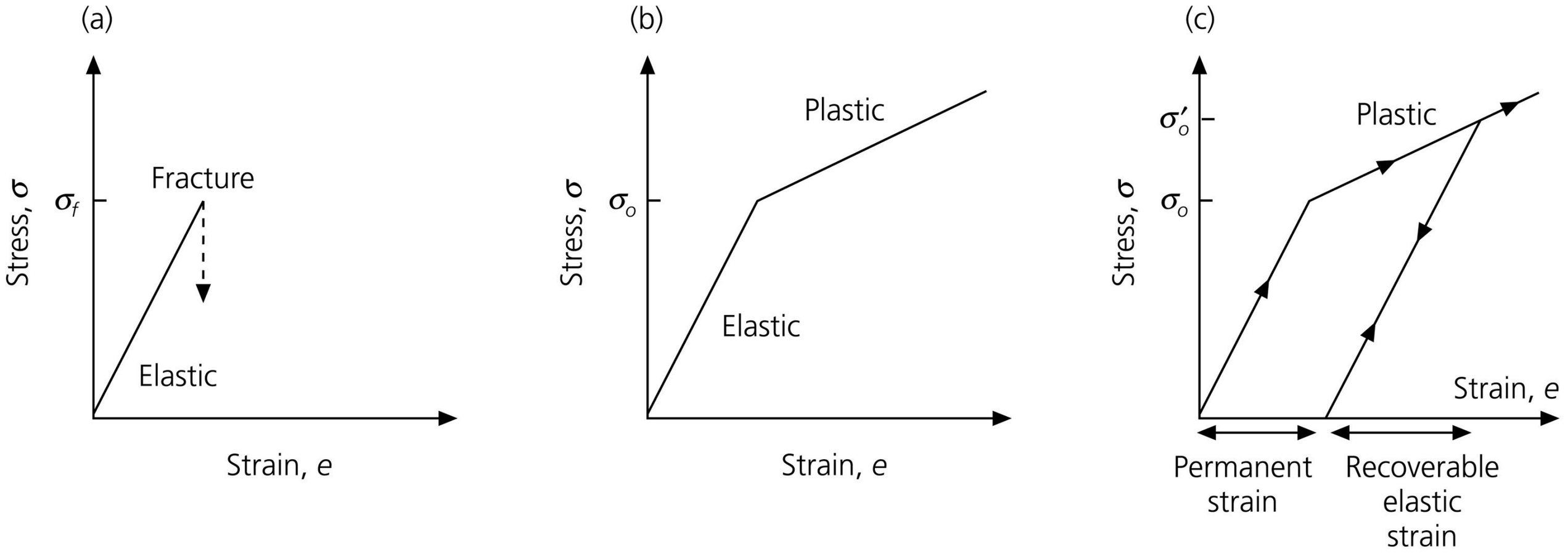

The mechanical properties of rocks deforming in the brittle regime are nearly insensitive to temperature, but very sensitive to strain-rate and **confining pressure**. Indeed, **friction** critically depends on the pressure acting across planes.

The fracture strength of rocks at the Earth's surface is the lowest and is controlled by the failure criteria only, but it increases with depth due to increasing lithostatic pressure.

Brittle & Ductile

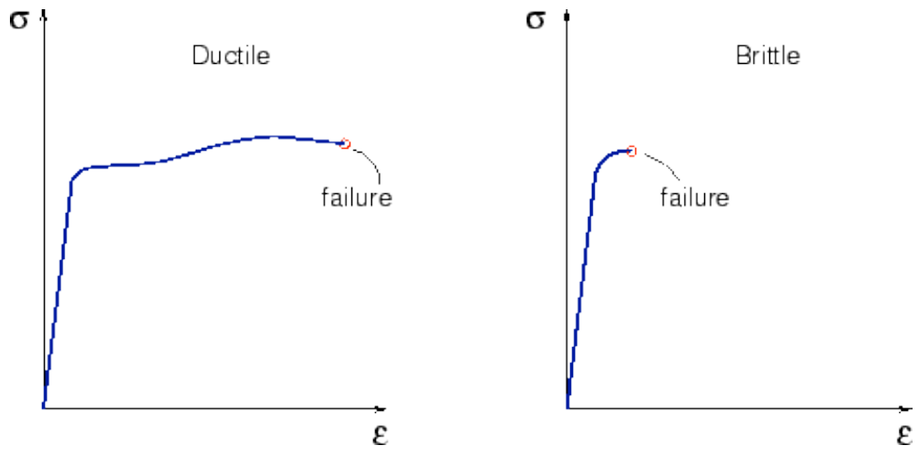

COMPRESSIVE FORCES

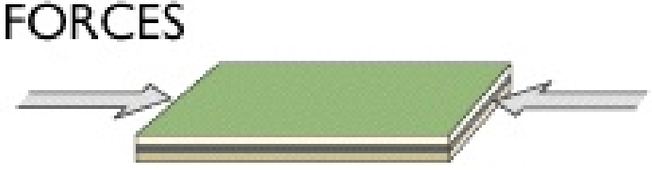

Folding

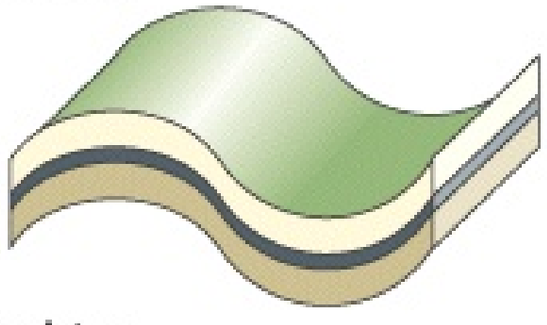

Faulting

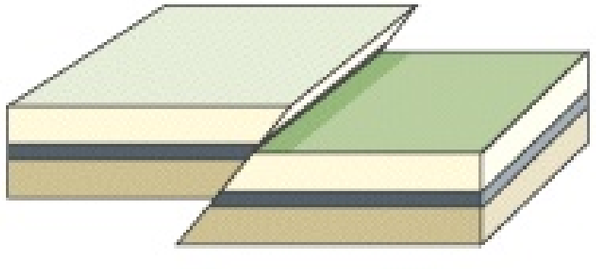

TENSIONAL FORCES

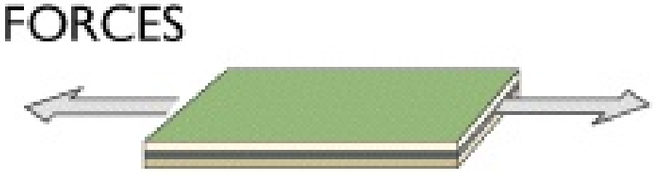

Stretching and thinning

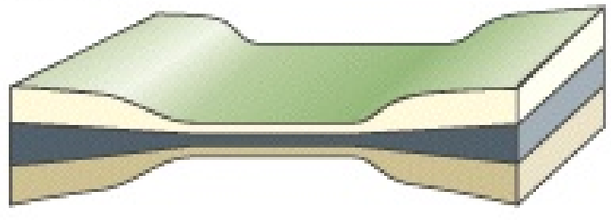

Faulting

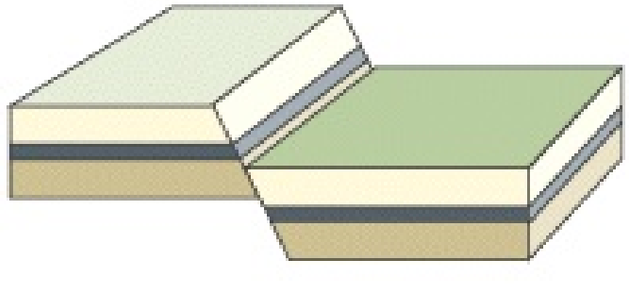

SHEARING FORCES

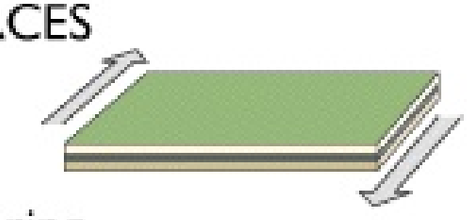

Shearing

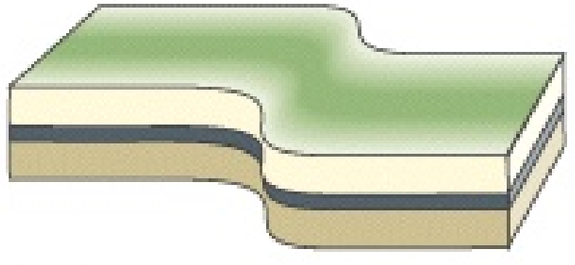

Faulting

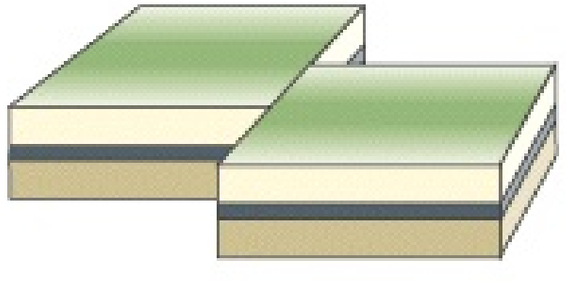

Normal Faulting Stresses

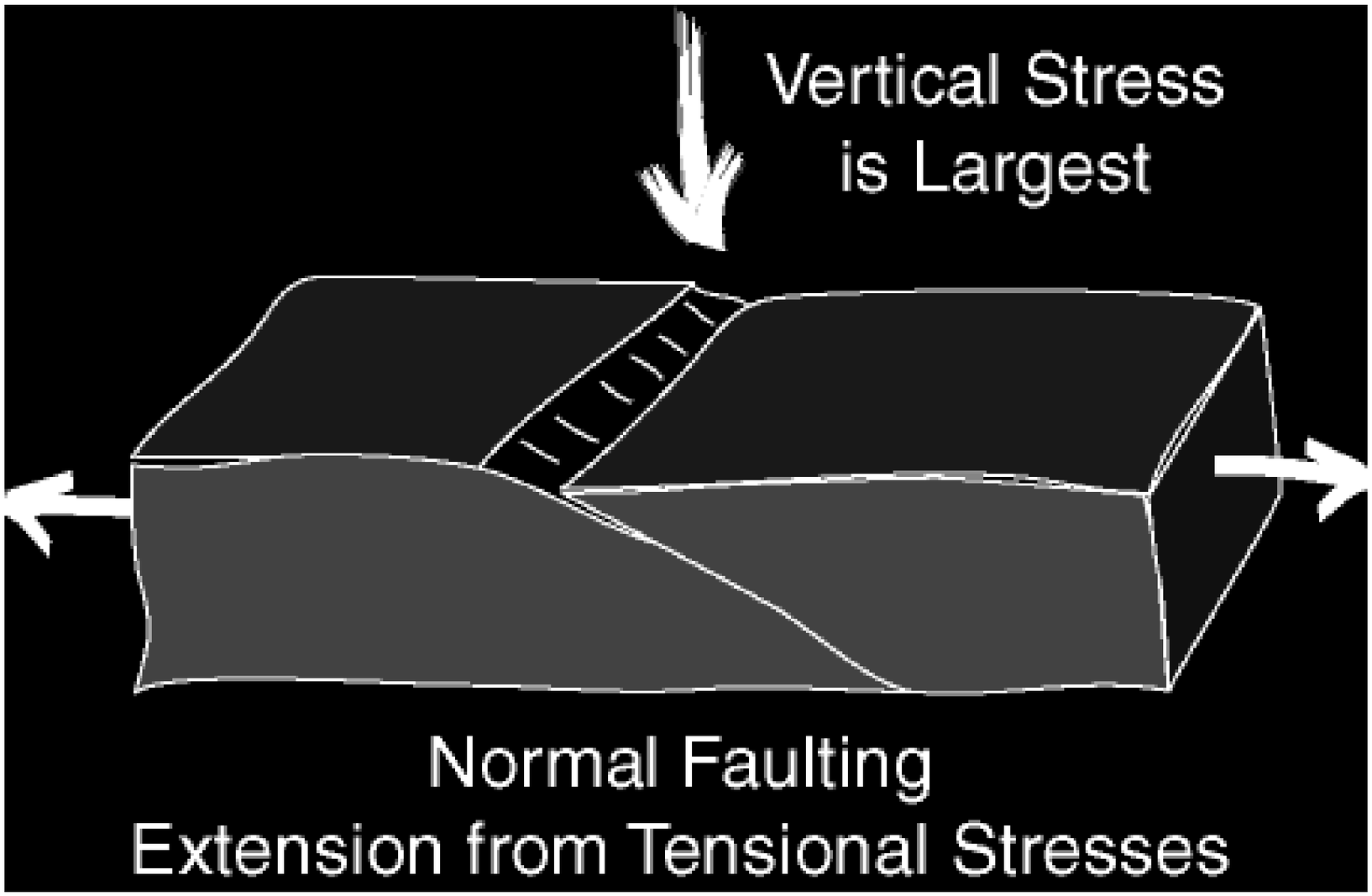

Reverse Faulting Stresses

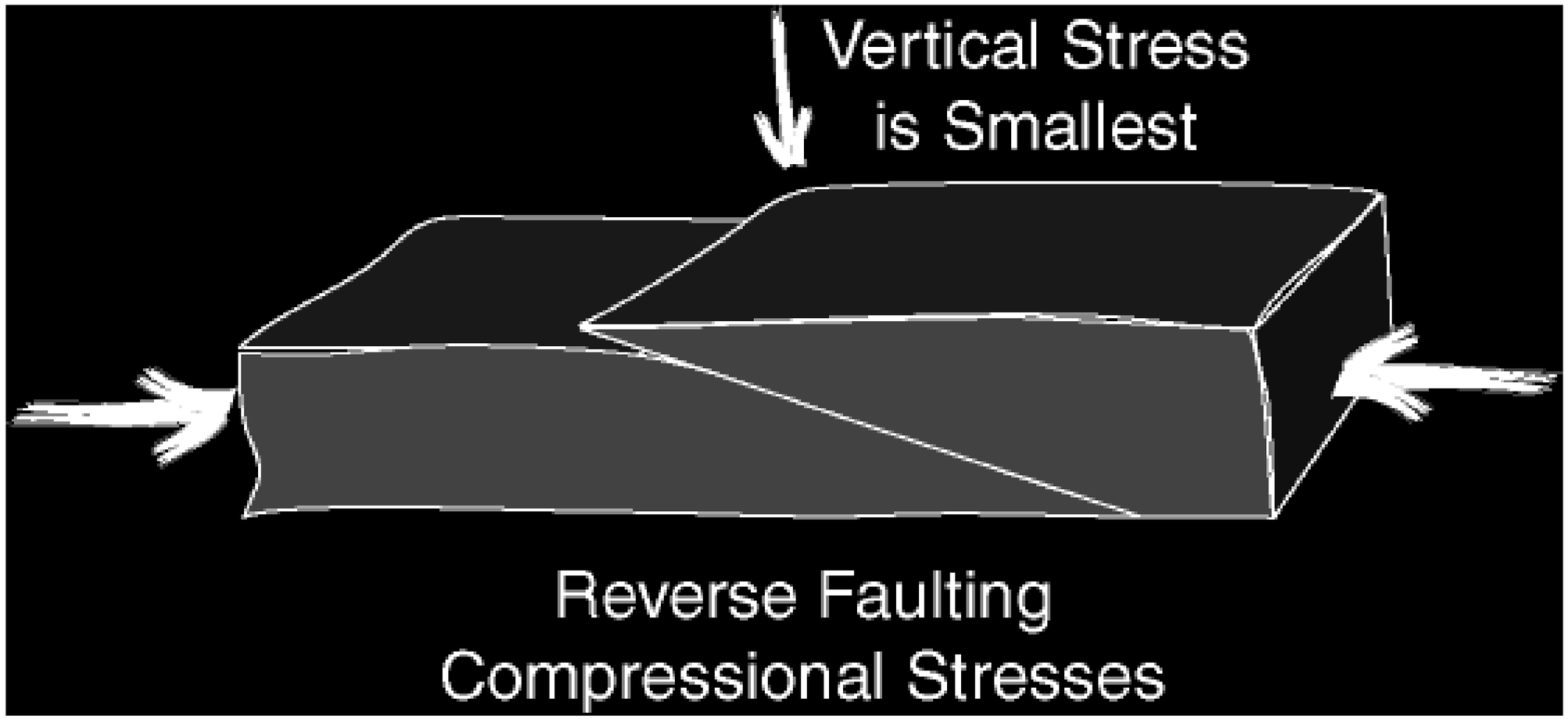

Strike-Slip Faulting Stresses

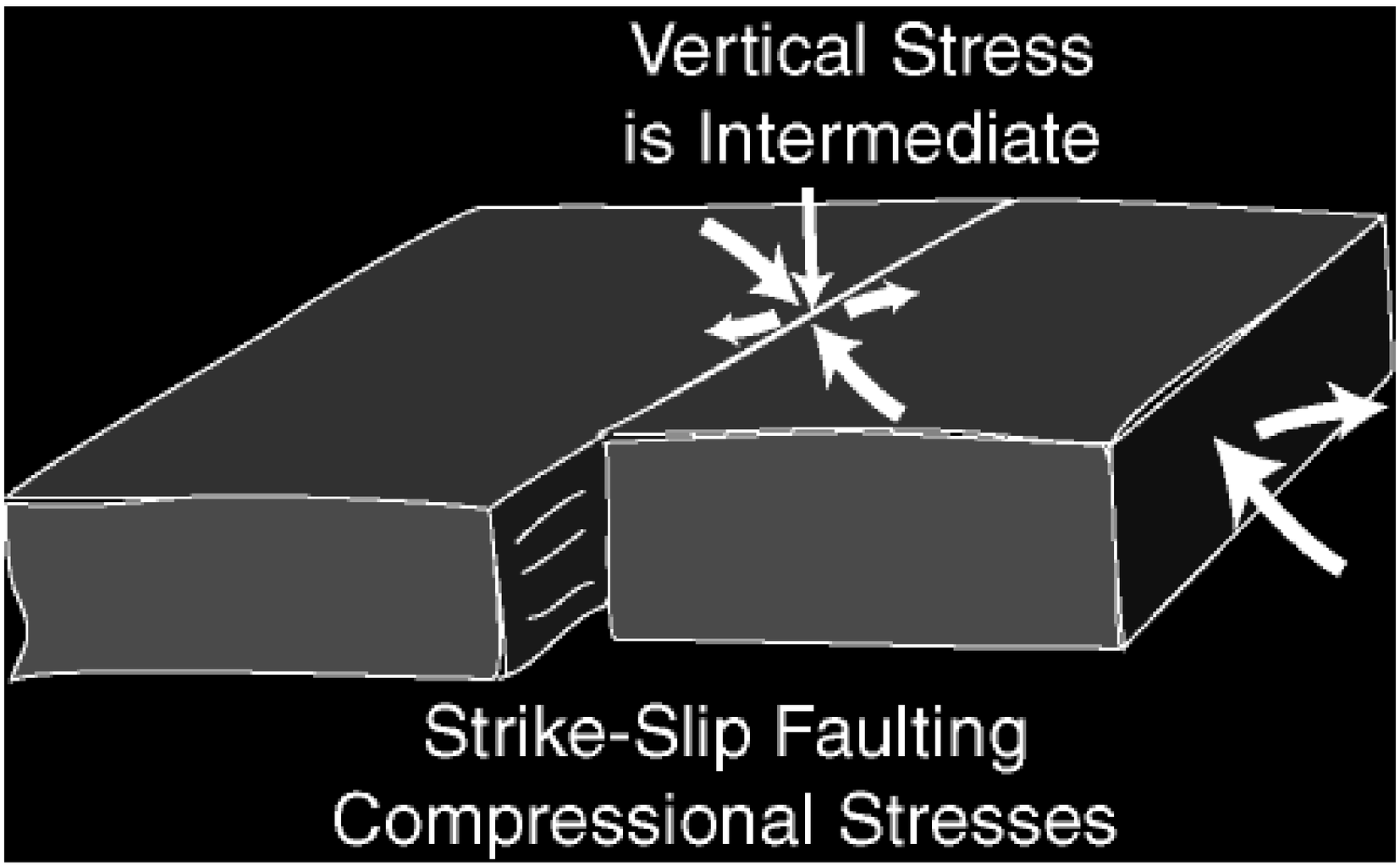

Fault Geometry Terminology: STRIKE

Strike is an angle use to describe the orientation of the fault surface with respect to North.

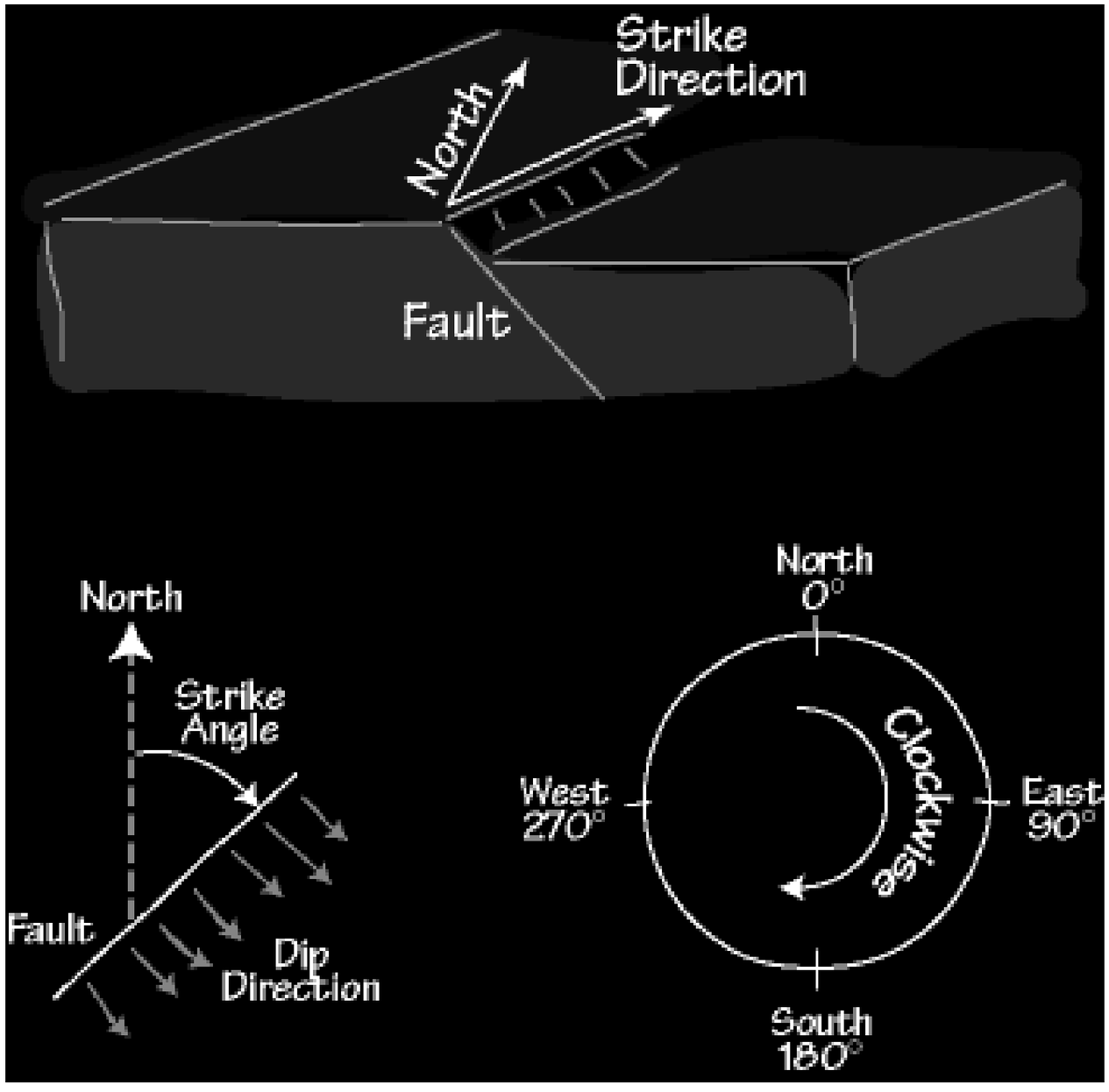

Fault Geometry Terminology: DIP

The orientation of the fault surface with respect to Earth's surface is defined by the fault dip.

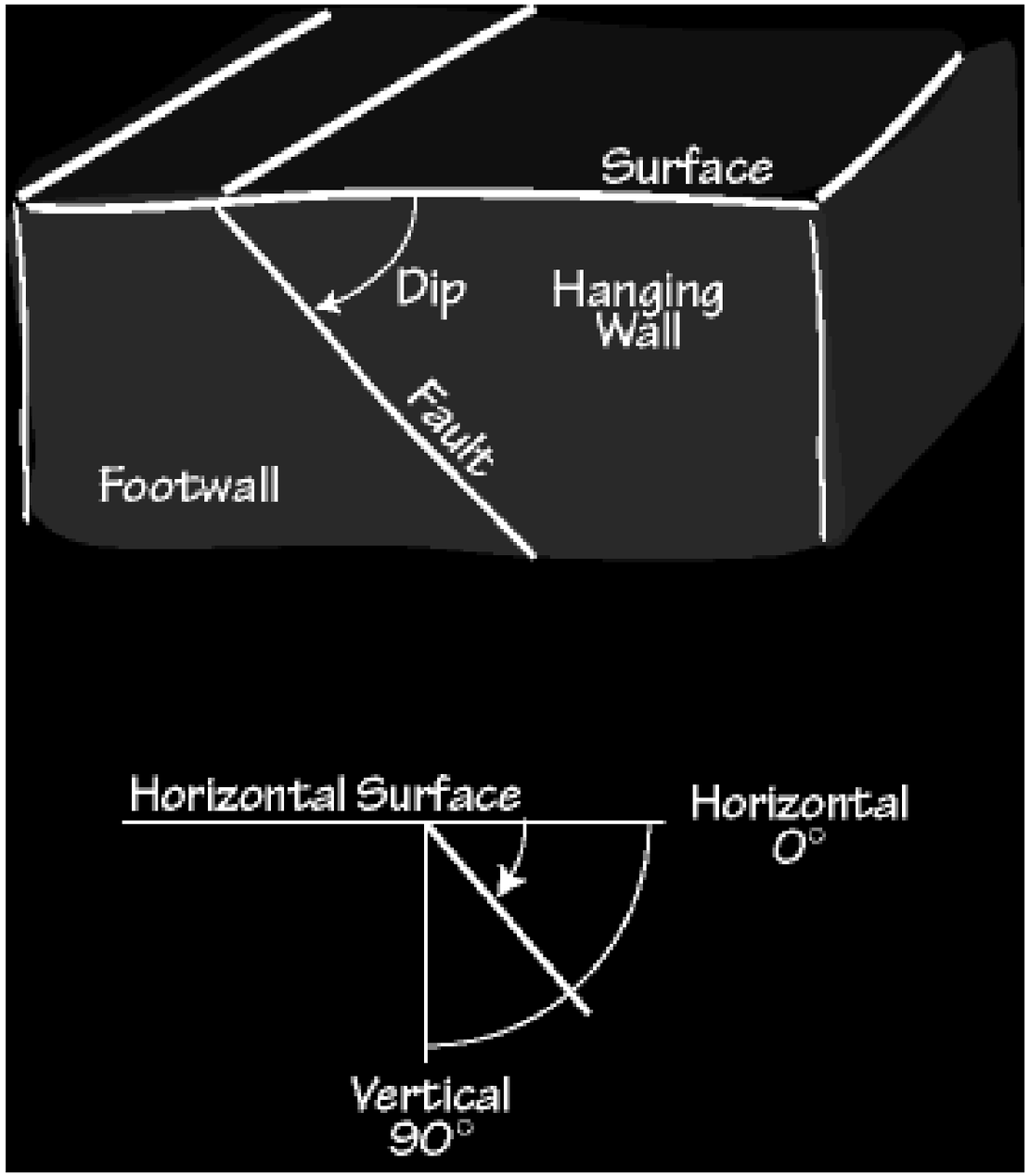

Fault Geometry Terminology: SLIP

Slip angle is used to describe the orientation of the movement of the hanging wall relative to the foot wall.

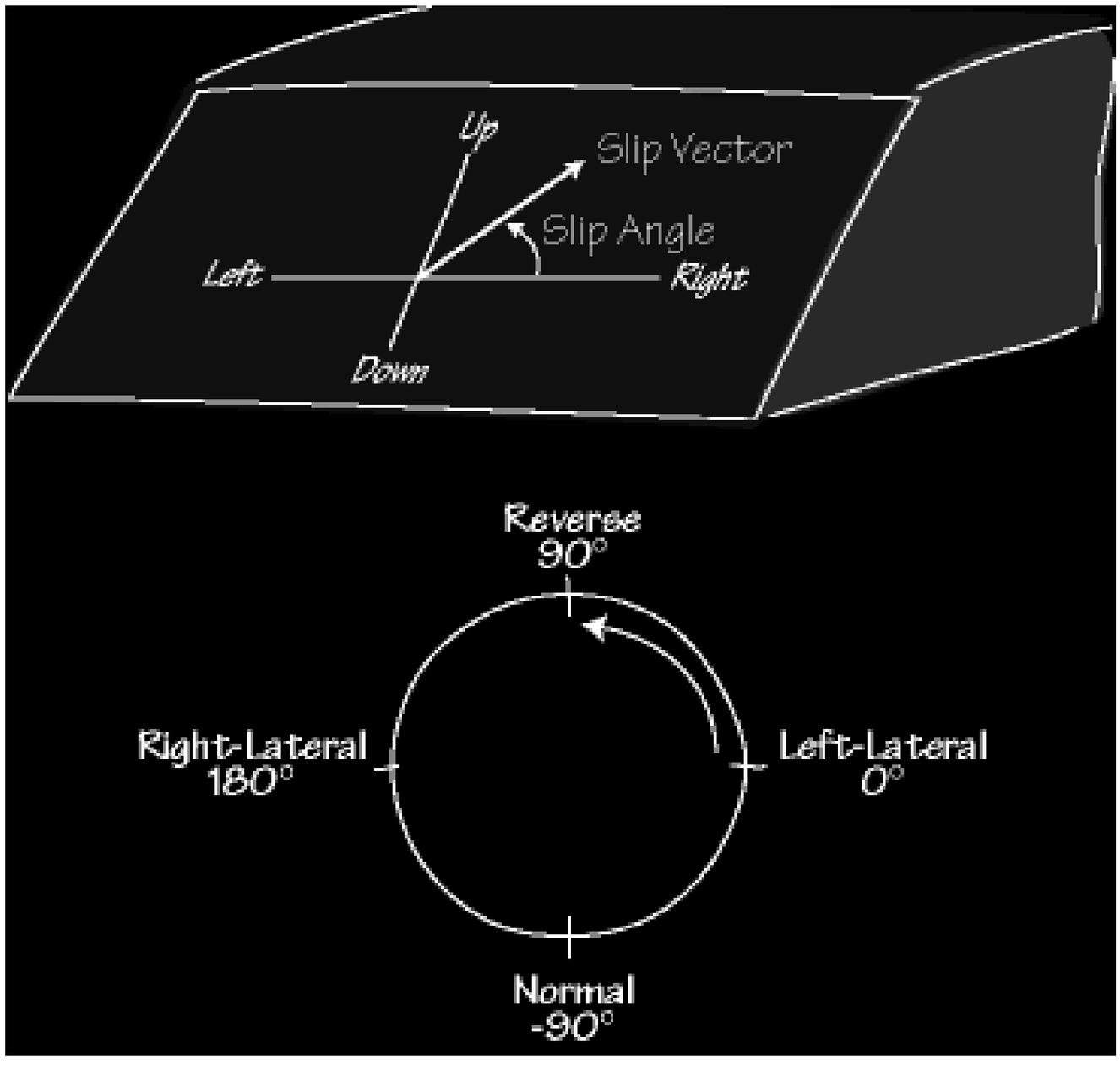

Hypocenter and Epicenter

The hypocenter (or focus) is the place where the rupture begins, the epicenter is the place directly above the hypocenter.

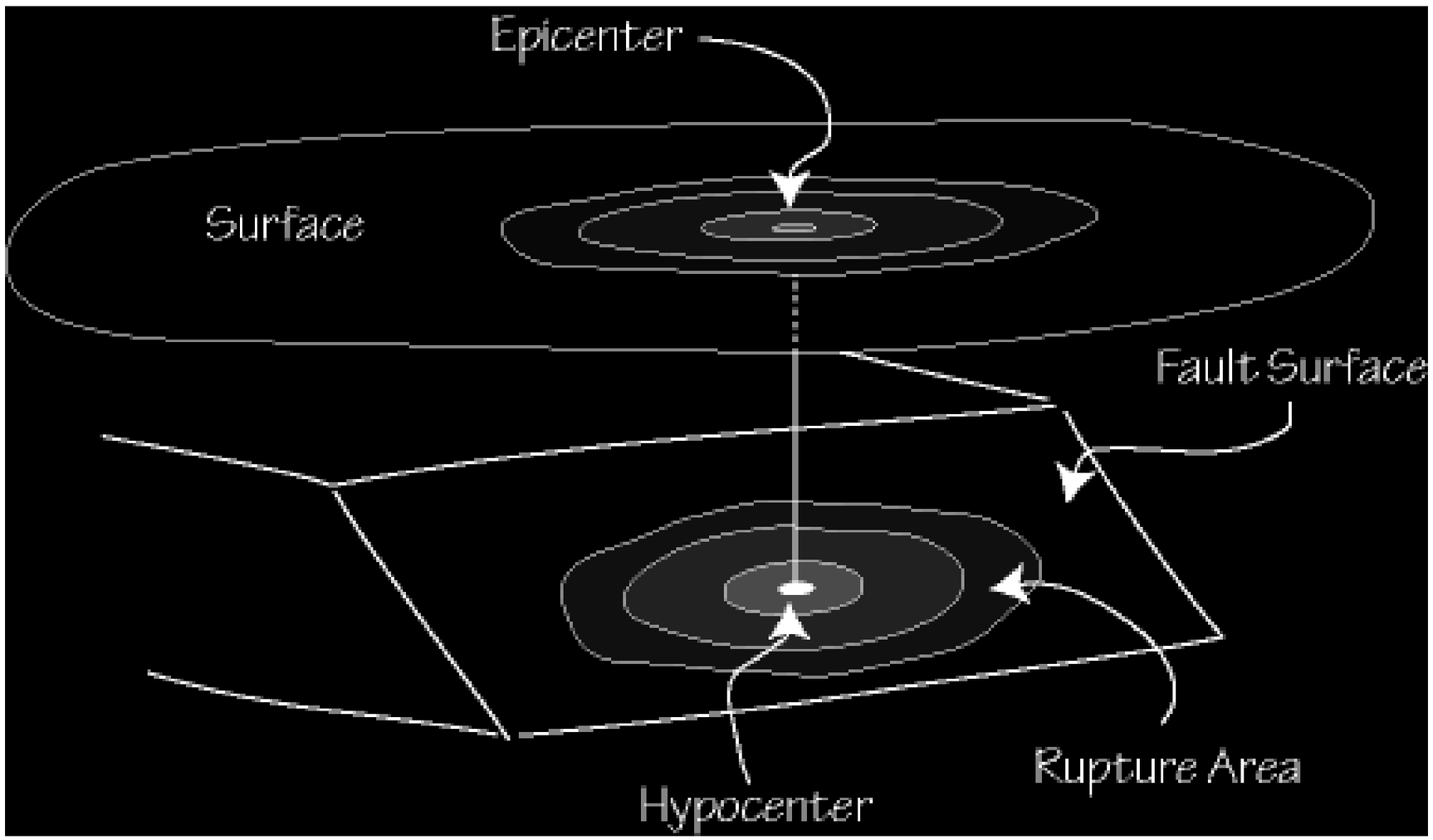

Elastic rebound (Reid)

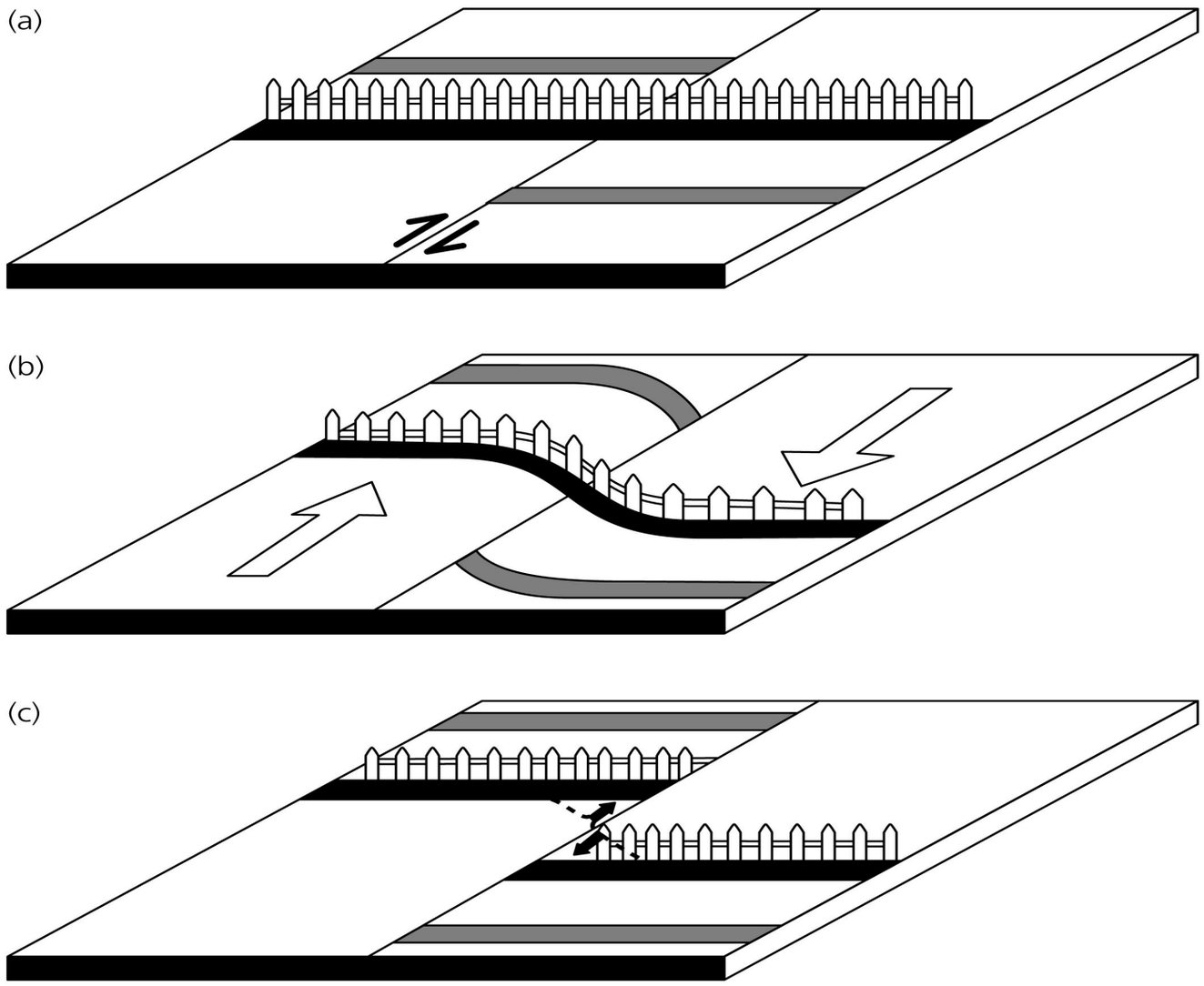

From an examination of the displacement of the ground surface which accompanied the 1906 San Francisco earthquake, Henry Fielding Reid, Professor of Geology at Johns Hopkins University, concluded that the earthquake must have involved an "elastic rebound" of previously stored elastic stress.

Reid, H.F., "The mechanics of the earthquake", v. 2 of "The California earthquake of April 18, 1906". Report of the State Earthquake Investigation Commission, Carnegie Institution of Washington Publication 87, 1910.

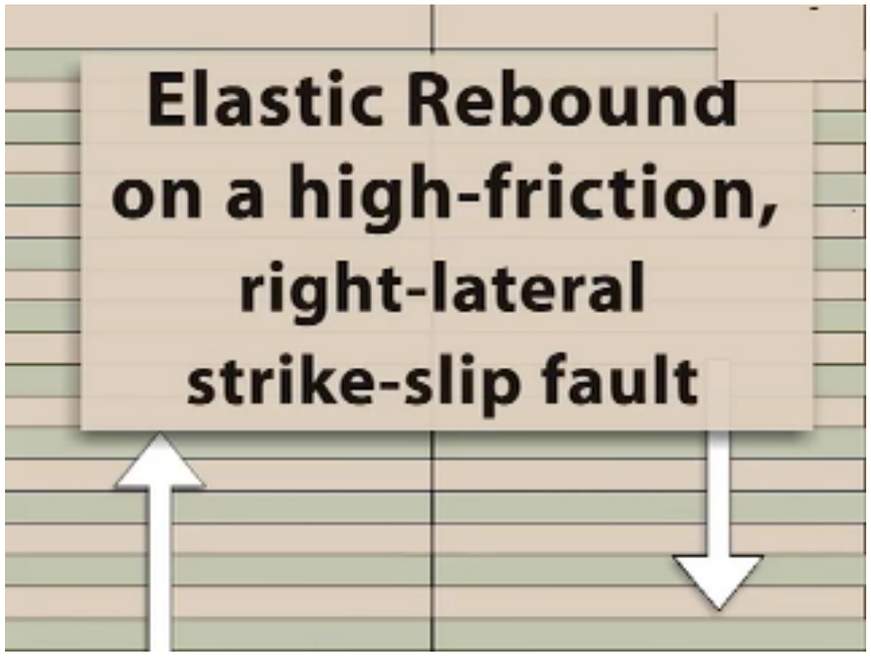

http://www.iris.edu/hq/programs/education_and_outreach/aotm/4

Earthquake rupture

Can be described by: a) formation and b) propagation of a crack.

The crack tip acts as a stress concentrator and if the stress exceeds some critical value then sudden slip occurs, and it drops to the dynamic frictional value; when the slip has stopped the stress reaches a final level

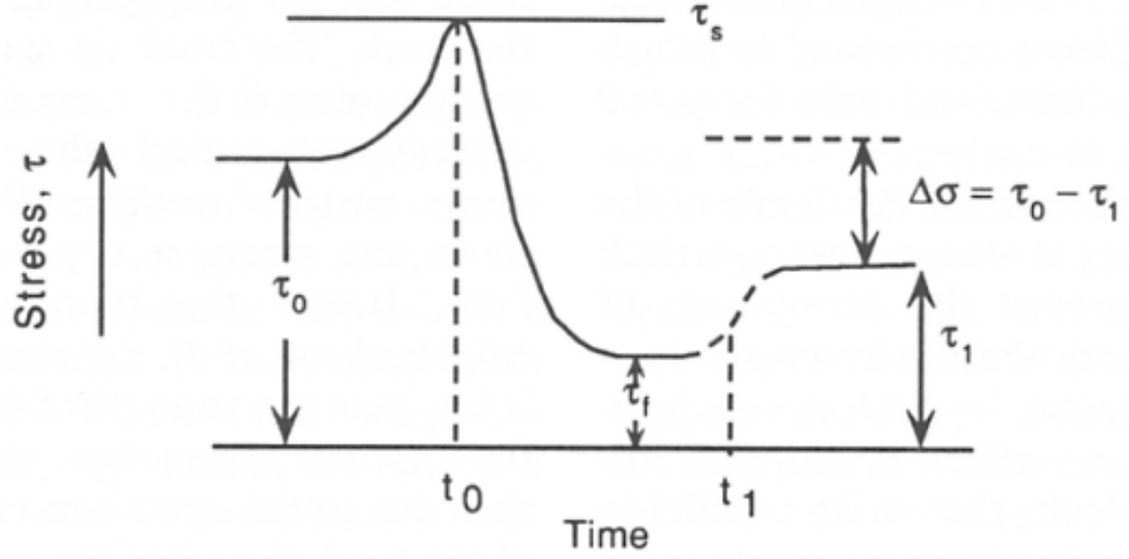

FIGURE 9.2 Stress at a point on a fault surface. As the rupture front approaches the point, stress increases to a value of τ_s, after which failure occurs at the point. The point slips to a displacement D, and stress is reduced to some value τ_f. The difference between the initial stress and the final stress, $\Delta\sigma$, is defined as the stress drop. (After Yamashita, 1976.)

Stick-slip

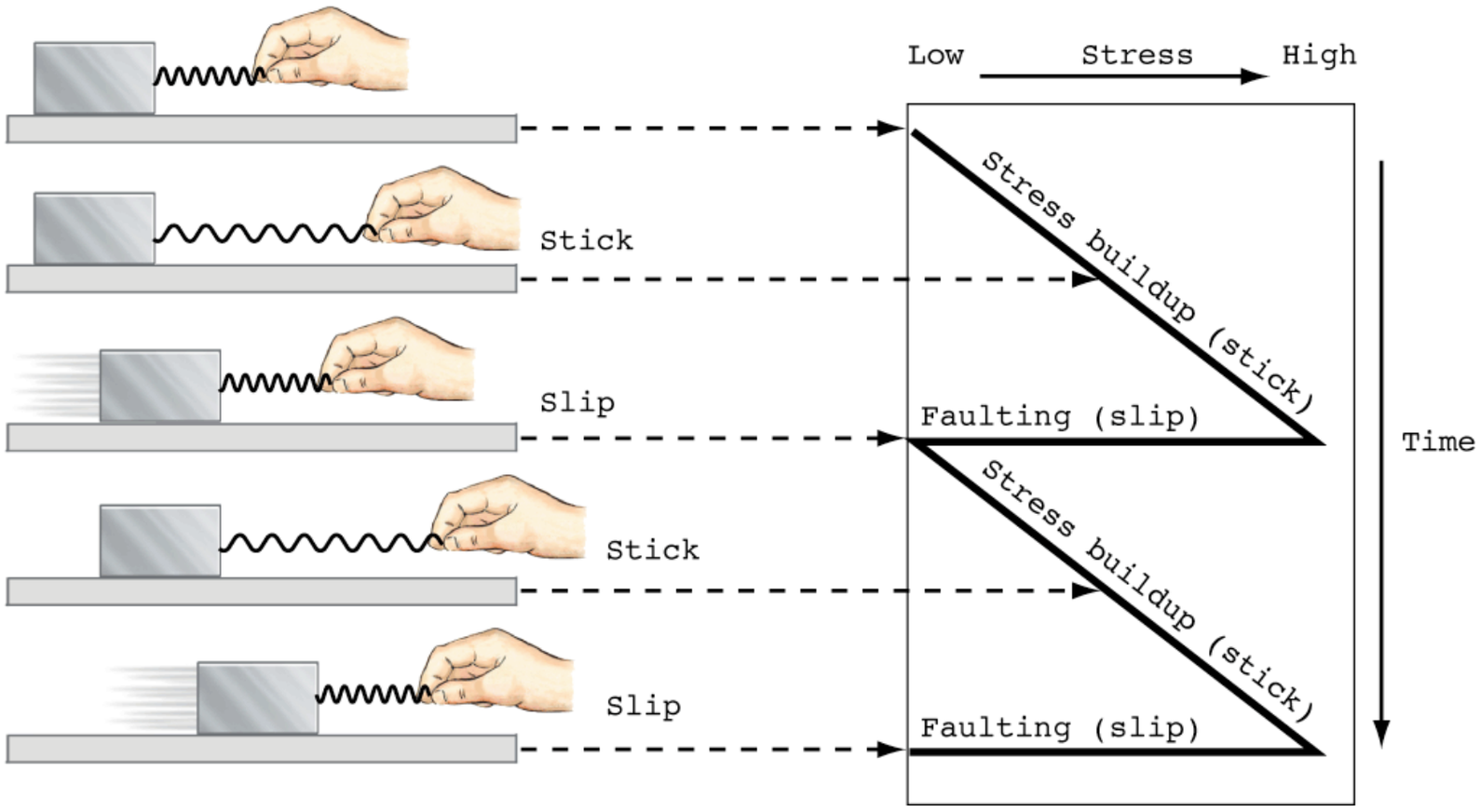

Earth, S. Marshak, W.W. Norton

Elastic strain accumulates during the interseismic period and is released during an earthquake. The elastic strain causes the earthquake –in the sense that the elastic energy stored around the fault drives earthquake rupture.
There are three basic stages in Reid's hypothesis.

1) Stress accumulation (e.g., due to plate tectonic motion)
2) Stress reaches or exceeds the (frictional) failure strength
3) Failure, seismic energy release (elastic waves), and fault rupture propagation

Stick-slip

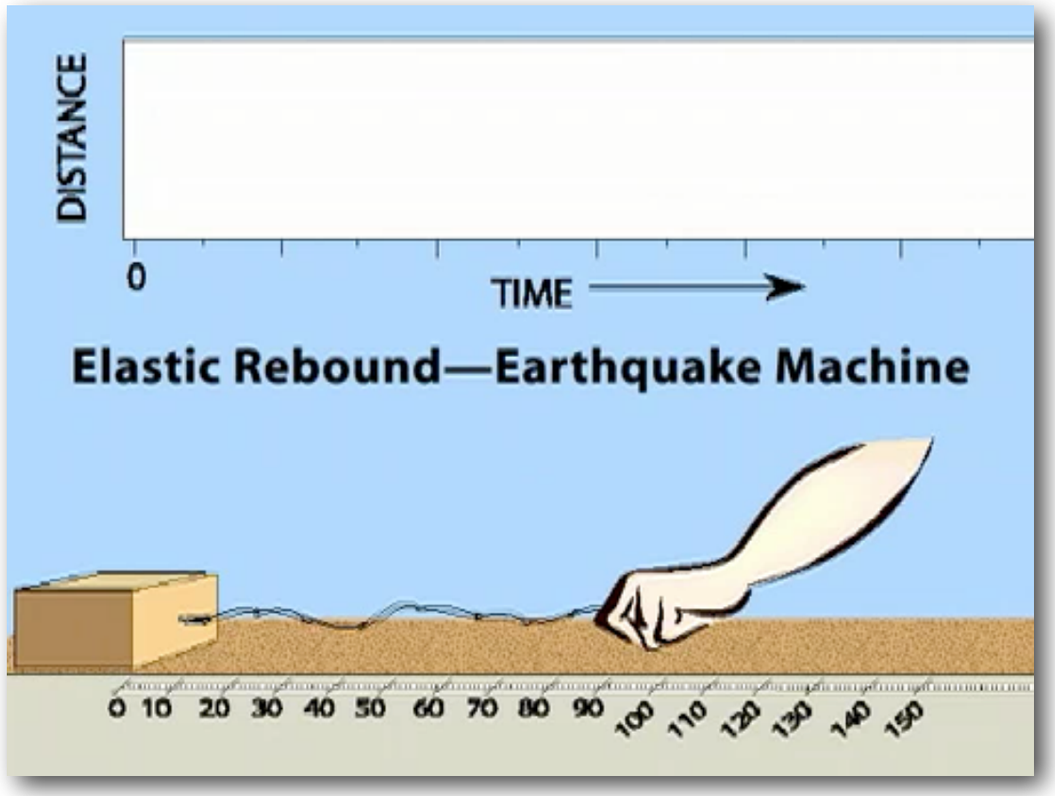

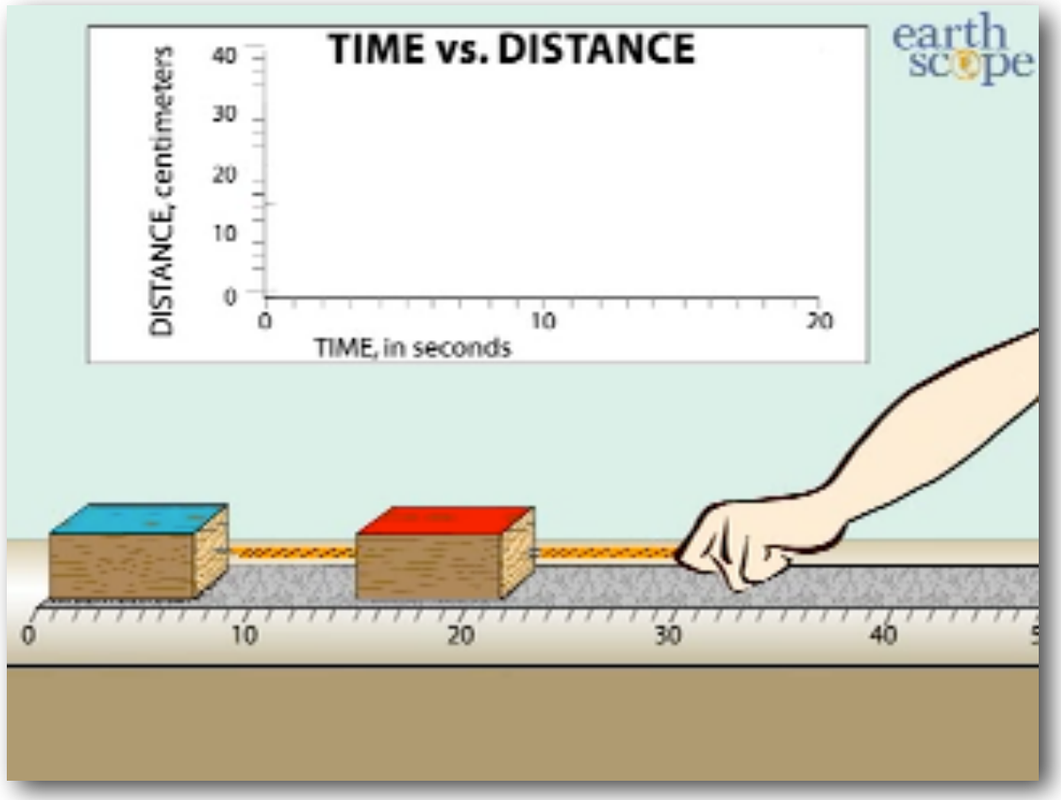

http://www.iris.edu/hq/programs/education_and_outreach/aotm/1

Stress cycle: prediction models

τ_1 is the shear stress at initiation of slip and reflects fault strength. τ_2 is the shear stress at which slip ceases and reflects fault friction.
(a) **Characteristic model** of stick-slip faulting. Each earthquake is identical in stress history, recurrence interval and slip.
(b) **Time-predictable model**. If slip is proportional to stress drop, and plate motions are steady, we can predict the time of the next earthquake based on the amount of slip during the previous earthquake.
(c) **Slip-predictable model**. Knowing the time of the last earthquake and assuming steady plate motion, we can predict the size of an earthquake expected at a particular time.

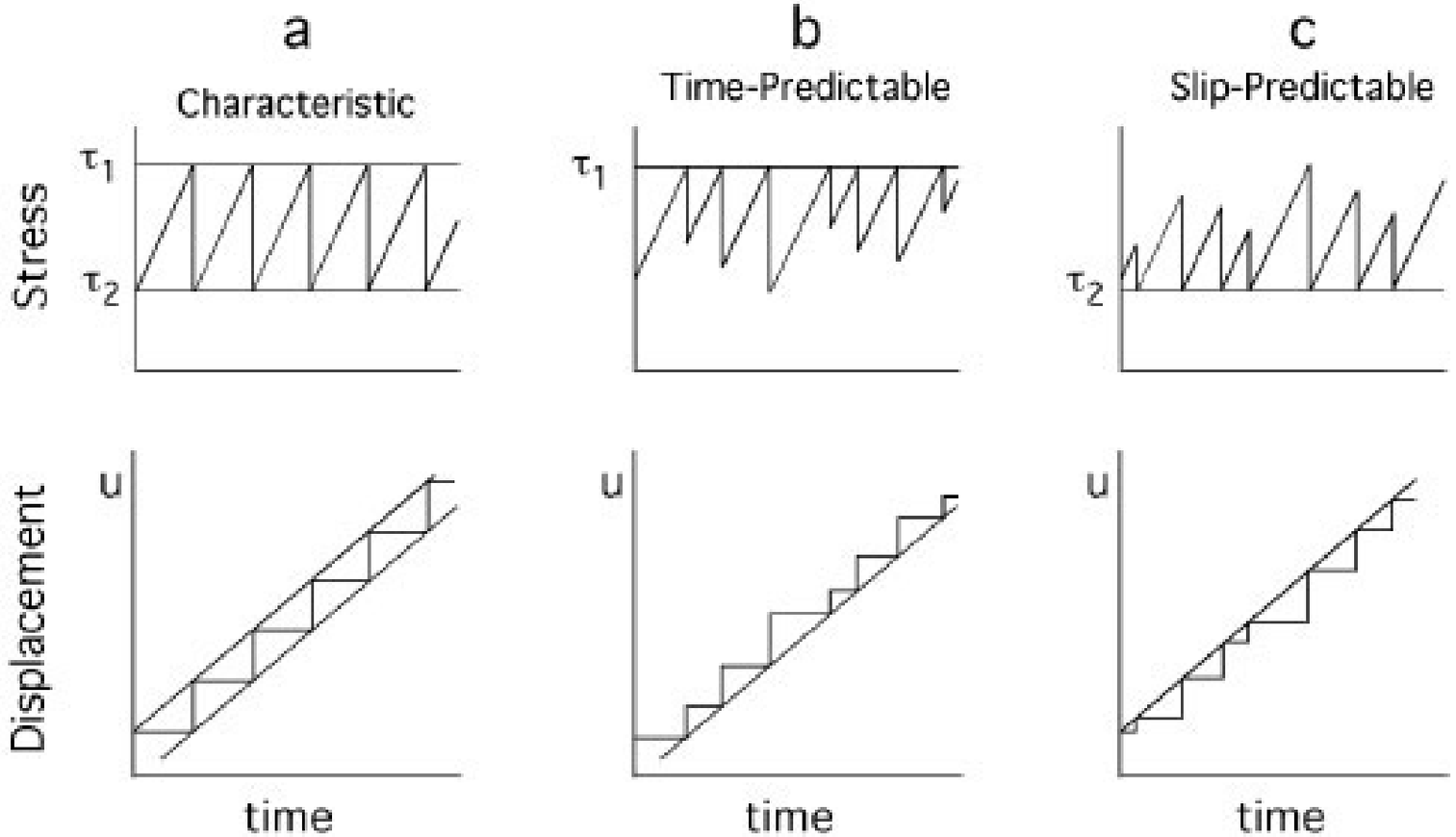

Stress cycle

The stress drop causes a time interval during which the stress builds up again to critical value. This type of frictional behaviour is known as **stick-slip**, or unstable sliding (as opposed to continue slip on smooth surfaces: stable sliding).
Earthquakes are generally thought to be **recurring slip episodes on preexisting faults**: the importance is no more on the strength of the rock but on the stress-stability cycle.

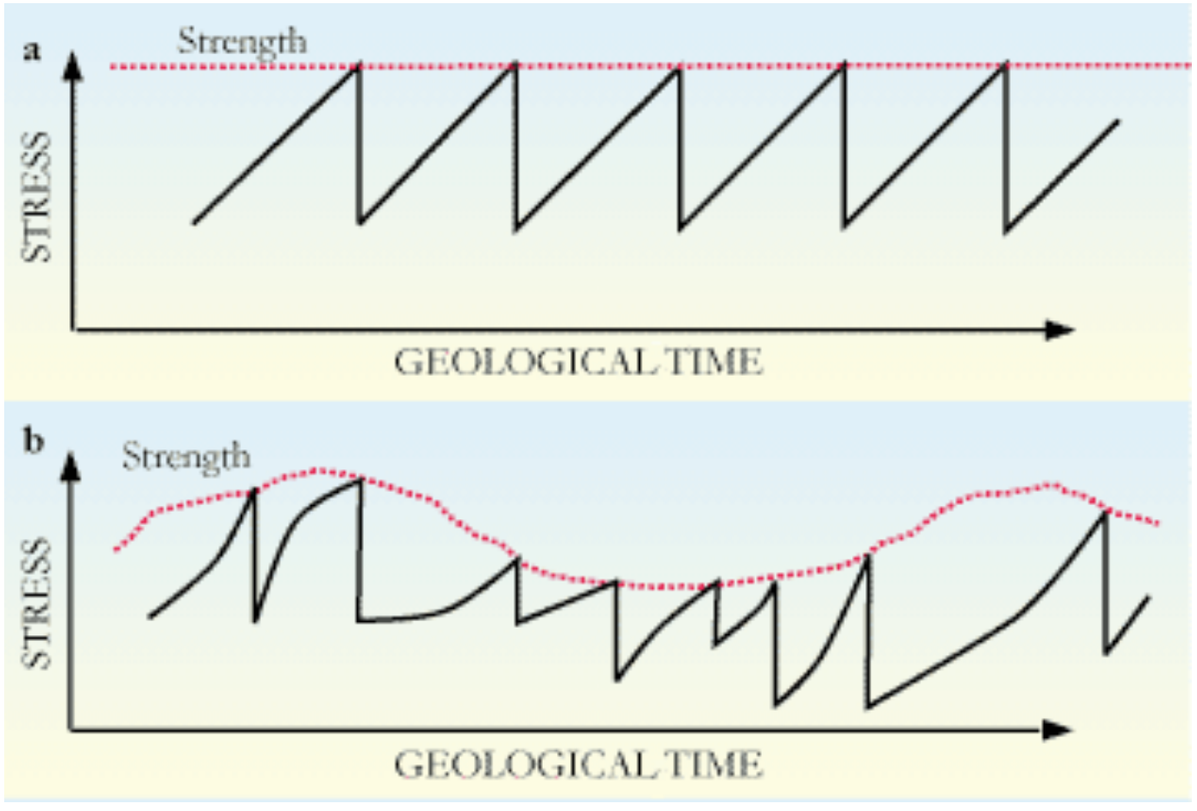

Maximum Intensity

Maximum Intensity is used to estimate the size of historical earthquakes, but suffers from dependence on depth, population, construction practices, site effects, regional geology, etc.

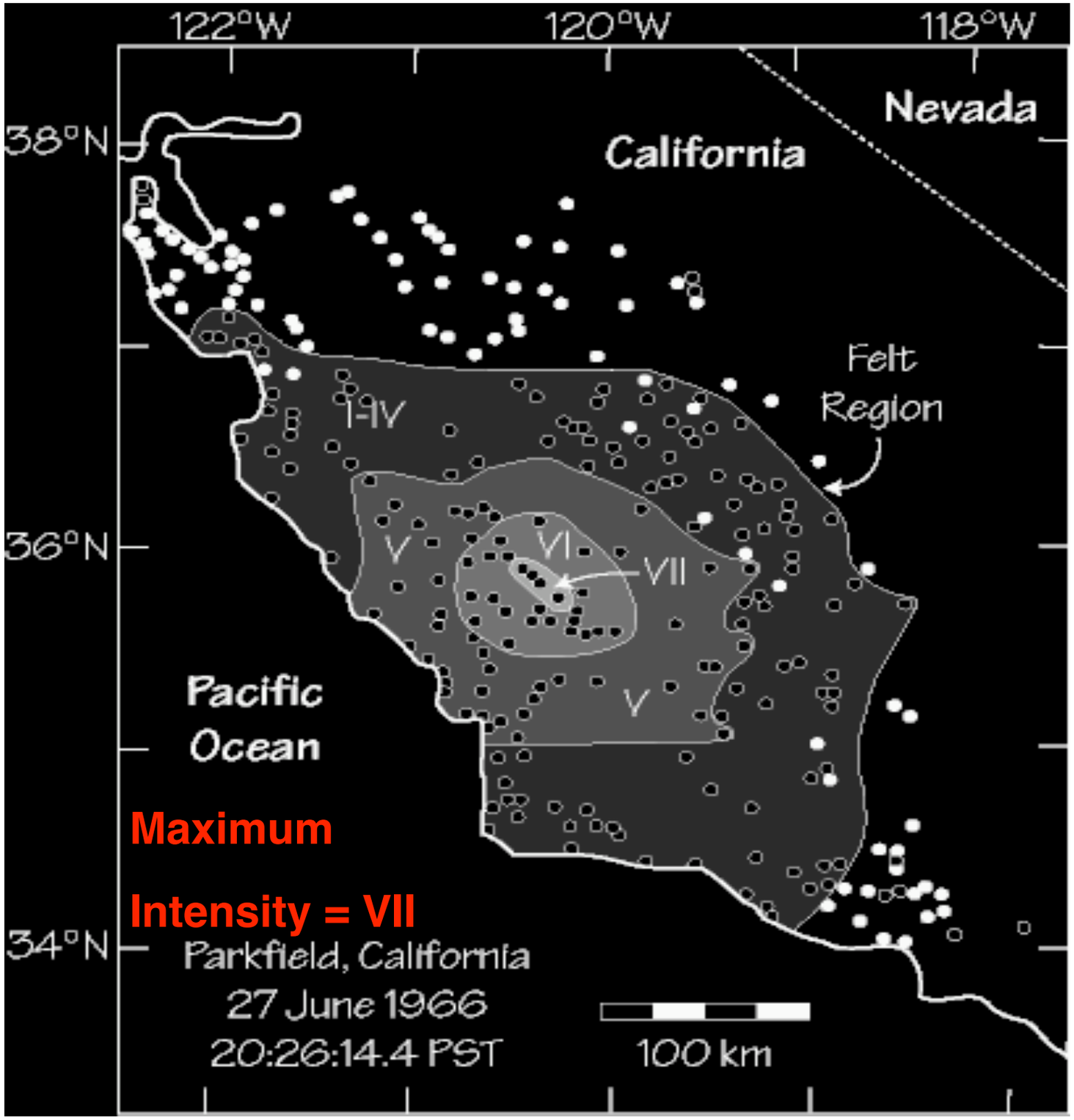

1906 SF and 1811-12 New Madrid

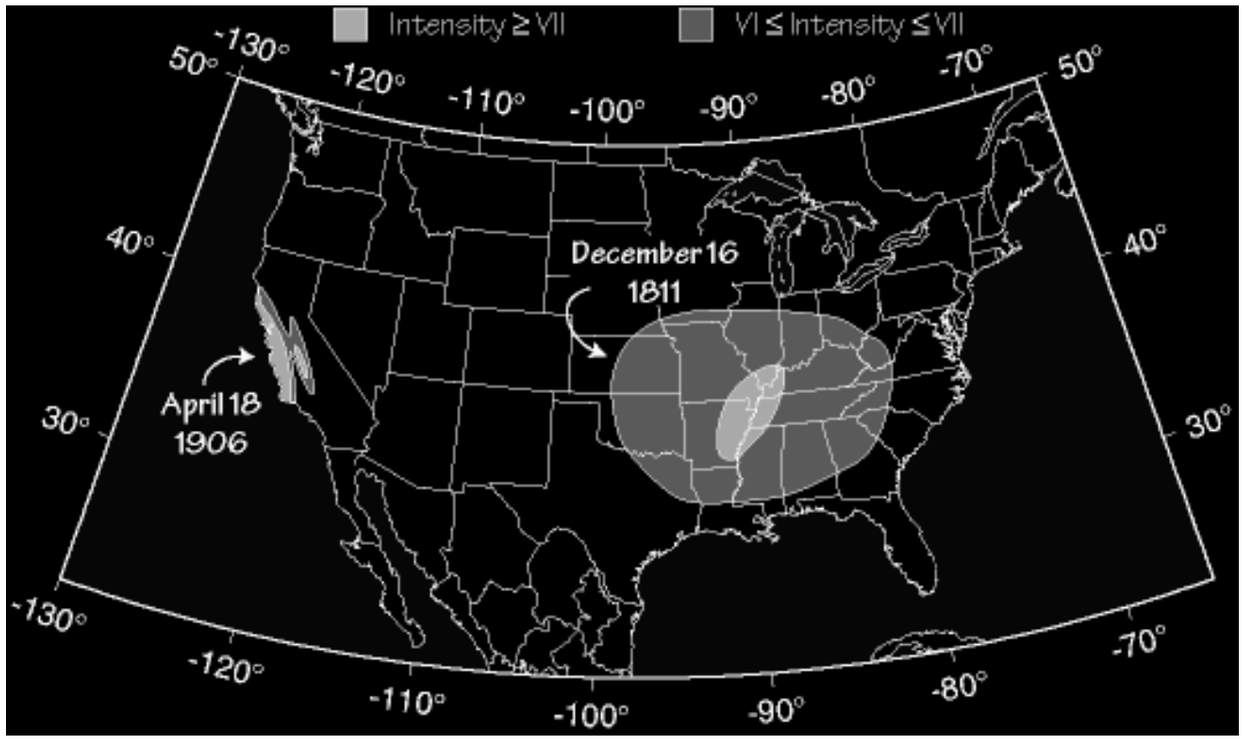

These earthquakes were roughly the same size, but the intensity patterns in the east are broader than in the west (wait for Q...)

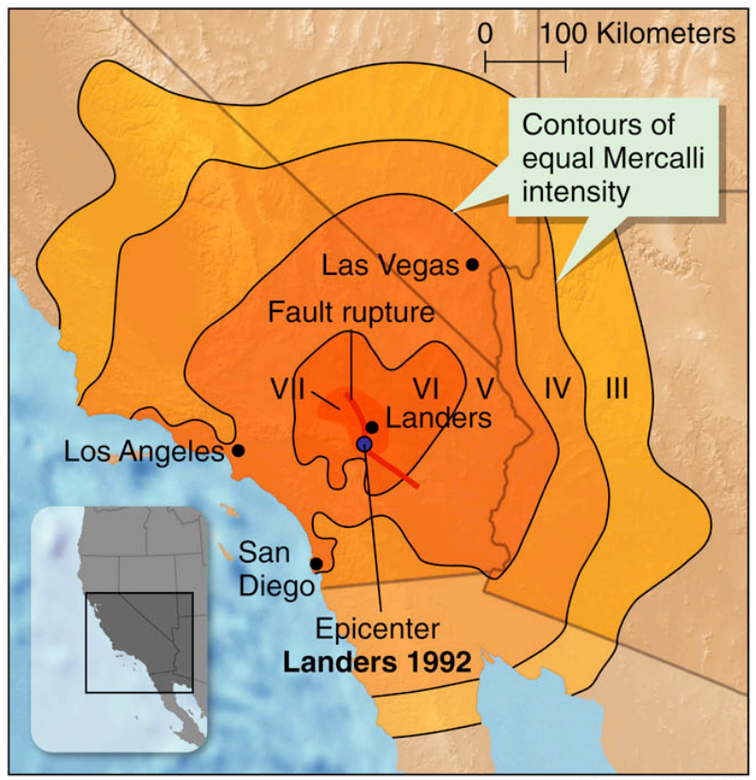

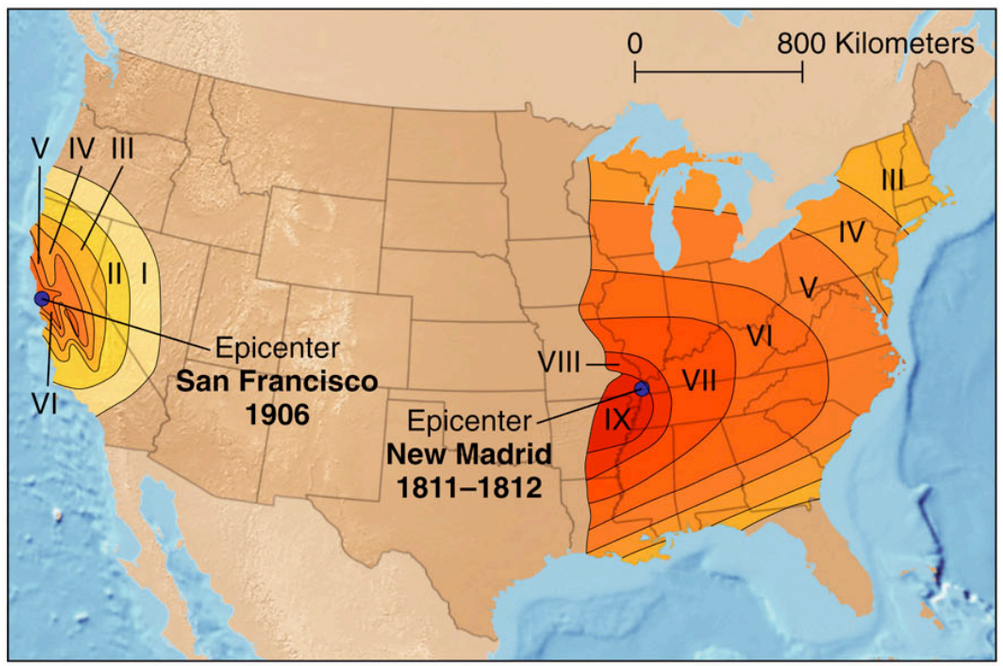

Mercalli Intensity and Richter Magnitude

Magnitude	Intensity	Description
1.0-3.0 **Micro**	**I**	**I.** Not felt except by a very few under especially favorable conditions.
3.0 - 3.9 **Minor**	**II - III**	**II.** Felt only by a few persons at rest, especially on upper floors of buildings. **III.** Felt quite noticeably by persons indoors, especially on upper floors of buildings. Many people do not recognize it as an earthquake. Standing motor cars may rock slightly. Vibrations similar to the passing of a truck. Duration estimated.
4.0 - 4.9 **Light**	**IV - V**	**IV.** Felt indoors by many, outdoors by few during the day. At night, some awakened. Dishes, windows, doors disturbed; walls make cracking sound. Sensation like heavy truck striking building. Standing motor cars rocked noticeably. **V.** Felt by nearly everyone; many awakened. Some dishes, windows broken. Unstable objects overturned. Pendulum clocks may stop.
5.0 - 5.9 **Moderate**	**VI - VII**	**VI.** Felt by all, many frightened. Some heavy furniture moved; a few instances of fallen plaster. Damage slight. **VII.** Damage negligible in buildings of good design and construction; slight to moderate in well-built ordinary structures; considerable damage in poorly built or badly designed structures; some chimneys broken.
6.0 - 6.9 **Strong**	**VII - IX**	**VIII**. Damage slight in specially designed structures; considerable damage in ordinary substantial buildings with partial collapse. Damage great in poorly built structures. Fall of chimneys, factory stacks, columns, monuments, walls. Heavy furniture overturned. **IX.** Damage considerable in specially designed structures; well-designed frame structures thrown out of plumb. Damage great in substantial buildings, with partial collapse. Buildings shifted off foundations.
7.0 and higher **Major great**	**VIII or higher**	**X.** Some well-built wooden structures destroyed; most masonry and frame structures destroyed with foundations. Rails bent. **XI.** Few, if any (masonry) structures remain standing. Bridges destroyed. Rails bent greatly. **XII.** Damage total. Lines of sight and level are distorted. Objects thrown into the air.

Intensity scales

MM	RF	JMA	MCS	MSK
I	I		II	I
II		I	III	II
	II			III
III	III		IV	
IV	IV	II	V	IV
V	V	III	VI	V
VI	VI	IV	VII	VI
	VII			
VII	VIII	V	VIII	VII
VIII			IX	VIII
	IX		X	
IX		VI	XI	IX
X	X		XII	X
XI		VII		XI
XII				XII

MM – Modified Mercalli; RF – Rossi-Forel; JMA – Japanese Meteorological Agency;
MCS – Mercalli-Cancani-Sieberg; MSK – Medvedev-Sponheuer-Karnik

Magnitude Scales - Richter

The concept of magnitude was introduced by Richter (1935) to provide an objective instrumental measure of the size of earthquakes. Contrary to seismic intensity, I, which is based on the assessment and classification of shaking damage and human perceptions of shaking, the magnitude M uses instrumental measurements of earth ground motion adjusted for epicentral distance and source depth.

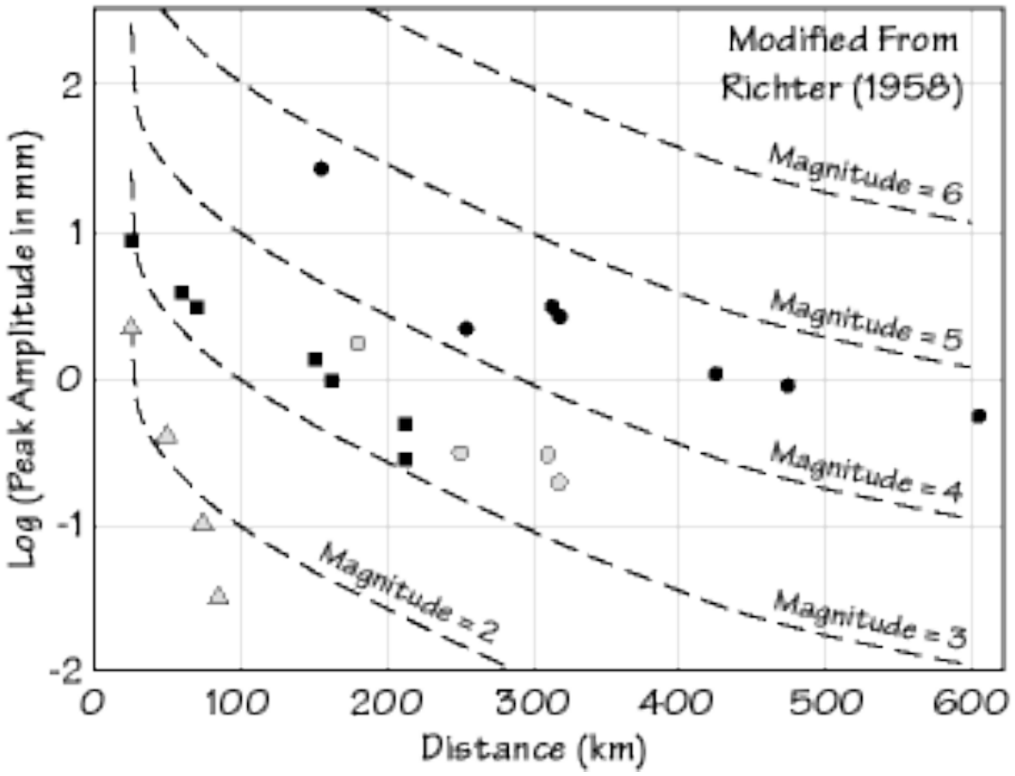

The original Richter scale was based on the observation that the amplitude of seismic waves systematically decreases with epicentral distance.

Data from local earthquakes in California

The relative size of events is calculated by comparison to a reference event, with M_L=0, such that A_0 was 1 μm at an epicentral distance, Δ, of 100 km with a Wood-Anderson instrument:

$$\mathbf{M_L = \log(A/A_0) = \log A - 2.48 + 2.76\Delta}.$$

Magnitude Scales - Richter

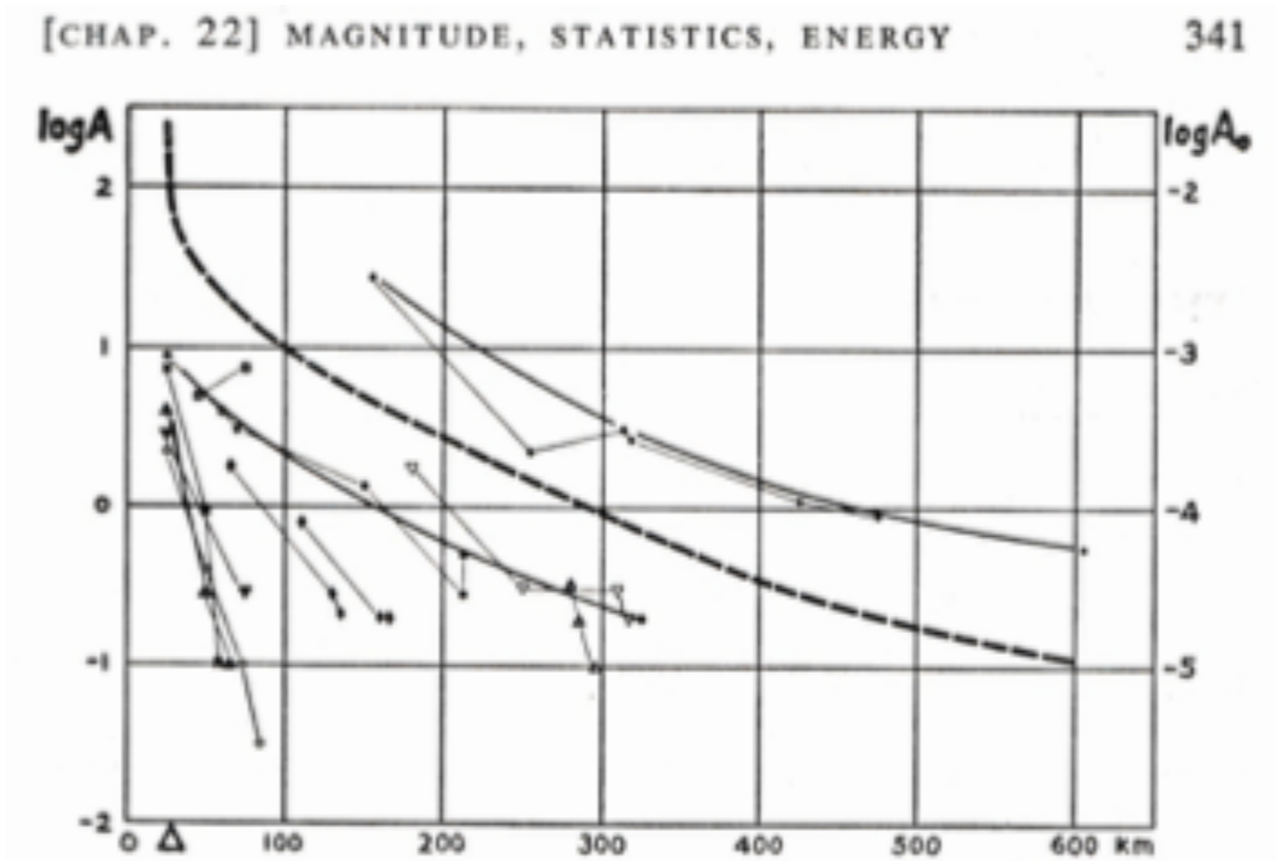

FIGURE 22-2 *Origin of the magnitude scale. Data for Southern California earthquakes of January, 1932. [Redrafted from the original notes.]*

"I found a paper by Professor K. Wadati of Japan in which he compared large earthquakes by plotting the maximum ground motion against distance to the epicenter. I tried a similar procedure for our stations, but the range between the largest and smallest magnitudes seemed unmanageably large. Dr. Beno Gutenberg then made the natural suggestion to plot the amplitudes logarithmically. I was lucky because **logarithmic plots are a device of the devil**. I saw that I could now rank the earthquakes one above the other. Also, quite unexpectedly the attenuation curves were roughly parallel on the plot. By moving them vertically, a representative mean curve could be formed, and individual events were then characterized by individual logarithmic differences from the standard curve. This set of logarithmic differences thus became the numbers on a new instrumental scale. Very perceptively, Mr. Wood insisted that this new quantity should be given a distinctive name to contrast it with the intensity scale. My amateur interest in astronomy brought out the term "magnitude," which is used for the brightness of a star."

Charles F. Richter - An Interview by Henry Spall, Earthquake Information Bulletin. Vol. 12, No. 1, January - February, 1980

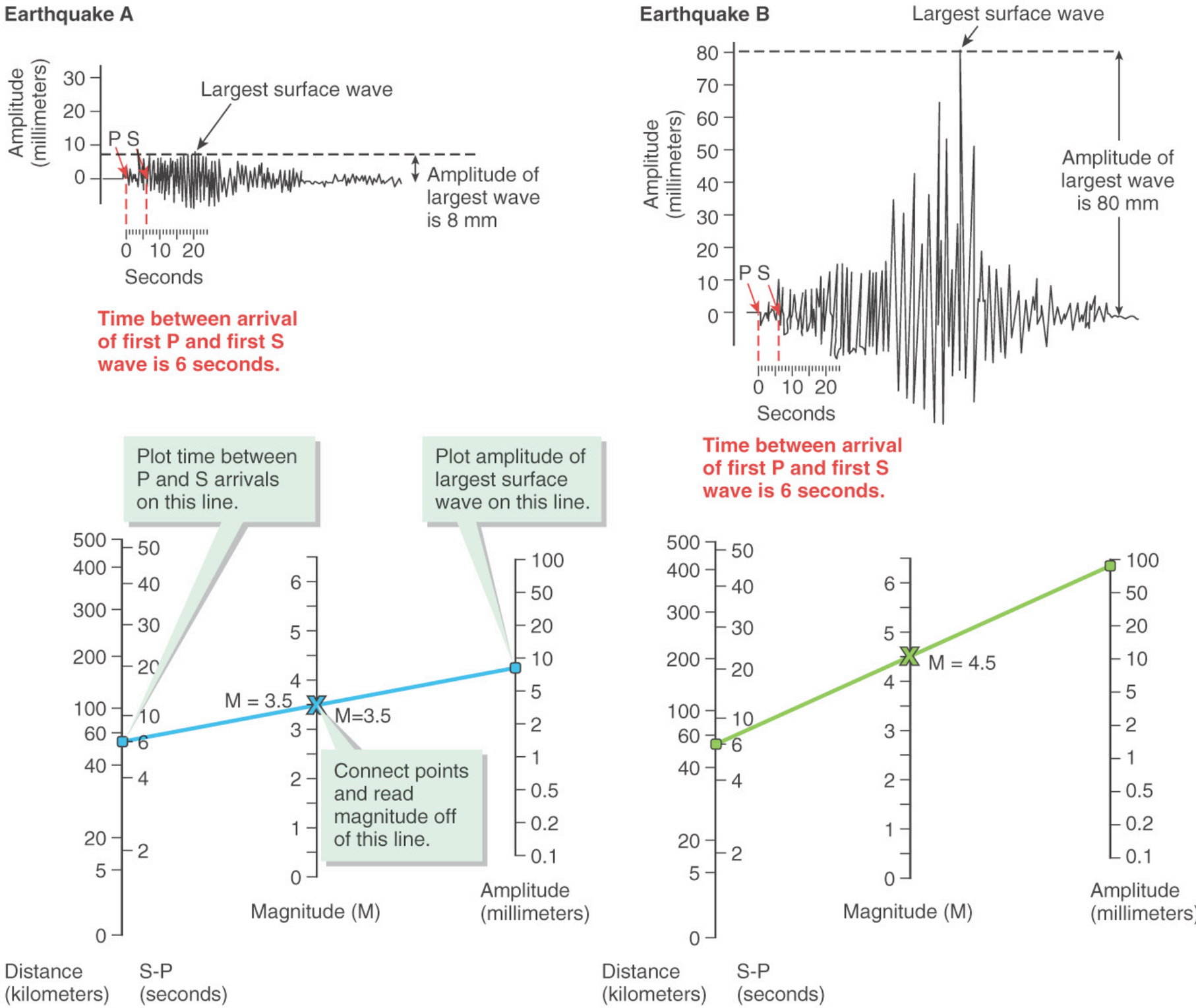

Wood-Anderson Seismometer

Richter also tied his formula to a specific seismic instrument.

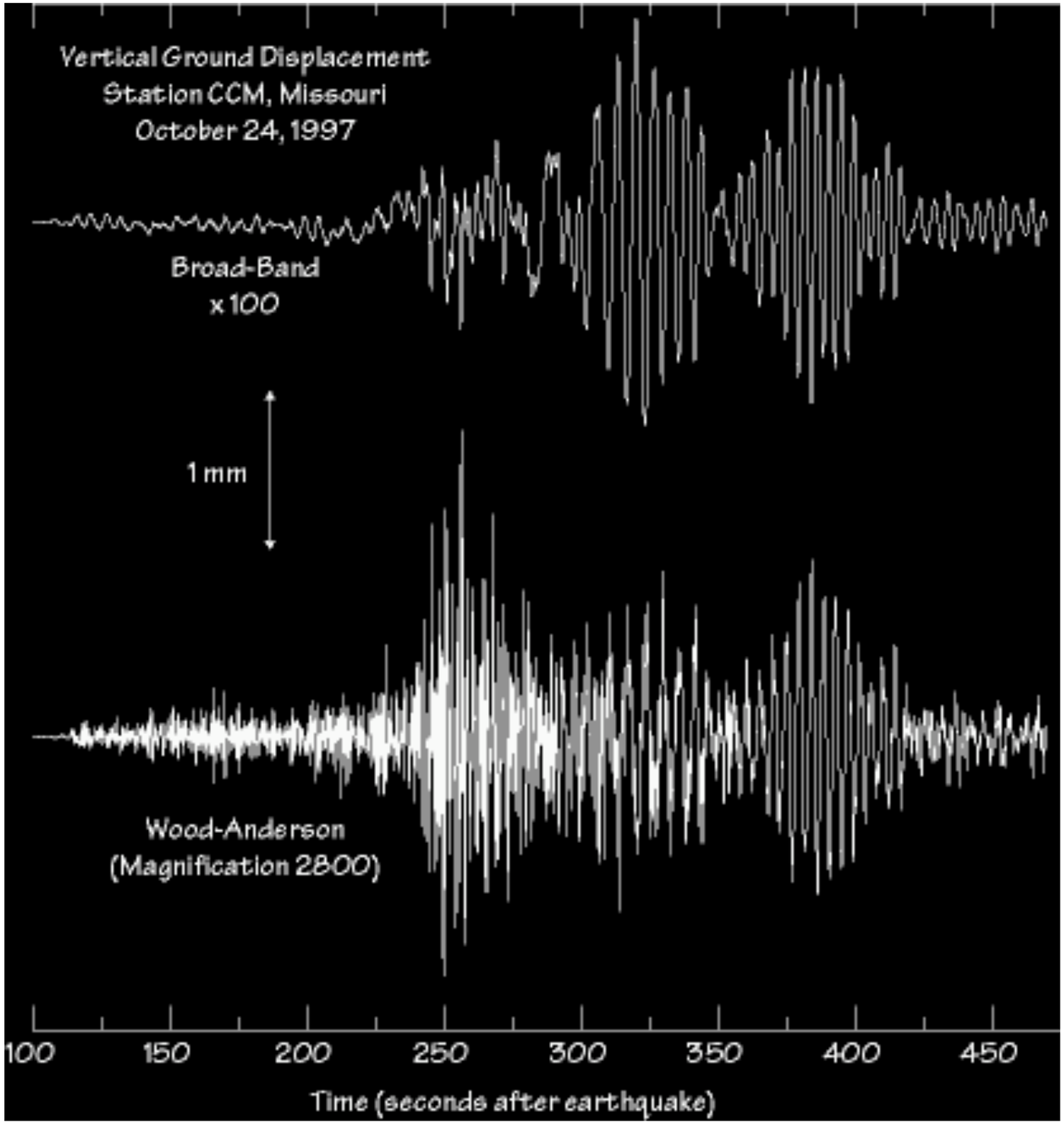

Magnitude Scales

The original M_L is suitable for the classification of local shocks in Southern California only since it used data from the standardized short-period Wood-Anderson seismometer network. The magnitude concept has then been extended so as to be applicable also to ground motion measurements from medium- and long-period seismographic recordings of both surface waves (M_s) and different types of body waves (m_b) in the teleseismic distance range.

The general form of all magnitude scales based on measurements of ground displacement amplitudes A and periods T is:

$$M = \log\left(\frac{A}{T}\right) + f(\Delta, h) + C_r + C_s$$

M seismic magnitude
A amplitude
T period
f correction for distance and depth
C_s correction for site
C_r correction for source region

M_L **Local magnitude**

m_b **body-wave magnitude** (1s)

M_s **surface wave magnitude** (20s)

Teleseismic M_S and mb

The two most common modern magnitude scales are:

- M_S, Surface-wave magnitude (Rayleigh Wave, 20s)
- m_b, Body-wave magnitude (P-wave)

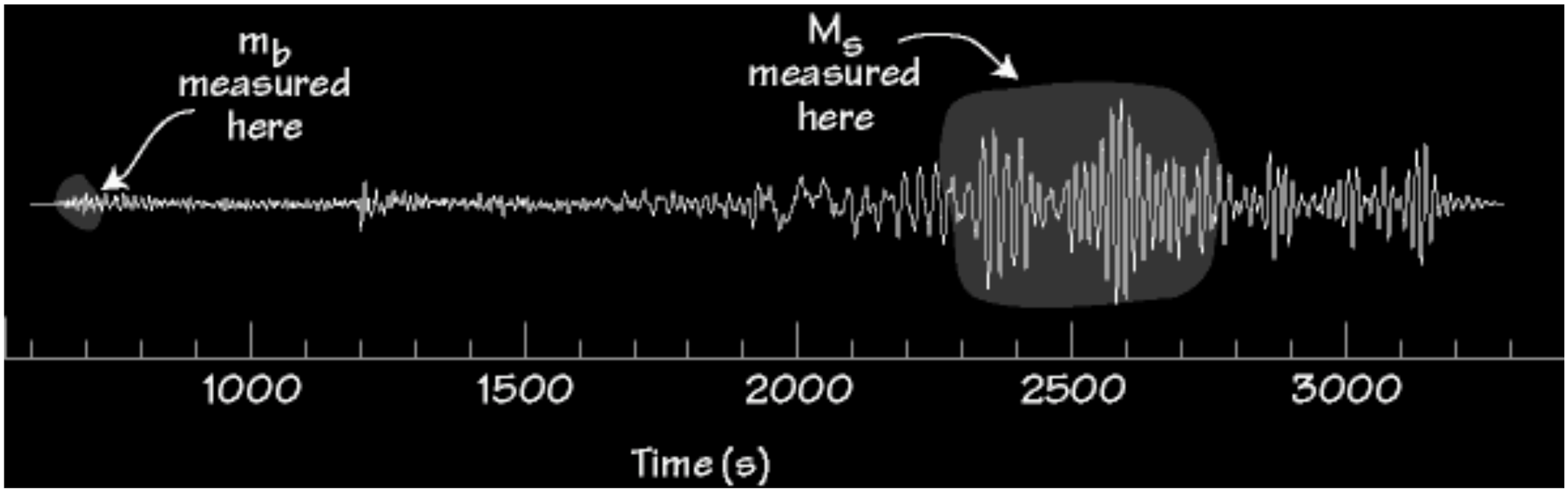

Example: m_b "Saturation"

m_b seldom gives values above 6.7 - it "saturates".

m_b must be measured in the first 5 seconds - that's the rule.

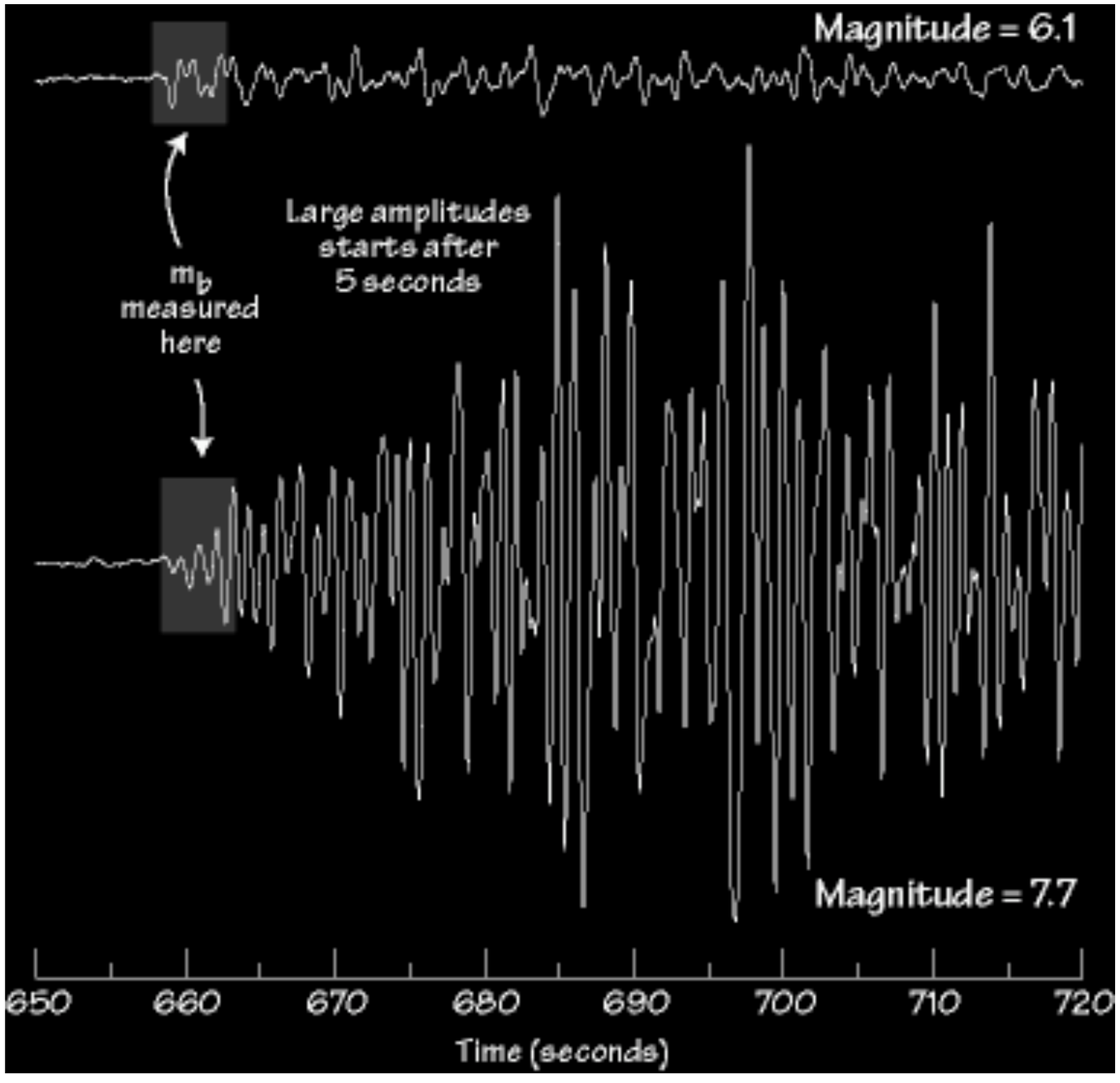

Saturation

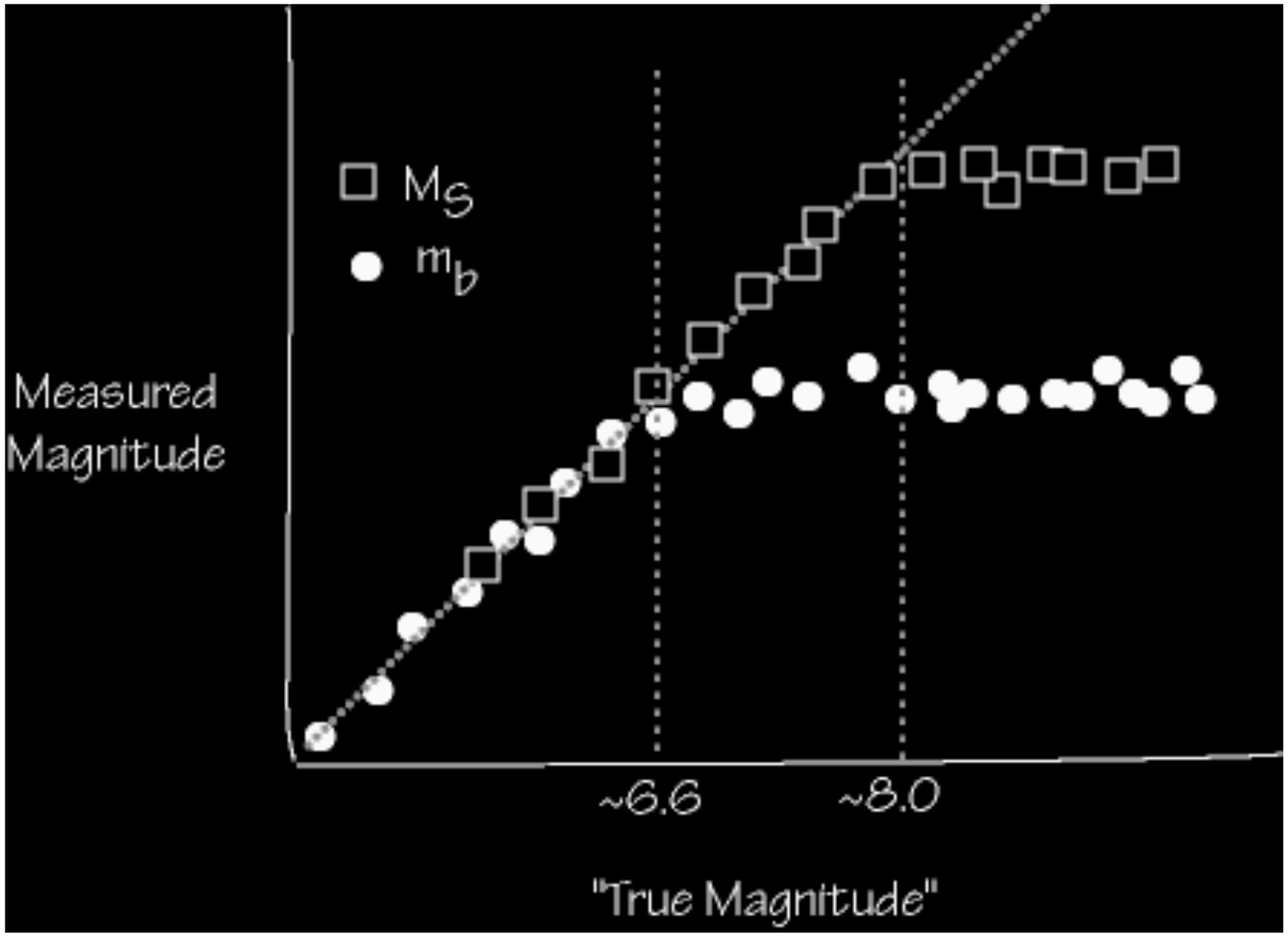

Equivalent Forces

The observable seismic radiation is through energy release as the fault surface moves: formation and propagation of a crack. This complex dynamical problem can be studied by kinematical equivalent approaches.

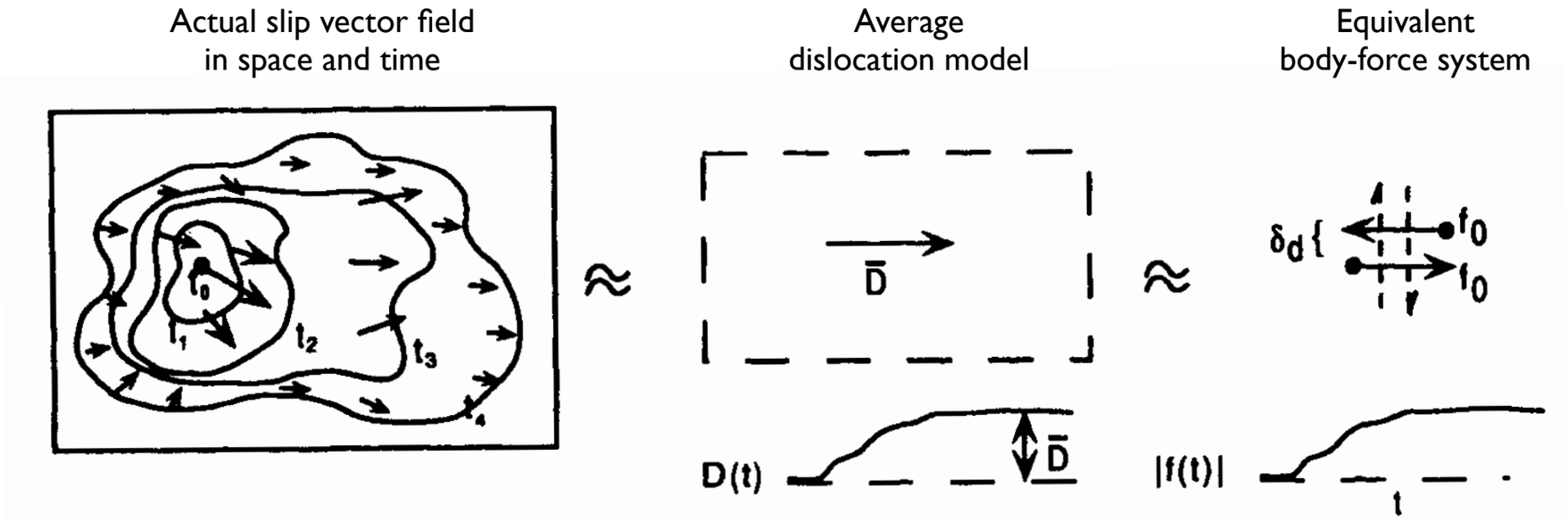

The scope is to develop a representation of the displacement generated in an elastic body in terms of the quantities that originated it: body forces and applied tractions and displacements over the surface of the body.

The actual slip process will be described by superposition of equivalent body forces acting in space (over a fault) and time (rise time).

Final source representation

$$u_n(\mathbf{x},t) = \iint_{\Sigma} [u_i] c_{ijpq} \nu_j * \frac{\partial G_{np}}{\partial \xi_q} d\Sigma$$

$$m_{pq} = [u_i] c_{ijpq} \nu_j \qquad u_n(\mathbf{x},t) = \iint_{\Sigma} m_{pq} * \frac{\partial G_{np}}{\partial \xi_q} d\Sigma$$

And if the source can be considered a point-source (for distances greater than fault dimensions), the contributions from different surface elements can be considered in phase.

Thus for an effective point source, one can define the moment tensor:

$$M_{pq} = \iint_{\Sigma} m_{pq} \, d\Sigma$$

$$u_n(\mathbf{x},t) = M_{pq} * G_{np,q}$$

Moment tensor decomposition

The moment tensor is symmetric (thus the roles of **u** and ν can be interchanged without affecting the displacement field, leading to the **fault plane-auxiliary plane** ambiguity), and it can be diagonalized and decomposed in an isotropic and deviatoric part:

$$M_{pq} = \begin{pmatrix} M_1 & 0 & 0 \\ 0 & M_2 & 0 \\ 0 & 0 & M_3 \end{pmatrix} = \frac{1}{3}\begin{pmatrix} tr(M) & 0 & 0 \\ 0 & tr(M) & 0 \\ 0 & 0 & tr(M) \end{pmatrix} + \begin{pmatrix} M'_1 & 0 & 0 \\ 0 & M'_2 & 0 \\ 0 & 0 & M'_3 \end{pmatrix}$$

For a shear dislocation, the equivalent point force is a **double-couple**, since internal faulting implies that the total force $\mathbf{f}^{[u]}$ and its total moment are null. The seismic moment has a **null trace** and **one of the eigenvalues is 0**.

$$M_{pq}(\text{doublecouple}) = \begin{pmatrix} M_0 & 0 & 0 \\ 0 & 0 & 0 \\ 0 & 0 & -M_0 \end{pmatrix} \quad \text{with } M_0 = \mu A[\bar{u}]$$

M_0 is called **seismic moment**, a scalar quantity related to the area of the fault and to the slip, averaged over the fault plane.

Moment tensor components

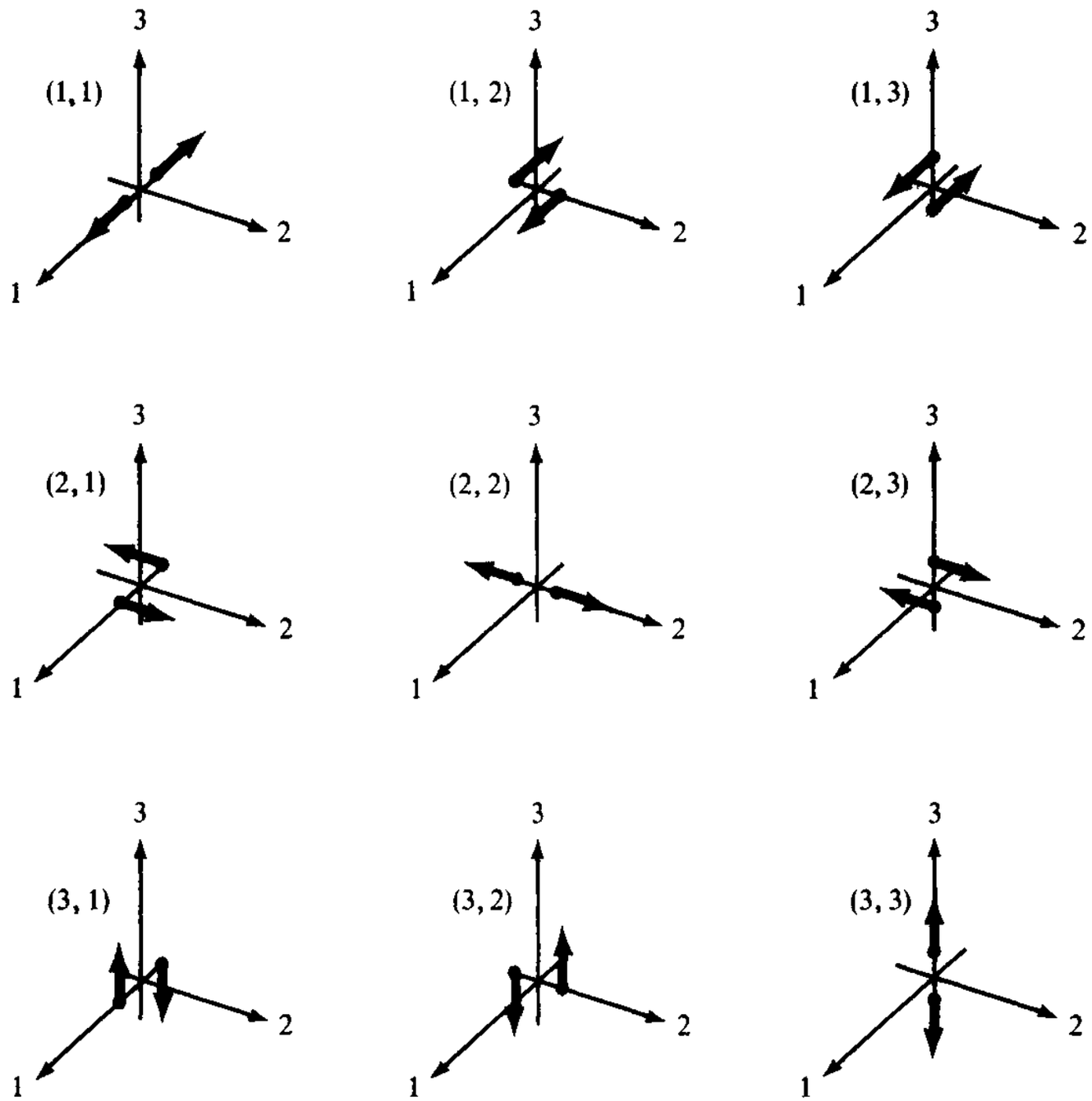

The nine possible couples that are required to obtain equivalent forces for a generally oriented displacement discontinuity in anisotropic media.

Point sources can be described by the seismic moment tensor **Mpq**, whose elements have clear physical meaning of **forces acting on particular planes**.

Moment tensor components

Figure 4.4-1: Equivalent body forces for a single force, single couple, and double couple.

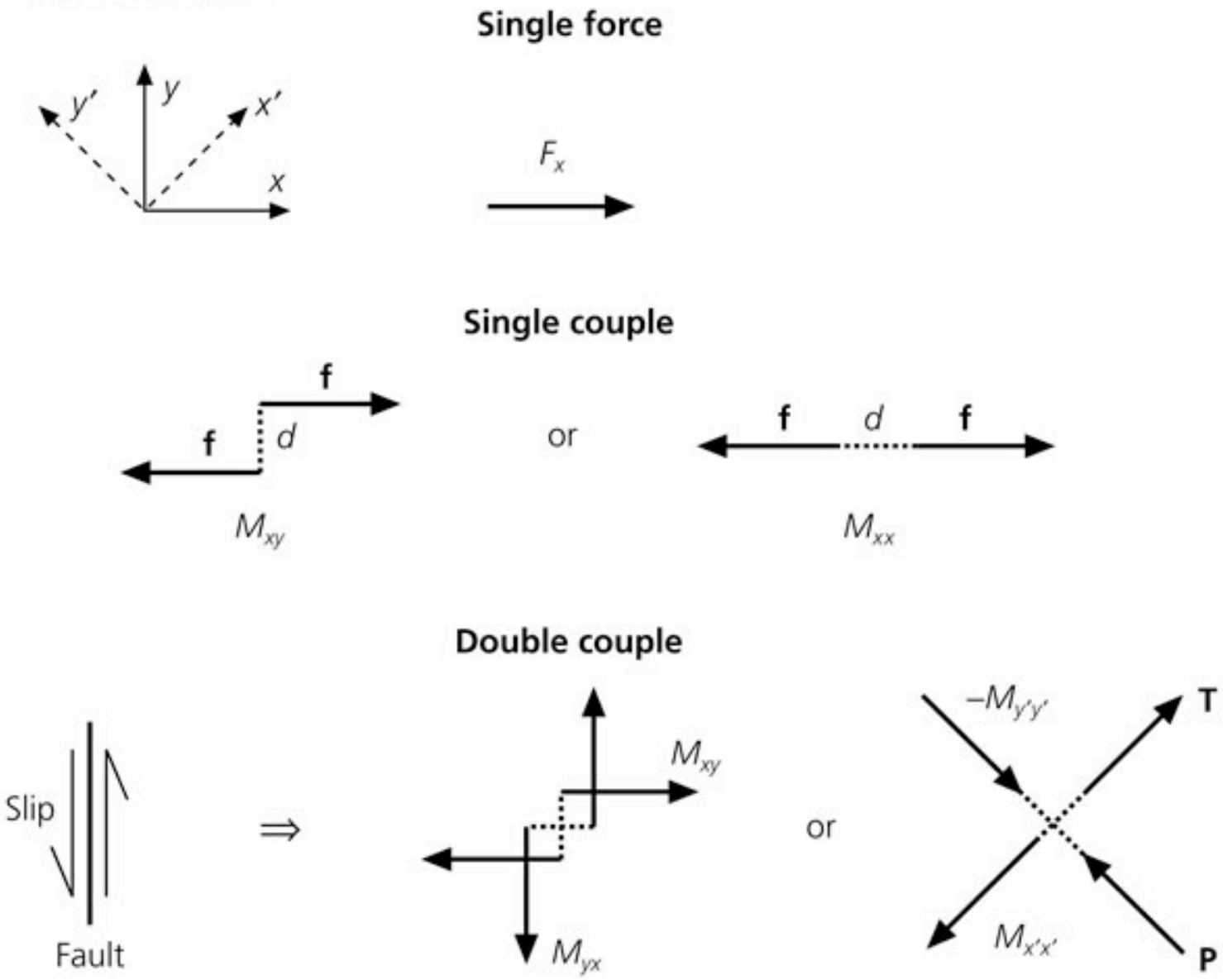

Point sources can be described by the seismic moment tensor M_{pq}, whose elements have clear physical meaning of **forces acting on particular planes**.

Angle and axis conventions

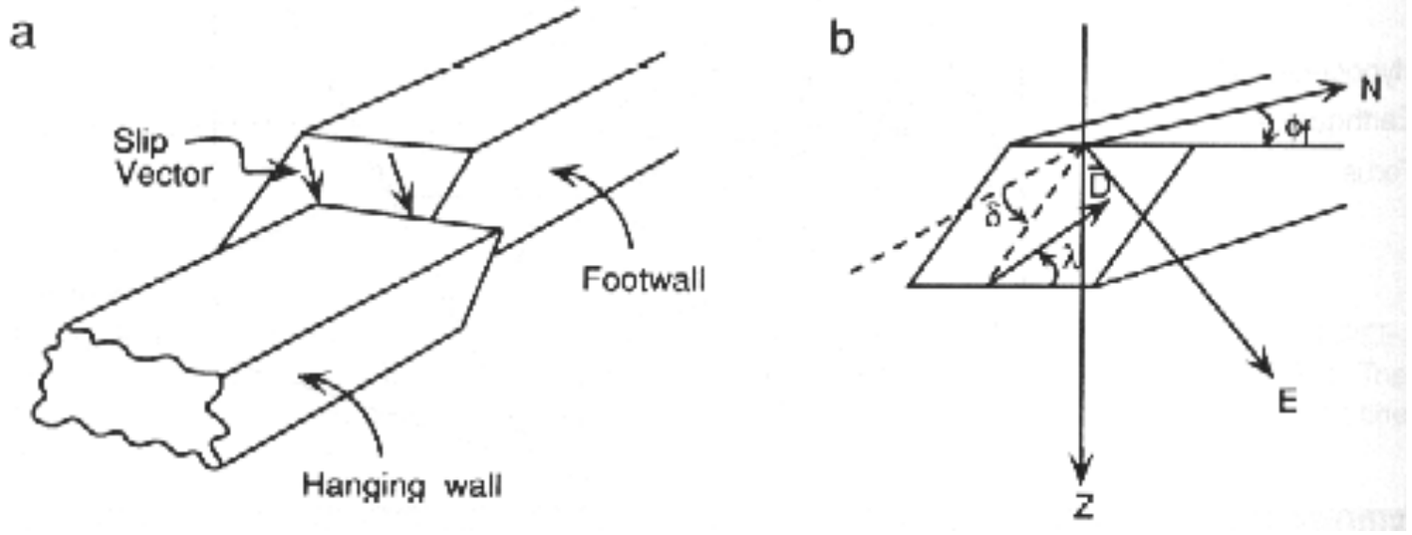

Convention for naming blocks, fault plane, and slip vector, i.e. strike, dip and rake

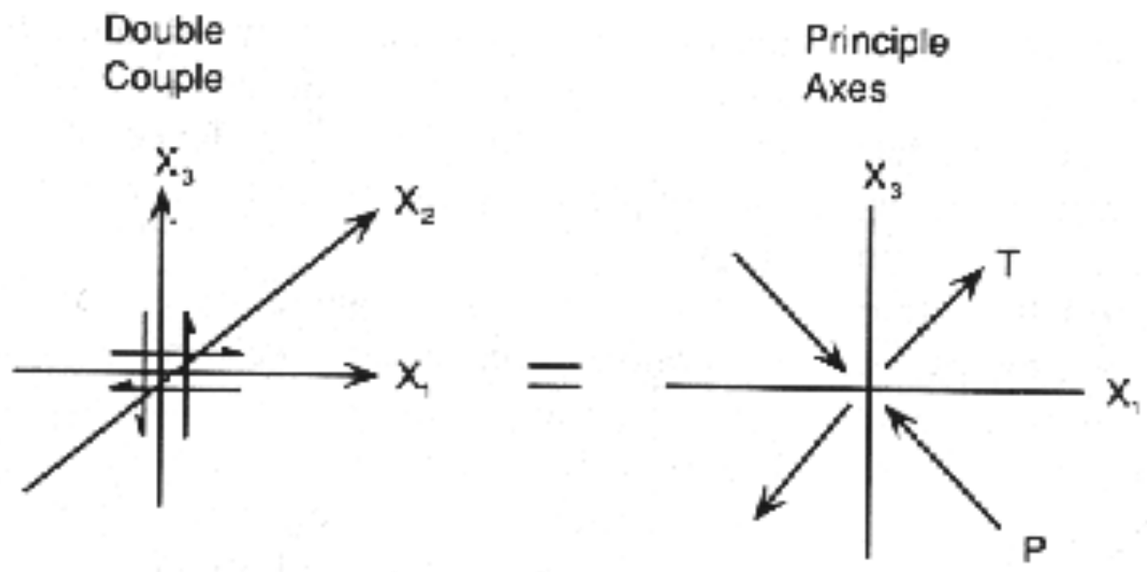

Force system or a double couple in the xz-plane

T and P axes are the directions of maximum positive or negative first break.

Moment tensor and fault vectors

The orthogonal eigenvectors to the above eigenvalues give the directions of the principal axes: **b**, corresponding to eigenvalue 0, gives the **null-axis**, **t**, corresponding to the positive eigenvalue, gives the **tension axis** (T) and **p** gives the **pressure axis** (P) of the tensor.

They are related to the **u** and **v** vector, defining respectively the slip vector and the fault plane:

$$\begin{cases} \mathbf{t} = \frac{1}{\sqrt{2}}(\mathbf{v} + \mathbf{u}) \\ \mathbf{b} = (\mathbf{v} \times \mathbf{u}) \\ \mathbf{p} = \frac{1}{\sqrt{2}}(\mathbf{v} - \mathbf{u}) \end{cases} \qquad \begin{cases} \mathbf{u} = \frac{1}{\sqrt{2}}(\mathbf{t} + \mathbf{p}); \frac{1}{\sqrt{2}}(\mathbf{t} - \mathbf{p}) \\ \mathbf{v} = \frac{1}{\sqrt{2}}(\mathbf{t} - \mathbf{p}); \frac{1}{\sqrt{2}}(\mathbf{t} + \mathbf{p}) \end{cases}$$

Moment tensor and fault plane solution

$$\mathbf{u}=\begin{cases}[\bar{u}]\left(\cos\lambda\cos\phi+\cos\delta\sin\lambda\sin\phi\right)\hat{\mathbf{e}}_x\\ [\bar{u}]\left(\cos\lambda\sin\phi-\cos\delta\sin\lambda\cos\phi\right)\hat{\mathbf{e}}_y\\ [\bar{u}]\left(-\sin\delta\sin\lambda\right)\hat{\mathbf{e}}_z\end{cases}\qquad \boldsymbol{\nu}=\begin{cases}\left(-\sin\delta\sin\phi\right)\hat{\mathbf{e}}_x\\ \left(-\sin\delta\cos\phi\right)\hat{\mathbf{e}}_y\\ \left(-\cos\delta\right)\hat{\mathbf{e}}_z\end{cases}$$

Figure 4.2-2: Fault geometry used in earthquake studies.

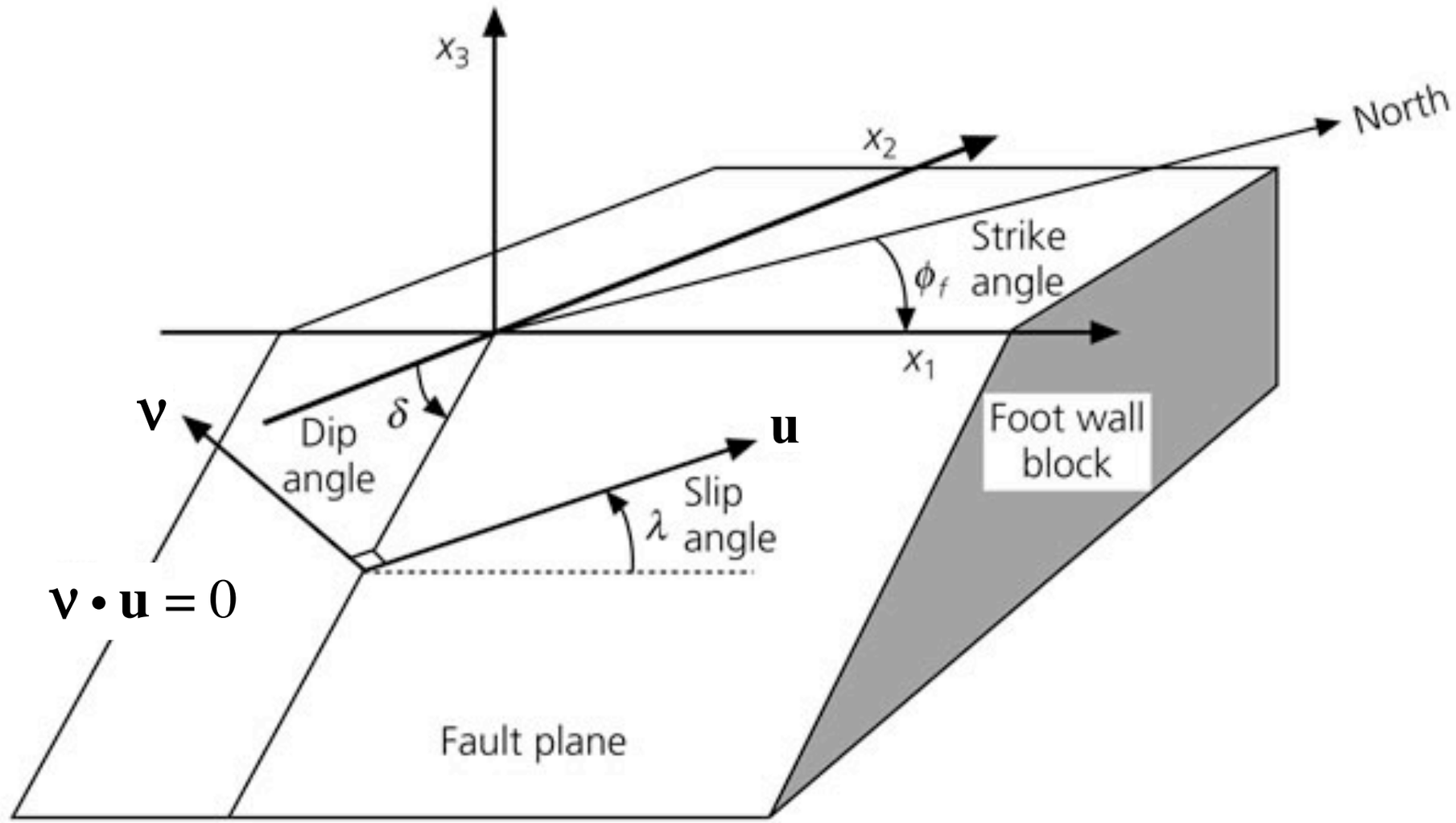

Moment tensor and fault plane solution

The slip vector and the fault normal can be expresses in terms of strike (φ), dip (δ) and rake(λ):

$$\mathbf{u}=\begin{cases} [\bar{u}]\left(\cos\lambda\cos\phi+\cos\delta\sin\lambda\sin\phi\right)\hat{\mathbf{e}}_x \\ [\bar{u}]\left(\cos\lambda\sin\phi-\cos\delta\sin\lambda\cos\phi\right)\hat{\mathbf{e}}_y \\ [\bar{u}]\left(-\sin\delta\sin\lambda\right)\hat{\mathbf{e}}_z \end{cases} \qquad \boldsymbol{\nu}=\begin{cases} \left(-\sin\delta\sin\phi\right)\hat{\mathbf{e}}_x \\ \left(-\sin\delta\cos\phi\right)\hat{\mathbf{e}}_y \\ \left(-\cos\delta\right)\hat{\mathbf{e}}_z \end{cases}$$

Then the Cartesian components of the simmetric moment tensor can be written as:

$$M_{xx} = -M_0\left(\sin\delta\cos\lambda\sin 2\phi+\sin 2\delta\sin\lambda\sin^2\phi\right) \qquad M_{xy} = M_0\left(\sin\delta\cos\lambda\sin 2\phi+0.5\sin 2\delta\sin\lambda\sin 2\phi\right)$$

$$M_{yy} = M_0\left(\sin\delta\cos\lambda\sin 2\phi-\sin 2\delta\sin\lambda\cos^2\phi\right) \qquad M_{xz} = -M_0\left(\cos\delta\cos\lambda\cos\phi+\cos 2\delta\sin\lambda\sin\phi\right)$$

$$M_{zz} = M_0\left(\sin 2\delta\sin\lambda\right) \qquad M_{yz} = -M_0\left(\cos\delta\cos\lambda\sin\phi-\cos 2\delta\sin\lambda\cos\phi\right)$$

GF for double couple

An important case to consider in detail is the radiation pattern expected when the source is a double-couple. The result for a moment time function $M_0(t)$ is:

$$u=\frac{A^{NF}}{4\pi\rho|x|^4}\int_{|x|/\alpha}^{|x|/\beta}\tau M_0(t-\tau)d\tau+$$

$$+\frac{A_P^{IF}}{4\pi\rho\alpha^2|x|^2}M_0\left(t-\frac{|x|}{\alpha}\right)-\frac{A_S^{IF}}{4\pi\rho\beta^2|x|^2}M_0\left(t-\frac{|x|}{\beta}\right)+$$

$$+\frac{A_P^{FF}}{4\pi\rho\alpha^3|x|}\dot{M}_0\left(t-\frac{|x|}{\alpha}\right)-\frac{A_S^{FF}}{4\pi\rho\beta^3|x|}\dot{M}_0\left(t-\frac{|x|}{\beta}\right)$$

$$A^{NF}=9\sin2\theta\cos\phi\hat{r}-6\left(\cos2\theta\cos\phi\hat{\theta}-\cos\theta\sin\phi\hat{\phi}\right)$$

Near field term

$$A_P^{IF}=4\sin2\theta\cos\phi\hat{r}-2\left(\cos2\theta\cos\phi\hat{\theta}-\cos\theta\sin\phi\hat{\phi}\right)$$

$$A_S^{IF}=-3\sin2\theta\cos\phi\hat{r}+3\left(\cos2\theta\cos\phi\hat{\theta}-\cos\theta\sin\phi\hat{\phi}\right)$$

Intermediate field term

$$A_P^{FF}=\sin2\theta\cos\phi\hat{r}$$

$$A_S^{FF}=\cos2\theta\cos\phi\hat{\theta}-\cos\theta\sin\phi\hat{\phi}$$

Far field term

NF DC (static) Radiation pattern

The static final displacement for a shear dislocation of strength M_0 is:

$$u = \frac{M_0(\infty)}{4\pi\rho|\mathbf{x}|^2}\left[A^{NF}\left(\frac{1}{2\beta^2}-\frac{1}{2\alpha^2}\right)+\frac{A_P^{IF}}{\alpha^2}+\frac{A_S^{IF}}{\beta^2}\right]=$$

$$=\frac{M_0(\infty)}{4\pi\rho|\mathbf{x}|^2}\left[\left(\frac{3}{2\beta^2}-\frac{1}{2\alpha^2}\right)\sin 2\theta\cos\phi\,\hat{\mathbf{r}}+\frac{1}{\alpha^2}\left(\cos 2\theta\cos\phi\,\hat{\boldsymbol{\theta}}-\cos\theta\sin\phi\,\hat{\boldsymbol{\phi}}\right)\right]$$

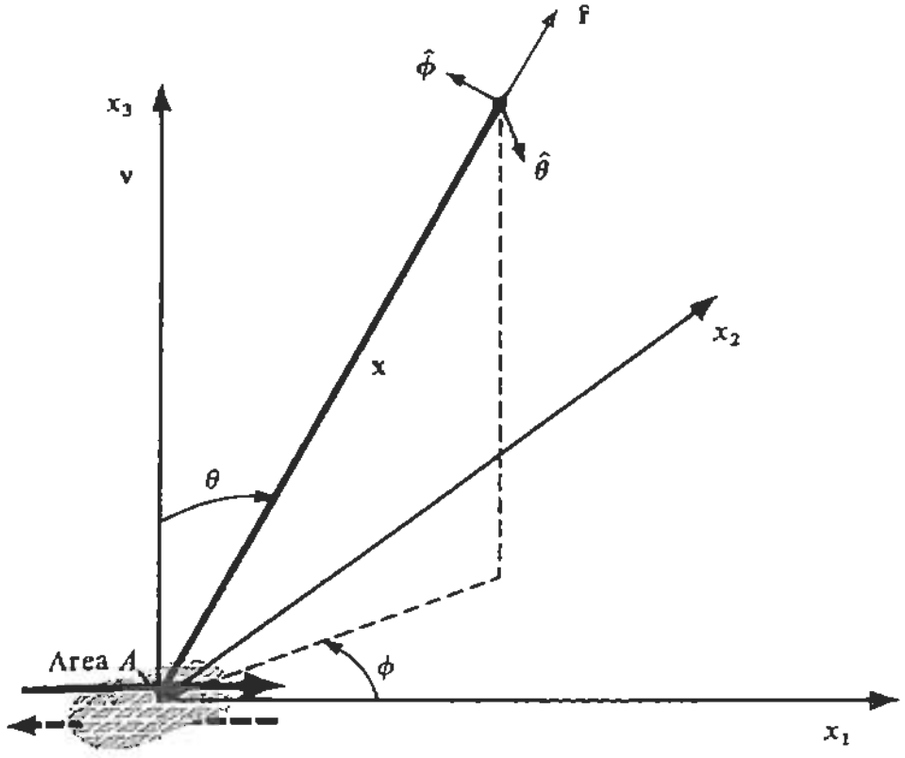

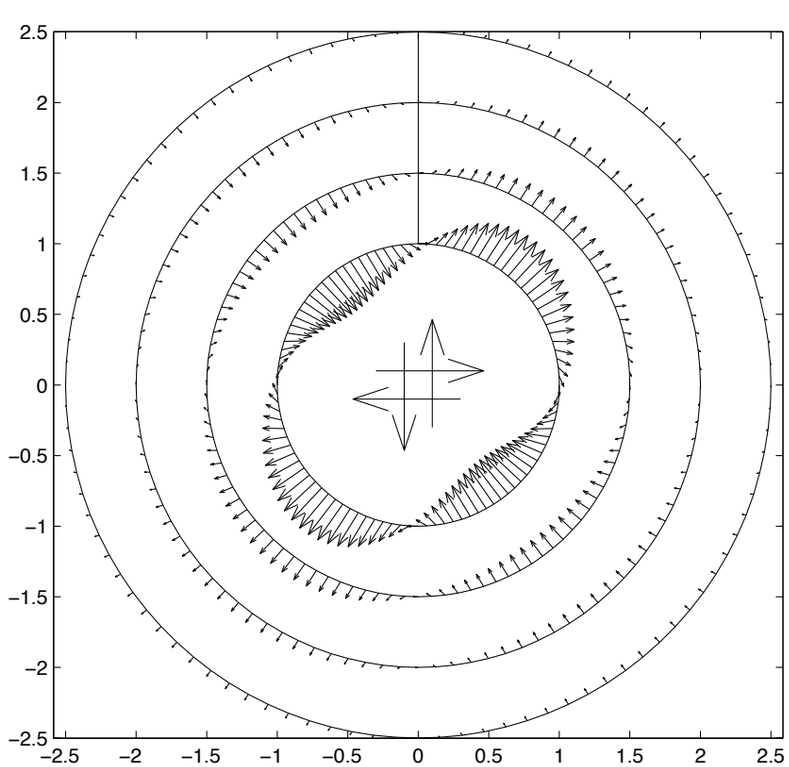

Figure 7: Near-field Static Displacement Field From a Point Double Couple Source ($\phi = 0$ plane); $\alpha = 3^{1/2}$, $\beta = 1$, $r = 0.1,\ 0.15,\ 0.20,\ 0.25$, $\rho = 1/4\pi$, $M_\infty = 1$; self-scaled displacements

Coseismic deformation

L'Aquila (Italy) earthquake, Mw 6.3.
Horizontal and Vertical surface displacement from InSAR Data
(assuming horizontal displacement is perpendicular to the fault strike ~N48W).

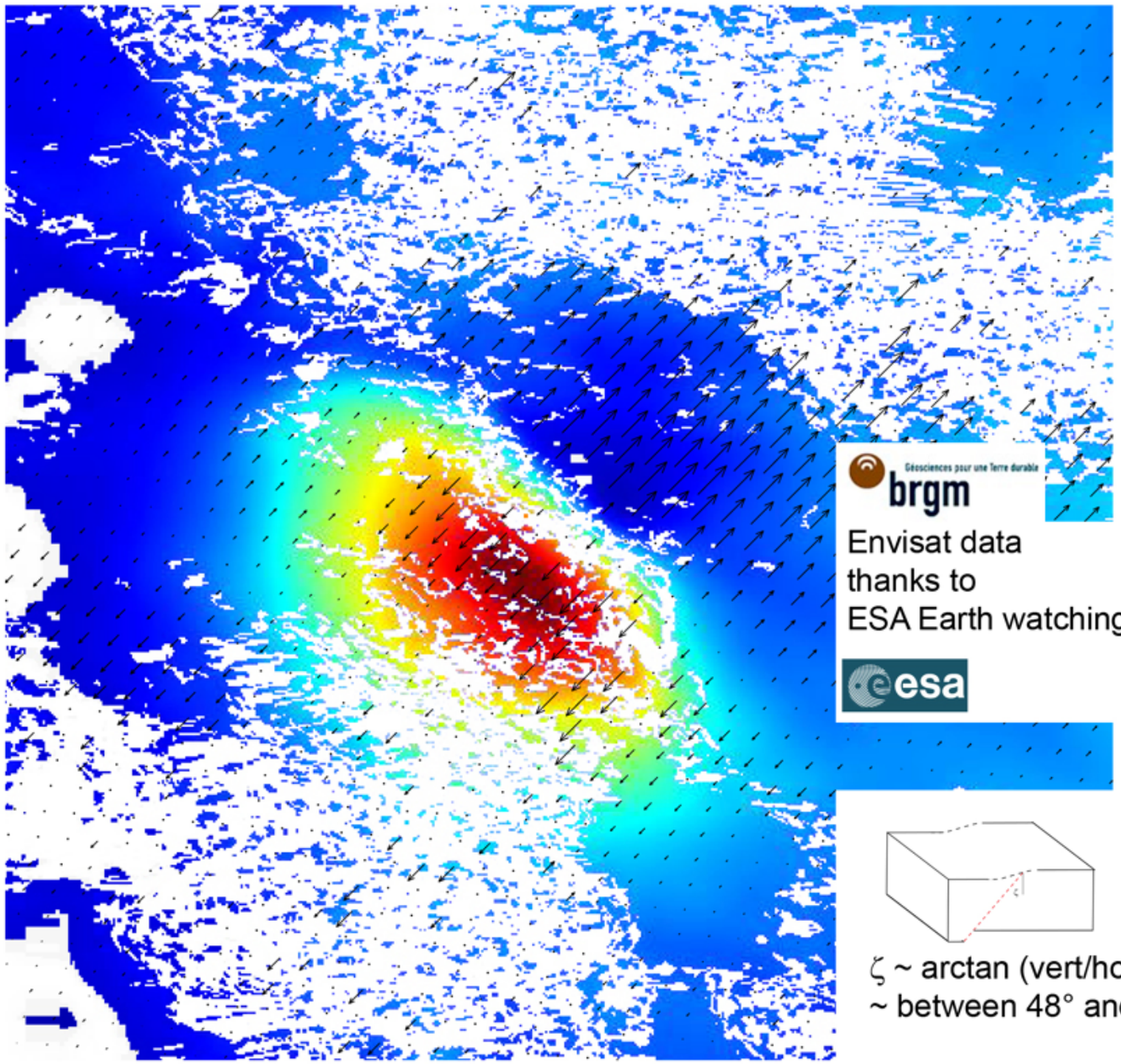

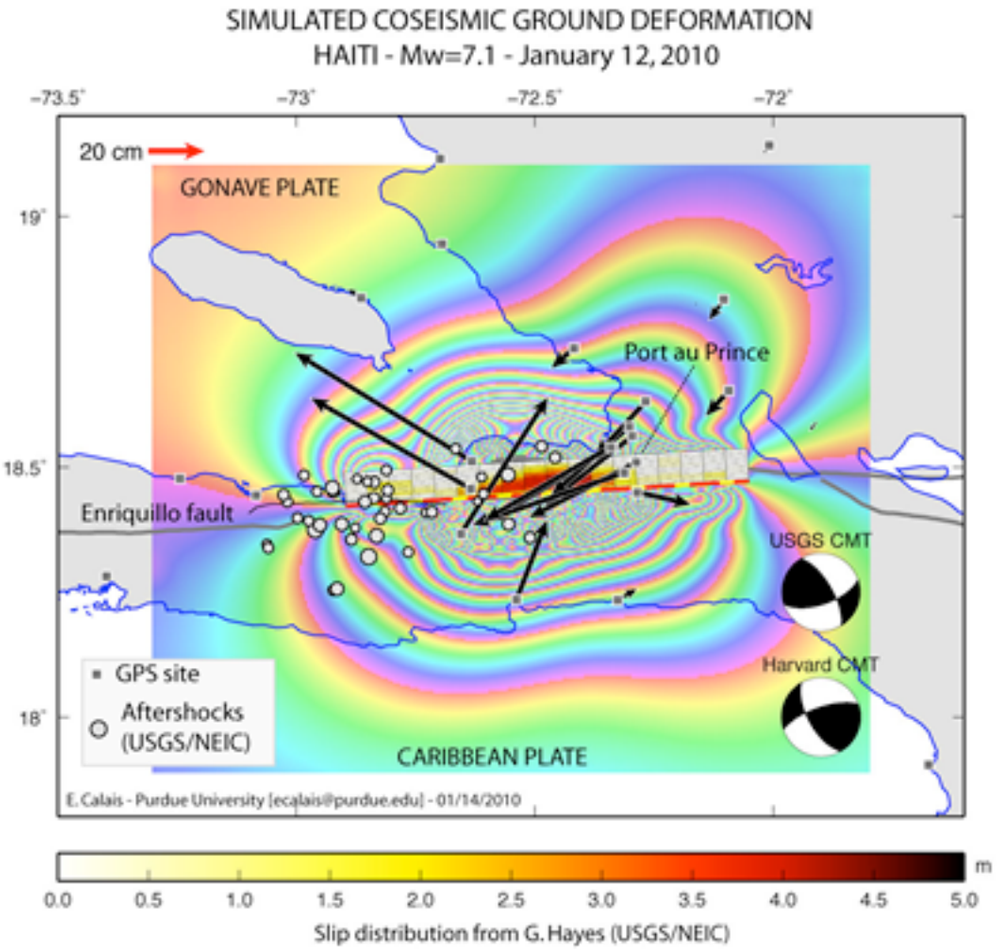

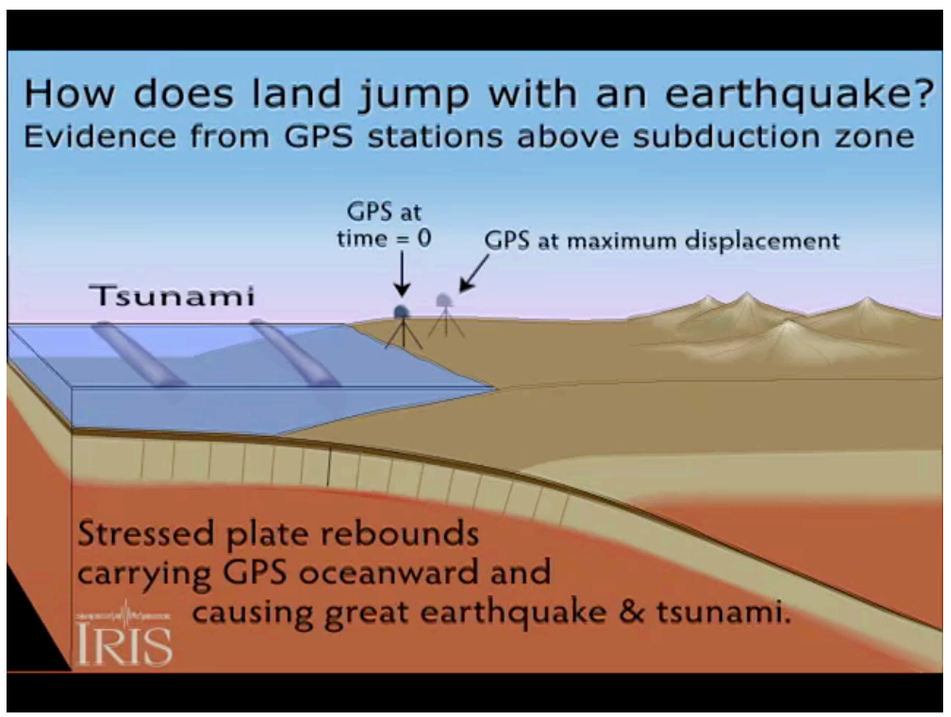

Co- & Post- seismic: Tohoku-oki

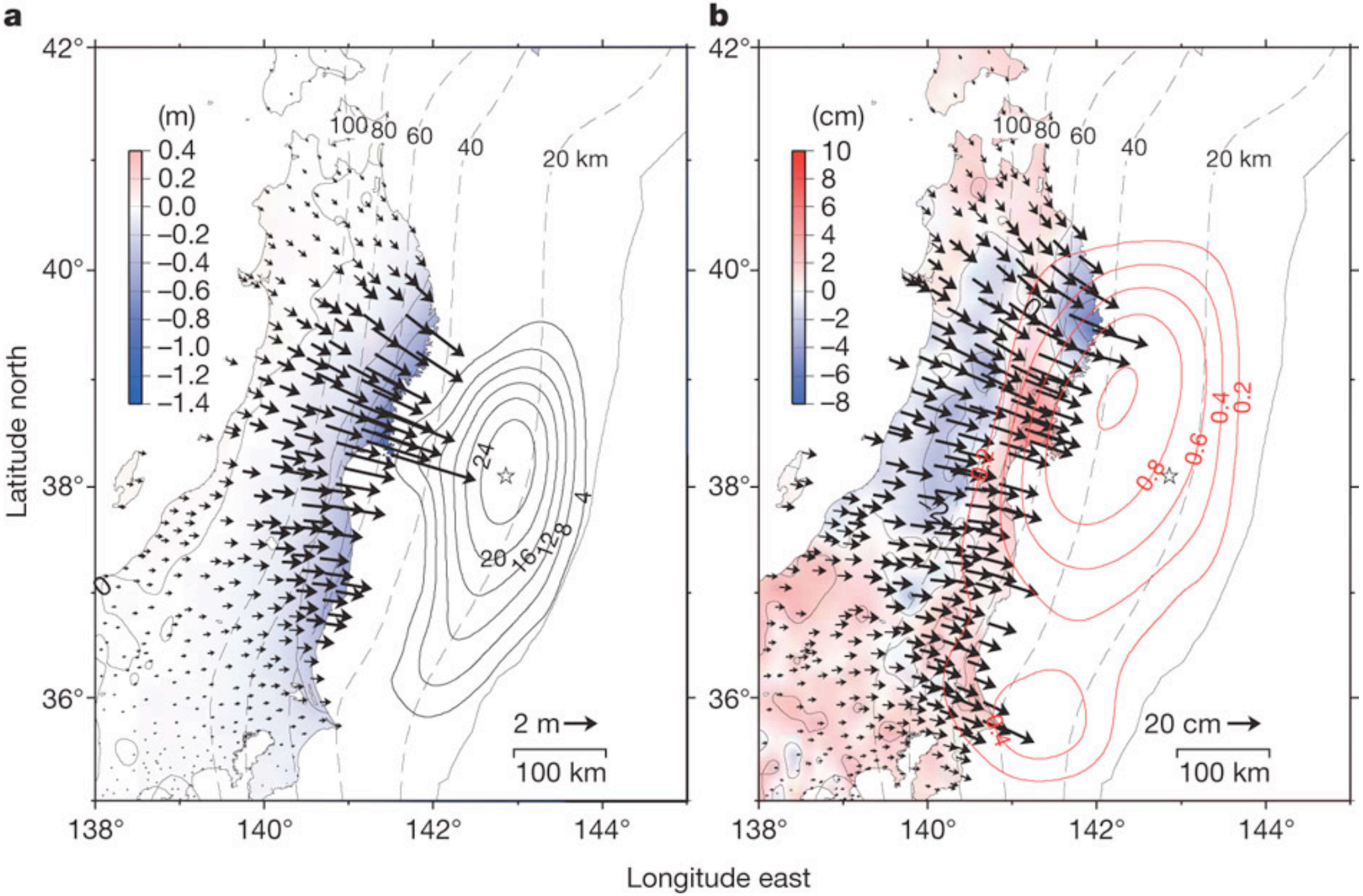

a, Coseismic displacements for 10–11 March 2011, relative to the Fukue site. The black arrows indicate the horizontal coseismic movements of the GPS sites. The colour shading indicates vertical displacement. The star marks the location of the earthquake epicentre. The dotted lines indicate the isodepth contours of the plate boundary at 20-km intervals28. The solid contours show the coseismic slip distribution in metres.
b, Postseismic displacements for 12–25 March 2011, relative to the Fukue site. The red contours show the afterslip distribution in metres. All other markings represent the same as in a.

From: Ozawa et al., 2011,, Nature, 475, 373–376.

Far field for a point d-c point source

From the representation theorem we have: $u_n(x,t) = M_{pq} * G_{np,q}$

that, in the far field and in a spherical coordinate system becomes:

$$u(x,t) = \frac{1}{4\pi\rho\alpha^3}\left(\sin 2\theta \cos\phi \hat{r}\right)\frac{\dot{M}\left(t - r/\alpha\right)}{r} +$$

$$\frac{1}{4\pi\rho\beta^3}\left(\cos 2\theta \cos\phi\hat{\theta} - \cos\theta \sin\phi\hat{\phi}\right)\frac{\dot{M}\left(t - r/\beta\right)}{r}$$

and both P and S radiation fields are proportional to the time derivative of the moment function (moment rate). If the moment function is a ramp of duration τ (**rise time**), the propagating disturbance in the far-field will be a **boxcar,** with the same duration, and whose amplitude is varying depending on the radiation pattern.

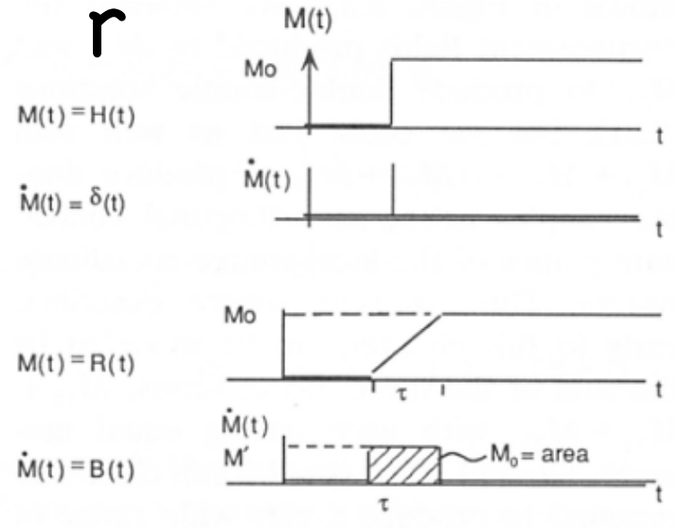

FIGURE 8.21 Far-field *P*- and *S*-wave displacements are proportional to $\dot{M}(t)$, the time derivative of the moment function $M(t) = \mu A(t)D(t)$. Simple step and ramp moment functions generate far-field impulses or boxcar ground motions.

FF DC Radiation pattern

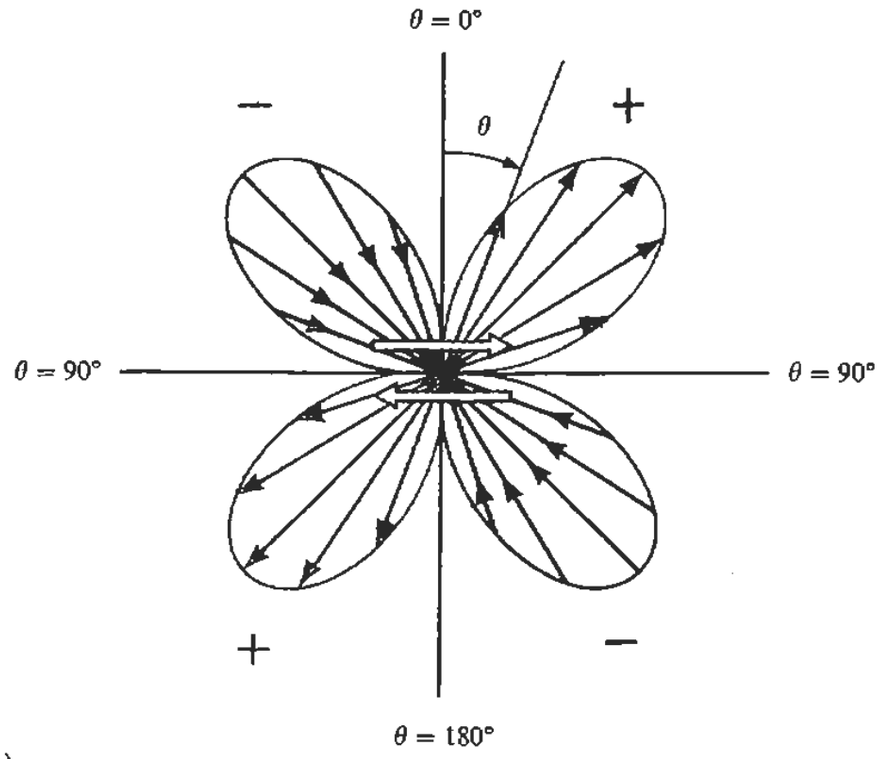

(a)

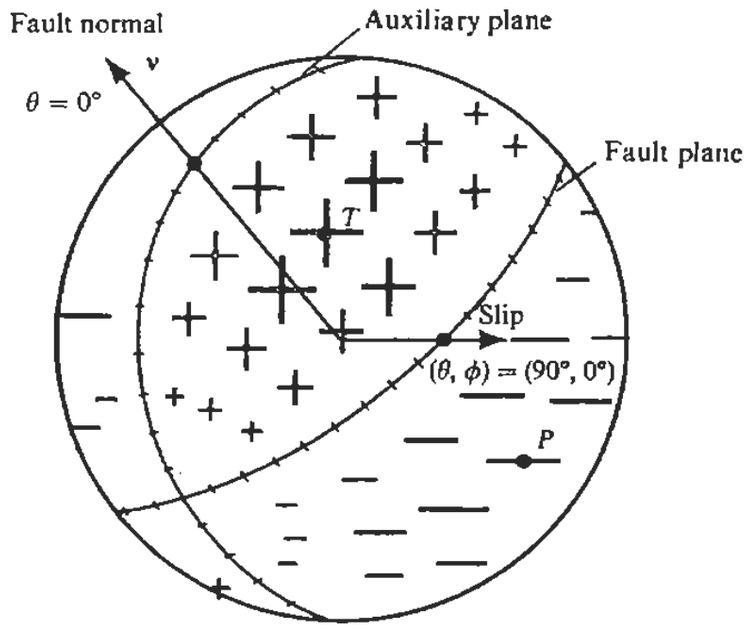

(b)

FIGURE **4.5**
Diagrams for the radiation pattern of the radial component of displacement due to a double couple, i.e., $\sin 2\theta \cos\phi\, \hat{\mathbf{r}}$. (**a**) The lobes are a locus of points having a distance from the origin that is proportional to $\sin 2\theta$. The diagram is for a plane of constant azimuth, and the pair of arrows at the center denotes the shear dislocation. Note the alternating quadrants of inward and outward directions. In terms of far-field P-wave displacement, plus signs denote outward displacement (if $\dot{M}_0(t - r/\alpha)$ is positive), and minus signs denote inward displacement. (**b**) View of the radiatiou pattern over a sphere centered on the origin. Plus and minus signs of various sizes denote variation (with θ, ϕ) of outward and inward motions. The fault plane and the auxiliary plane are nodal liues (on which $\sin 2\theta \cos\phi = 0$). An equal-area projection has been used (see Fig. 4.17). Point P marks the pressure axis, and T the tension axis.

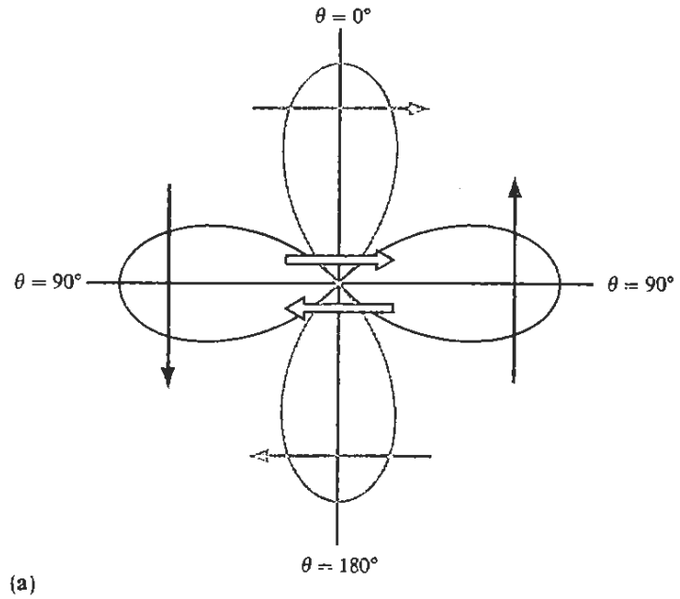

(a)

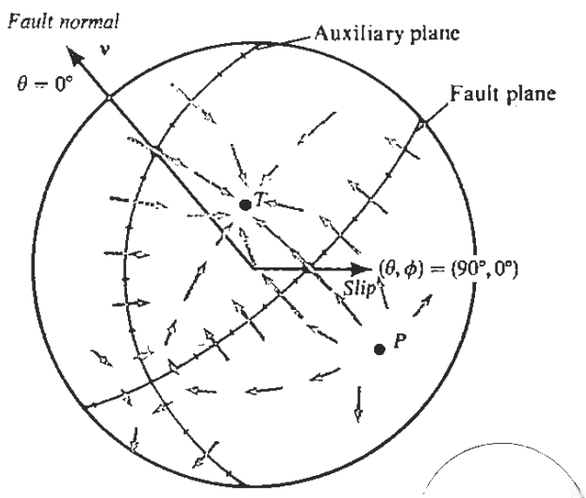

(b)

FIGURE **4.6**
Diagrams for the radiation pattern of the transverse component of displacement due to a double couple, i.e., $\cos 2\theta \cos\phi\, \hat{\theta} - \cos\theta \sin\phi\, \hat{\phi}$. (**a**) The four-lobed pattern in plane $\{\phi = 0, \phi = \pi\}$. The central pair of arrows shows the sense of shear dislocation, and arrows imposed on each lobe show the direction of particle displacement associated with the lobe. If applied to the far-field S-wave displacement, it is assumed that $\dot{M}_0(t - r/\beta)$ is positive. (**b**) Off the two planes $\theta = \pi/2$ and $\{\phi = 0, \phi = \pi\}$, the $\hat{\phi}$ component is nonzero, hence (a) is of limited use. This diagram is a view of the radiation pattern over a whole sphere centered on the origin, and arrows (with varying size and direction) in the spherical surface denote the variation (with θ, ϕ) of the transverse motions. There are no nodal lines (where there is zero motion), but nodal points do occur. Note that the nodal point for transverse motion at $(\theta, \phi) = (45°, 0)$ is a maximum in the radiation pattern for longitudinal motion (Fig. 4.5b). But the maximum transverse motion (e.g., at $\theta = 0$) occurs on a nodal line for the longitudinal motion. The stereographic projection has been used (see Fig. 4.16). It is a conformal projection, meaning that it preserves the angles at which curves intersect and the shapes of small regions, but it does not preserve relative areas.

Fault types and focal mechanisms

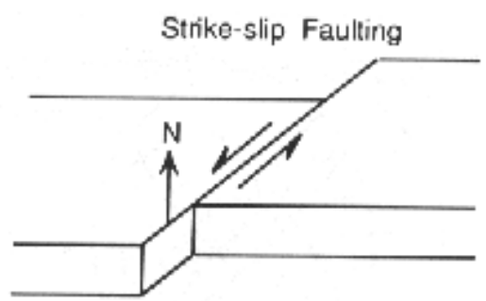

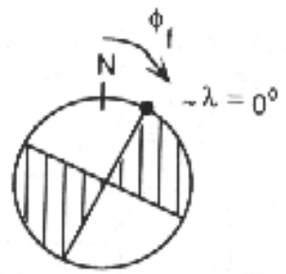

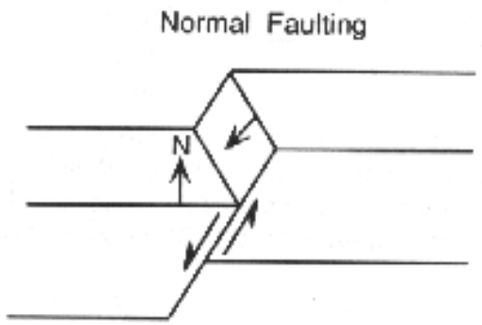

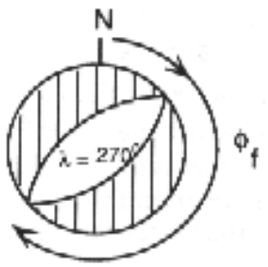

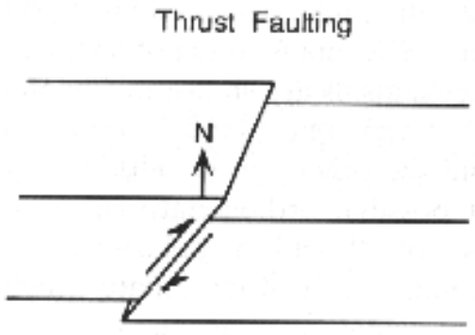

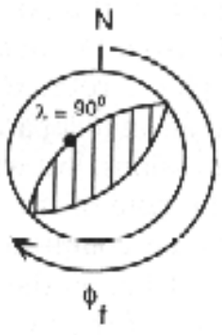

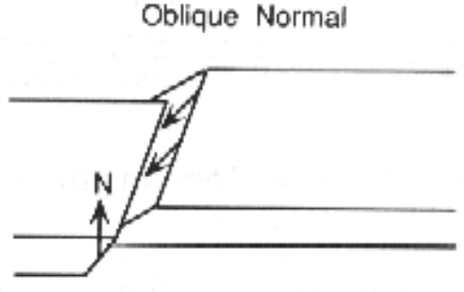

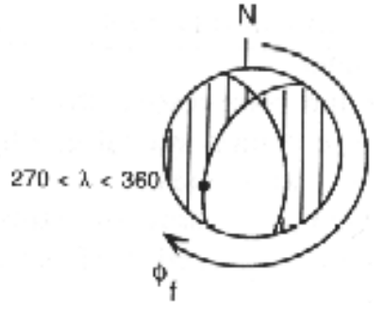

Basis fault types and their appearance in the focal mechanisms.

Dark regions indicate compressional P-wave motion.

The Principal Mechanisms

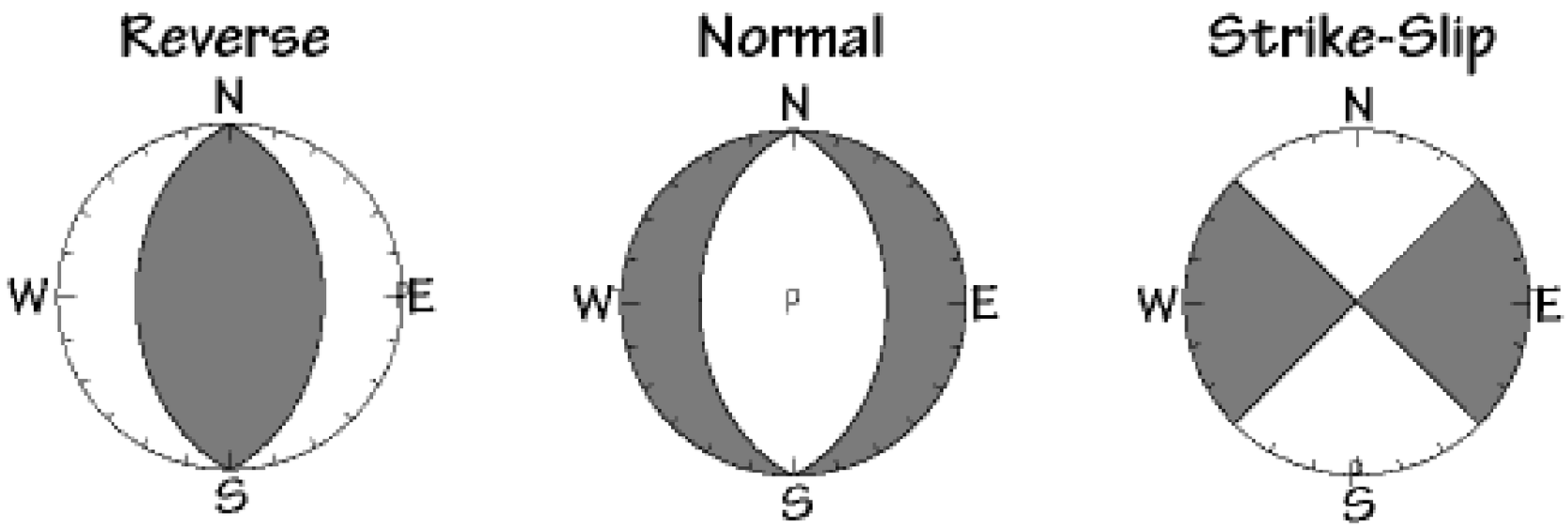

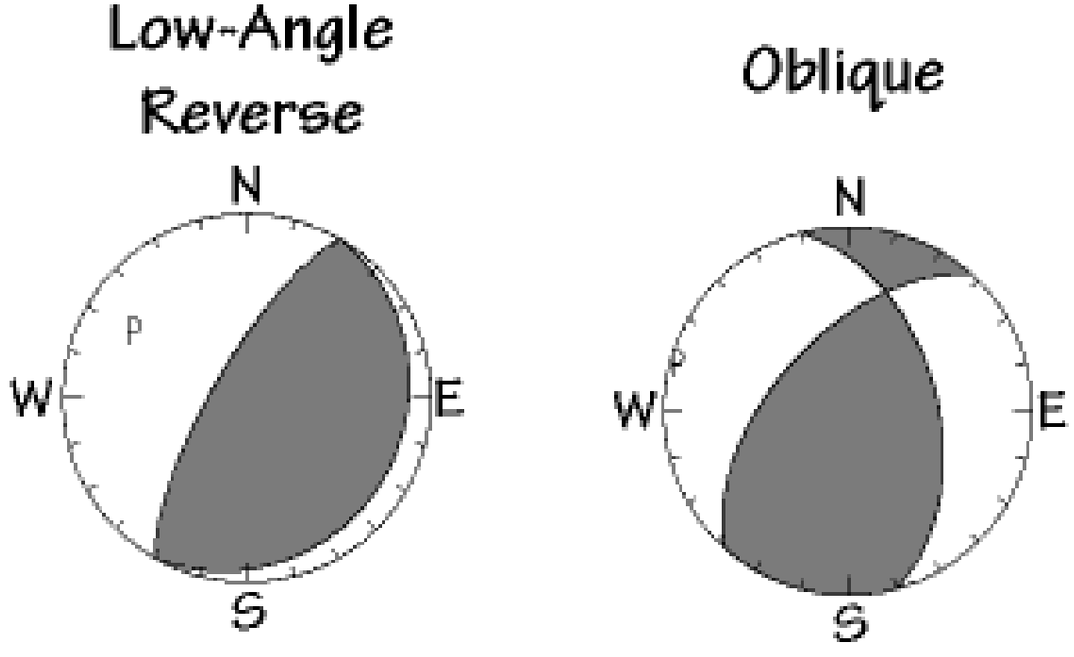

FM & stress axes

Figure 4.2-16: Relation between fault planes and stress axes.

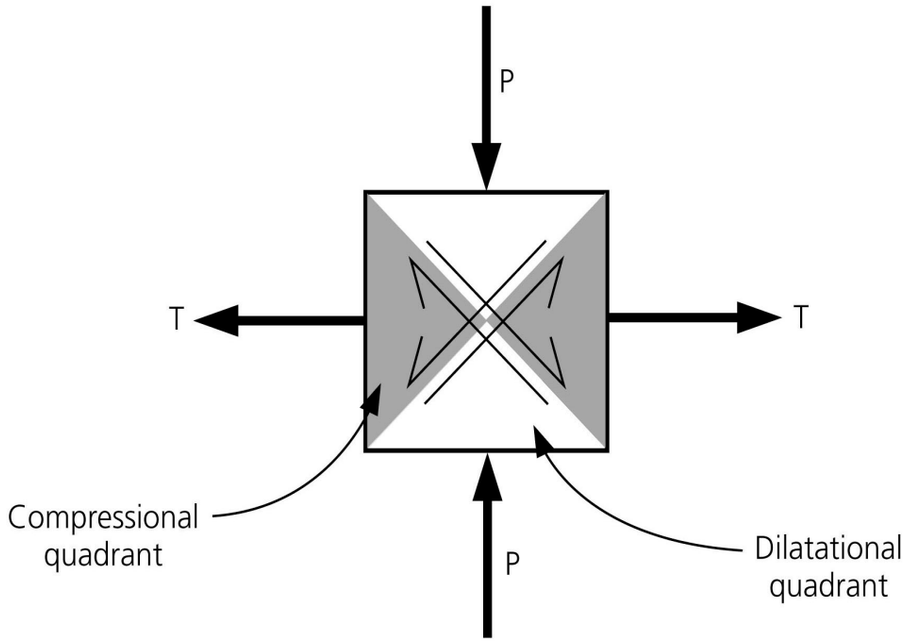

Faults

45° Dipping thrust

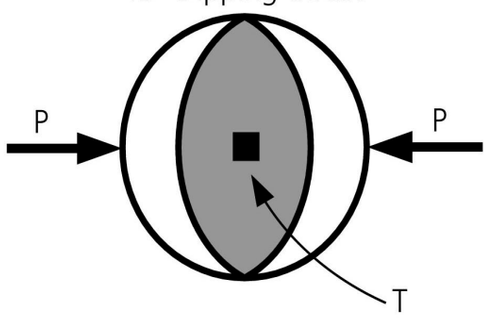

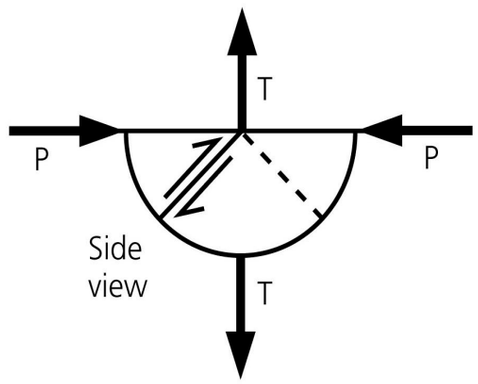

45° Dipping normal

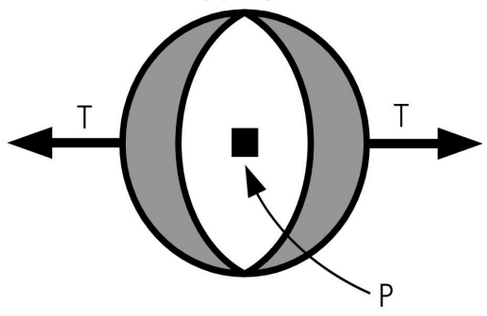

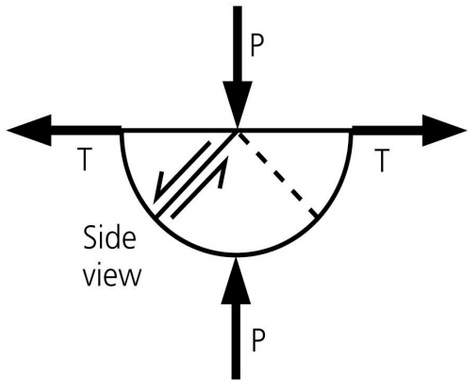

To obtain P and T axes:

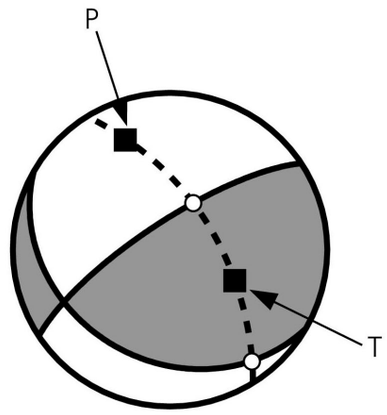

On the meridian connecting the poles, the points half-way between the nodal planes are the **P** and **T** axes

Focal Mechanisms - Examples

Figure 4.2-17: Examples of focal mechanisms and first motions.

Thrust faulting, Vanuatu Islands, July 3, 1985
Location: 17.2°S, 167.8°E. Depth: 30 km
Strike: 352°, Dip: 26°, Slip: 97°

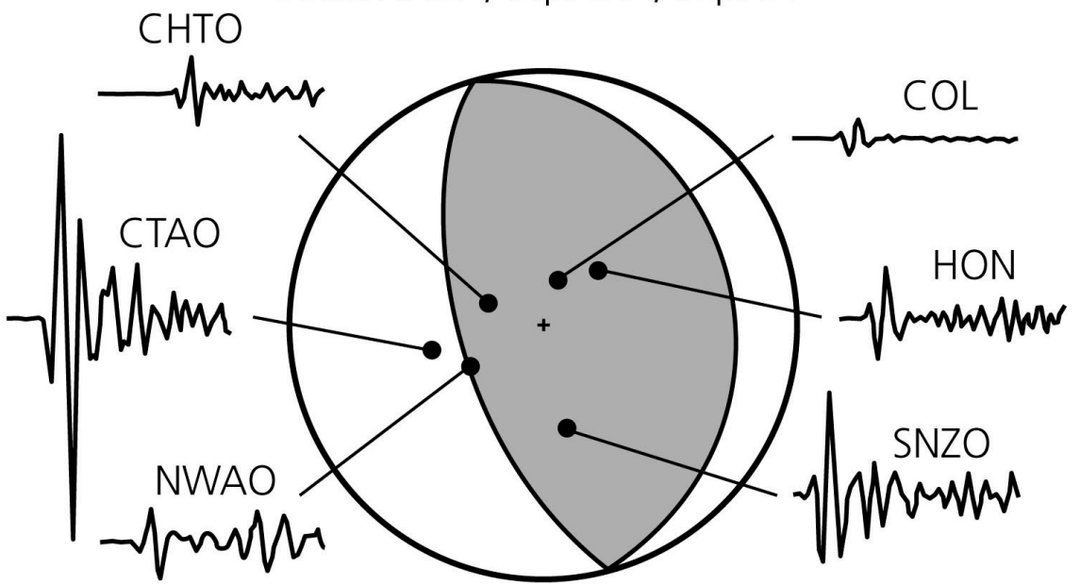

Strike-slip faulting, west of Oregon, March 13, 1985
Location: 43.5°N, 127.6°W. Depth: 10 km
Strike: 302°, Dip: 90°, Slip: 186°

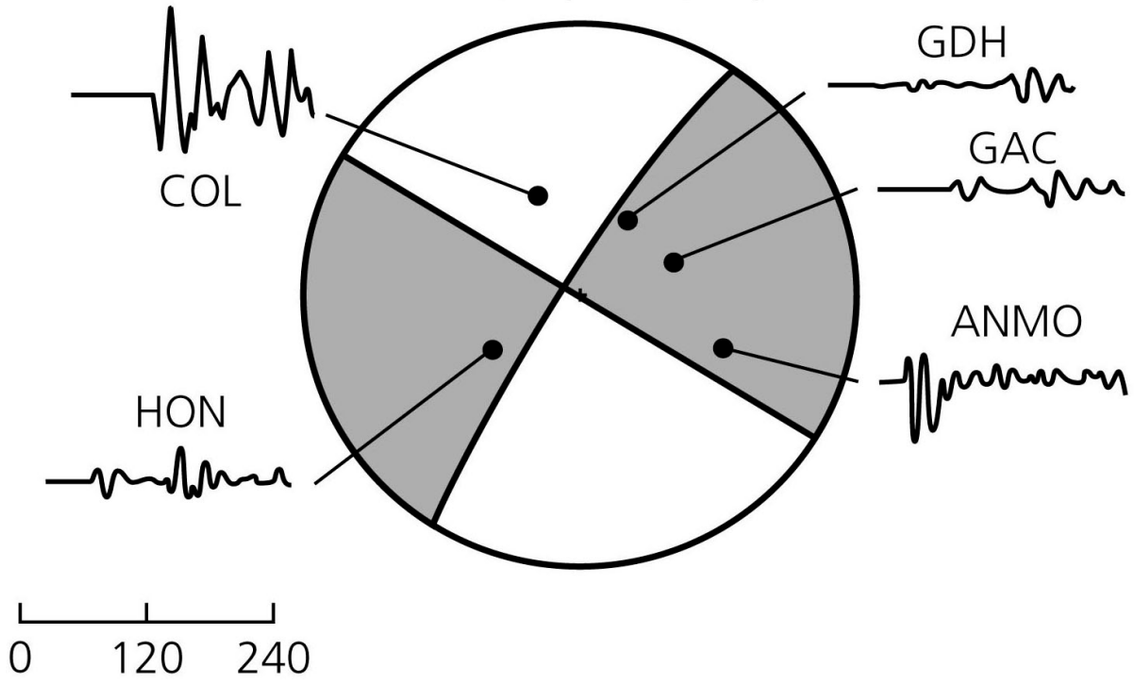

Normal faulting, mid-Indian rise, May 16, 1985
Location: 29.1°S, 77.7°E. Depth: 10 km
Strike: 8°, Dip: 70°, Slip: 270°

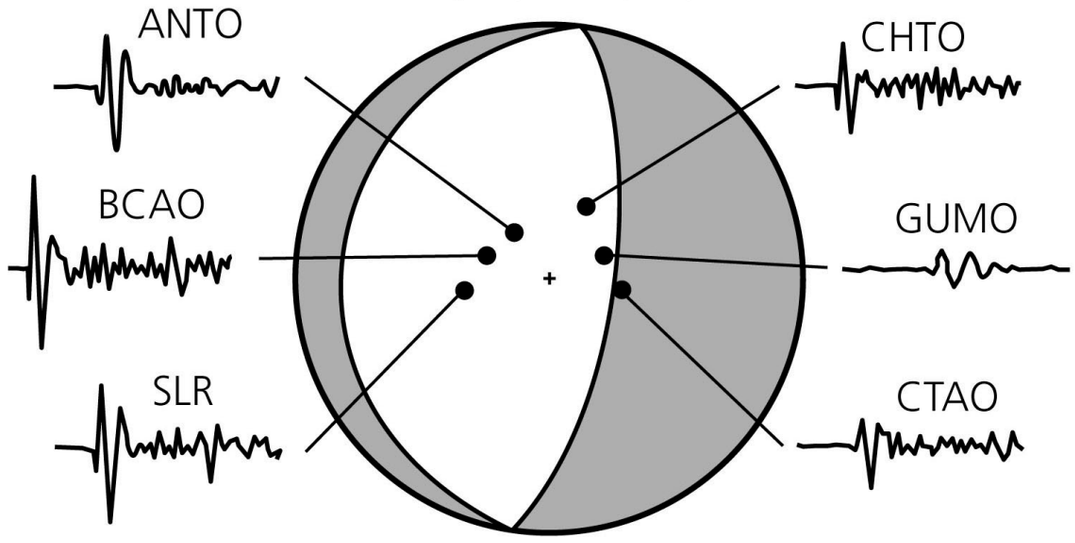

Double couple RP & surface waves

Figure 4.3-12: Surface wave amplitude radiation patterns for several focal mechanisms.

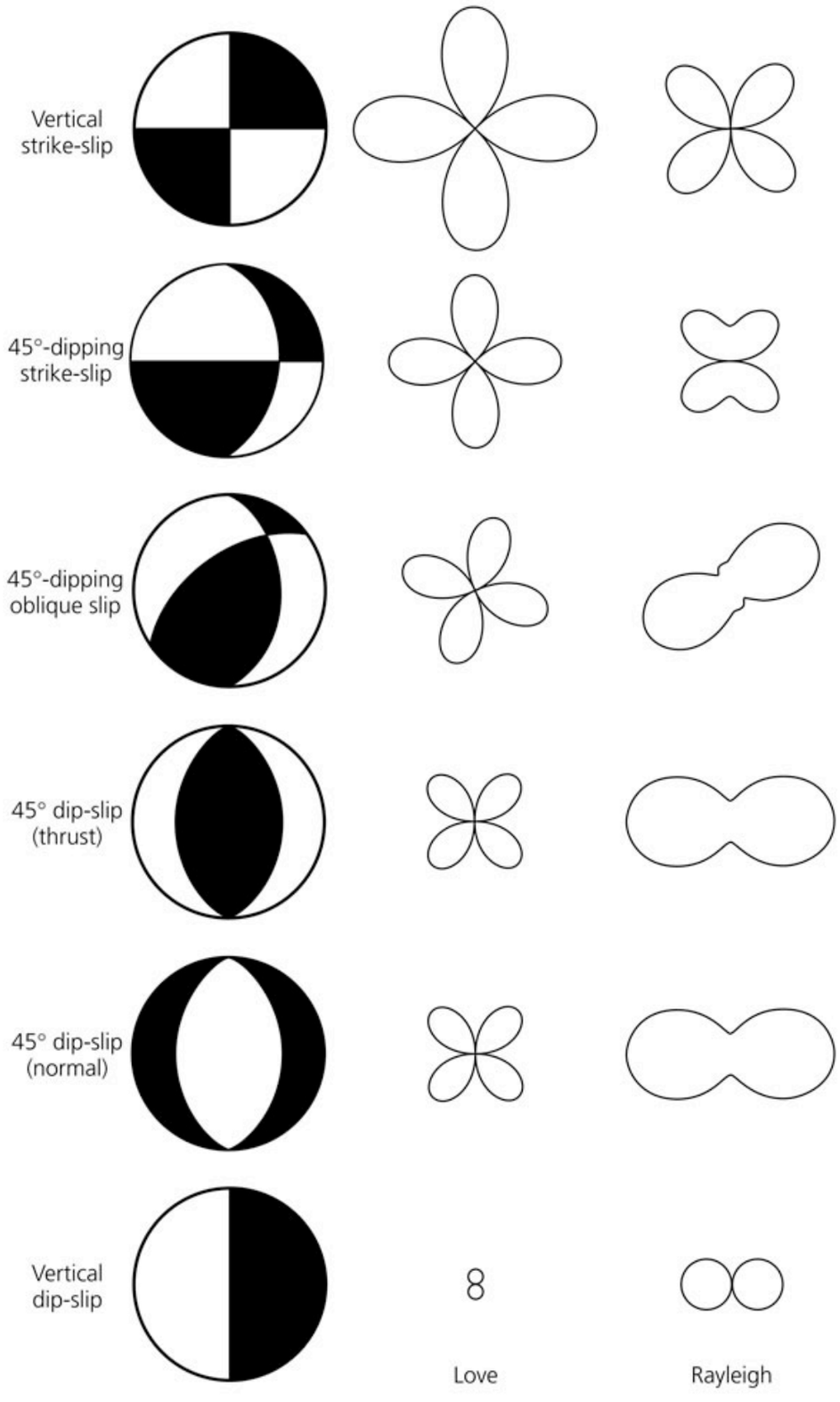

Haskell dislocation model

Haskell N. A. (1964). Total energy spectral density of elastic wave radiation from propagating faults, Bull. Seism. Soc. Am. **54**, 1811–1841

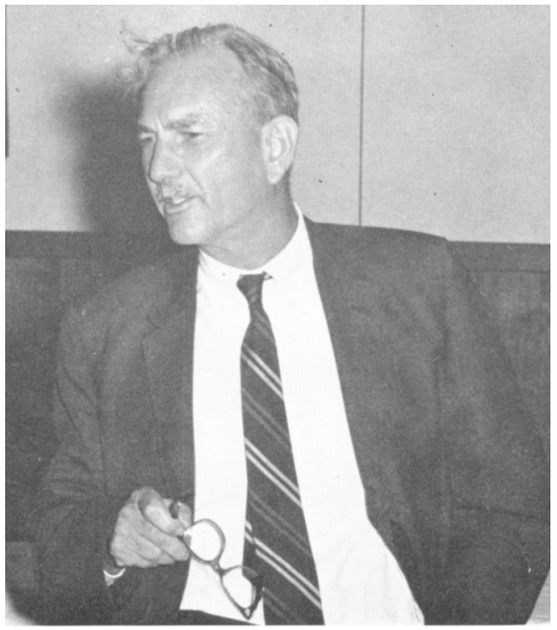

Norman A. Haskell

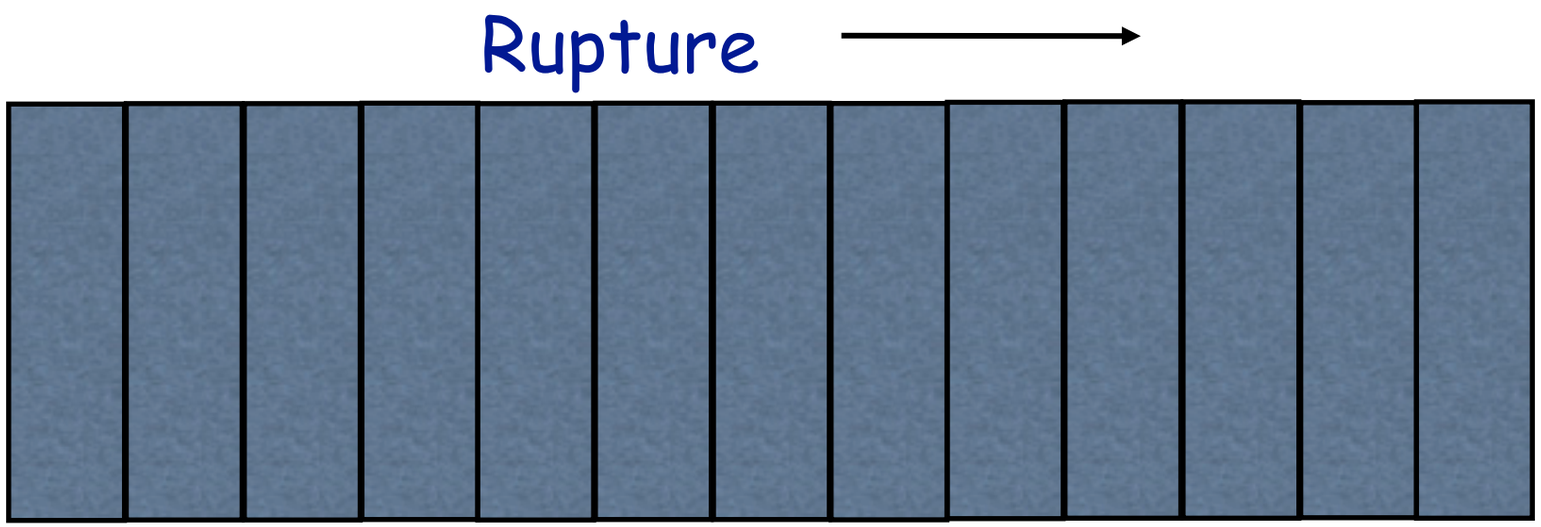

Sumatra earthquake, Dec 28, 2004

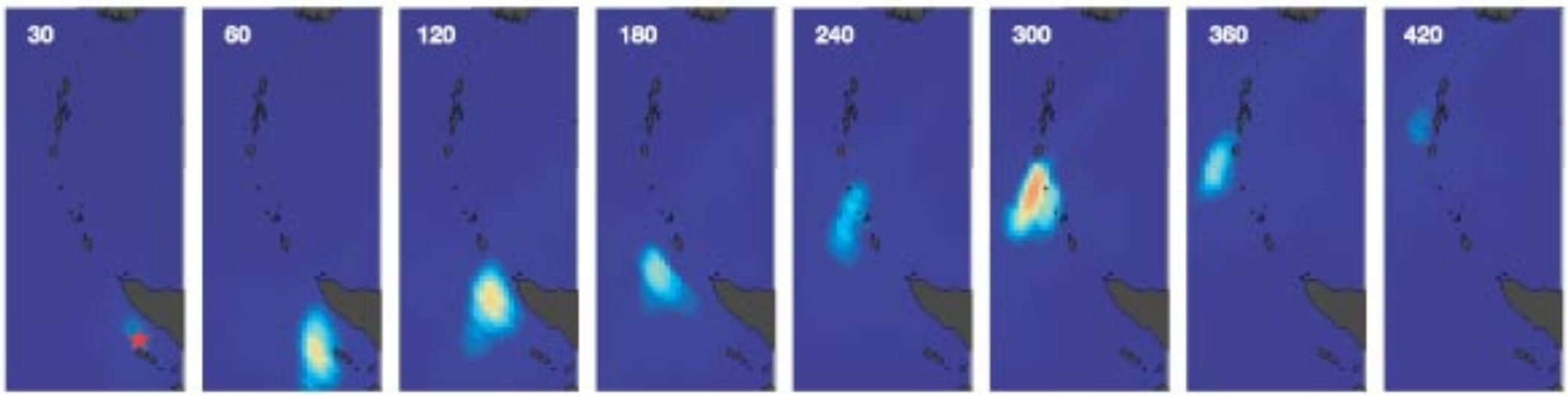

Ishii et al., Nature 2005 doi:10.1038/nature03675

Haskell source model: far field

For a single segment (point source)

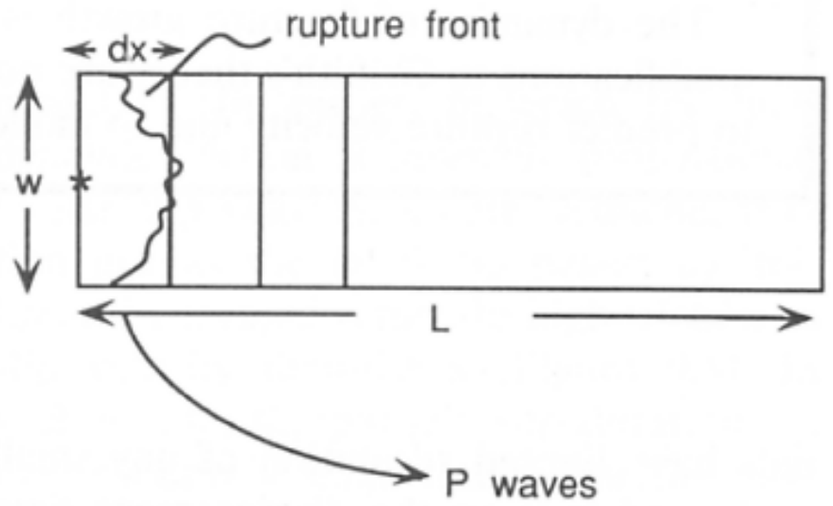

FIGURE 9.5 Geometry of a one-dimensional fault of width *w* and length *L*. The individual segments of the fault are of length *dx*, and the moment of a segment is *m dx*. The fault ruptures with velocity v_r.

$$u_r(r,t) = \sum_{i=1}^{N} u_i\left(r_i, t - r_i/\alpha - \Delta t_i\right) =$$

$$= \frac{R_i^P \mu}{4\pi\rho\alpha^3} W \sum_{i=1}^{N} \frac{\dot{D}_i}{r_i}\left(t - \Delta t_i\right)dx \approx$$

$$\approx \frac{R_i^P \mu}{4\pi\rho\alpha^3} \frac{W}{r} \sum_{i=1}^{N} \dot{D}(t) * \delta\left(t - \frac{x}{v_r}\right)dx \approx$$

$$\approx \frac{R_i^P \mu}{4\pi\rho\alpha^3} \frac{W}{r} \dot{D}(t) * \int_0^L \delta\left(t - \frac{x}{v_r}\right)dx =$$

$$= \frac{R_i^P \mu}{4\pi\rho\alpha^3} \frac{W}{r} v_r \dot{D}(t) * B(t; T_r)$$

Haskell source model: far field

$$u_r(r,t) \propto \dot{D}(t) * v_r H(z)\Big|_{t-x/v_r}^{t} = v_r \dot{D}(t) * B(t;T_r)$$

resulting in the convolution of two boxcars: the first with duration equal to the rise time and the second with duration equal to the **rupture time** (L/v_r)

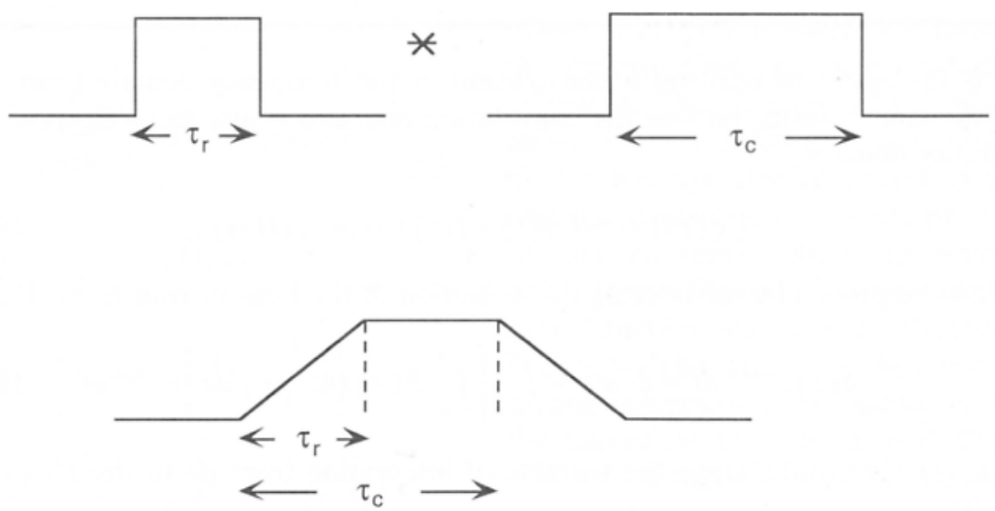

FIGURE 9.6 The convolution of two boxcars, one of length τ_r and the other of length τ_c ($\tau_c > \tau_r$). The result is a trapezoid with a rise time of τ_r, a top of length $\tau_c - \tau_r$, and a fall of width τ_r.

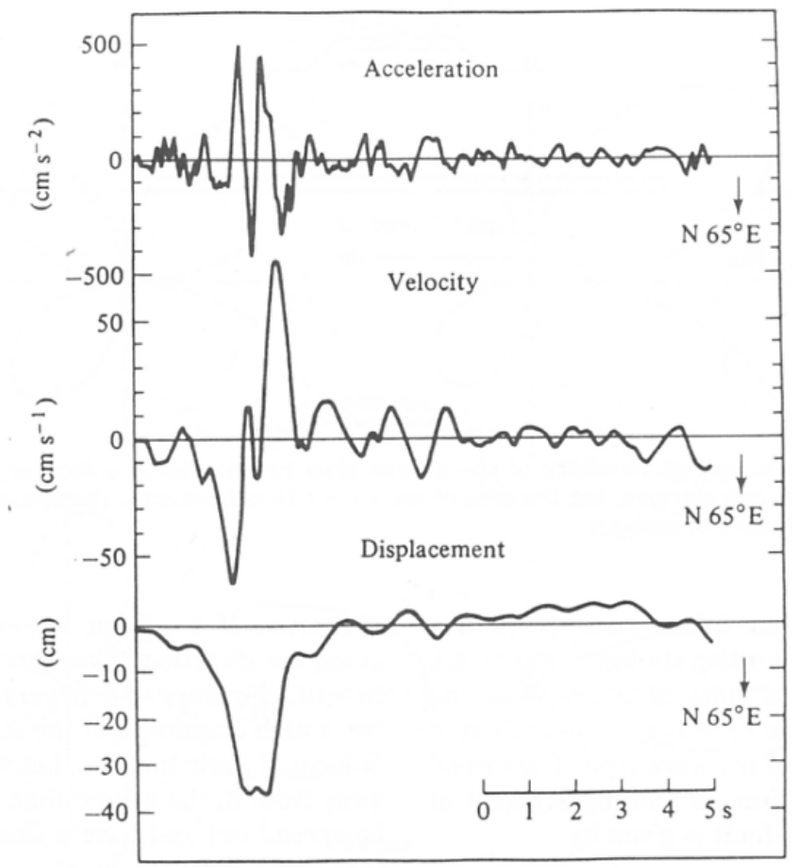

FIGURE 9.7 A recording of the ground motion near the epicenter of an earthquake at Parkfield, California. The station is located on a node for *P* waves and a maximum for *SH*. The displacement pulse is the *SH* wave. Note the trapezoidal shape. (From Aki, *J. Geophys. Res.* 73, 5359–5375, 1968; © copyright by the American Geophysical Union.)

Haskell source model: directivity

The body waves generated from a breaking segment will arrive at a receiver before than those that are radiated by a segment that ruptures later.
If the path to the station is not perpendicular, the waves generated by different

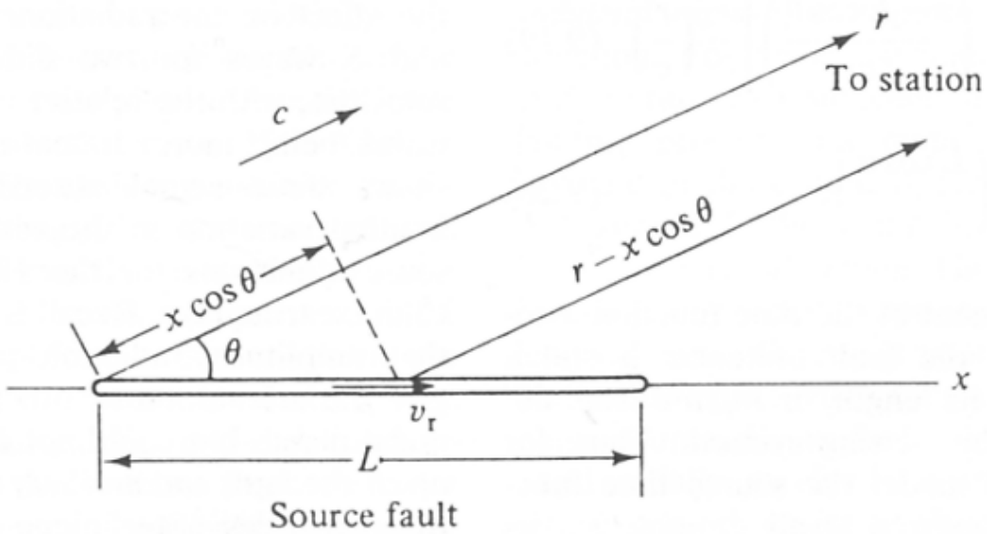

FIGURE 9.8 Geometry of a rupturing fault and the path to a remote recording station. (From Kasahara, 1981.)

$$T_r = \left[\frac{L}{v_r} + \left(\frac{r - L\cos\theta}{c}\right)\right] - \frac{r}{c} =$$

$$= \frac{L}{v_r} - \left(\frac{L\cos\theta}{c}\right) = \frac{L}{v_r}\left(1 - \frac{v_r}{c}\cos\theta\right)$$

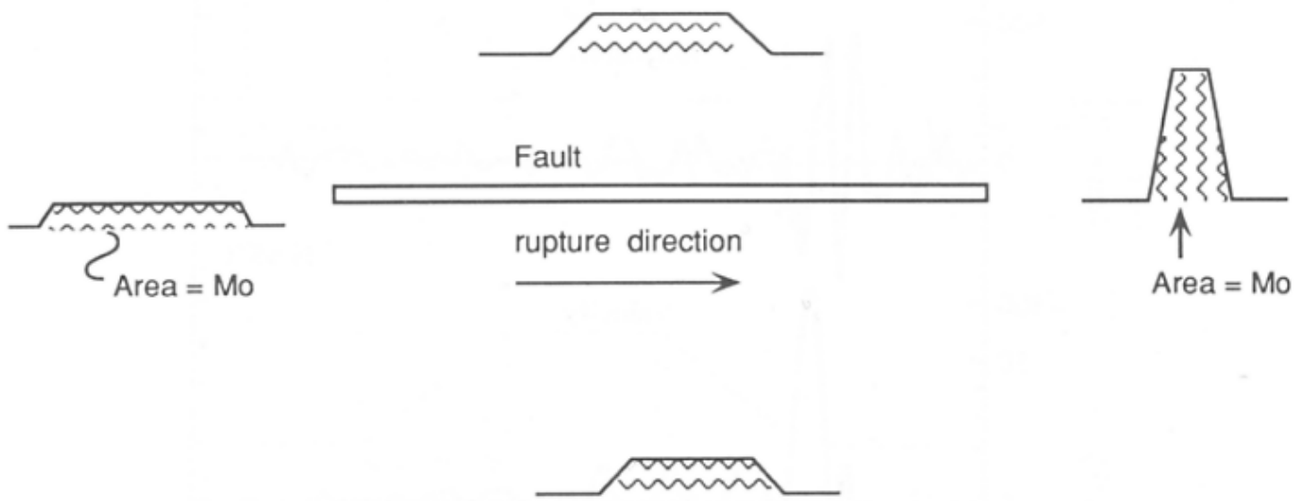

FIGURE 9.9 Azimuthal variability of the source time function for a unilaterally rupturing fault. The duration changes, but the area of the source time function is the seismic moment and is independent of azimuth.

Directivity example

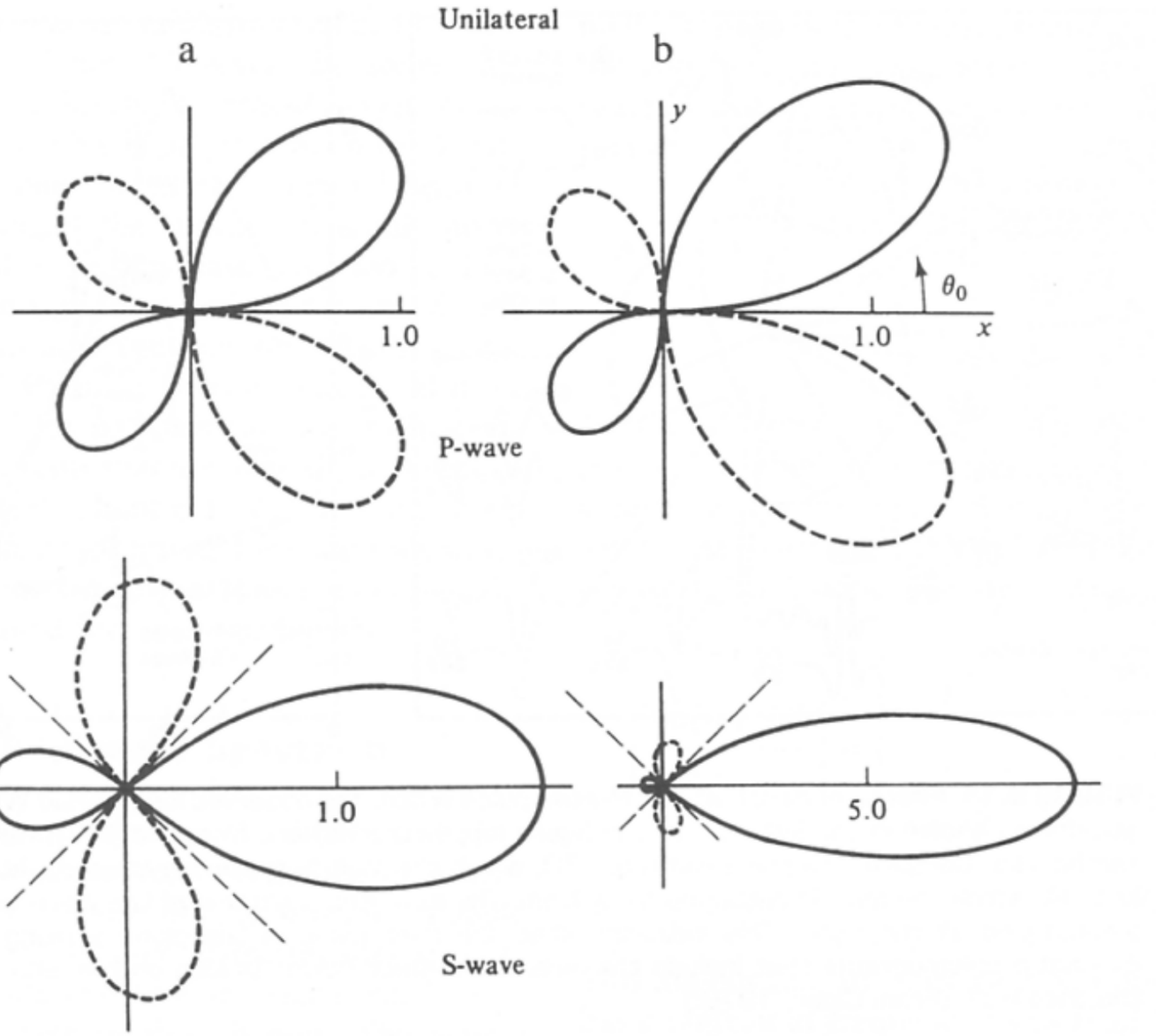

FIGURE 9.10 The variability of *P*- and *SH*-wave amplitude for a propagating fault (from left to right). For the column on the left $v_r/v_s = 0.5$, while for the column on the right $v_r/v_s = 0.9$. Note that the effects are amplified as rupture velocity approaches the propagation velocity. (From Kasahara, 1981.)

Ground motion scenarios

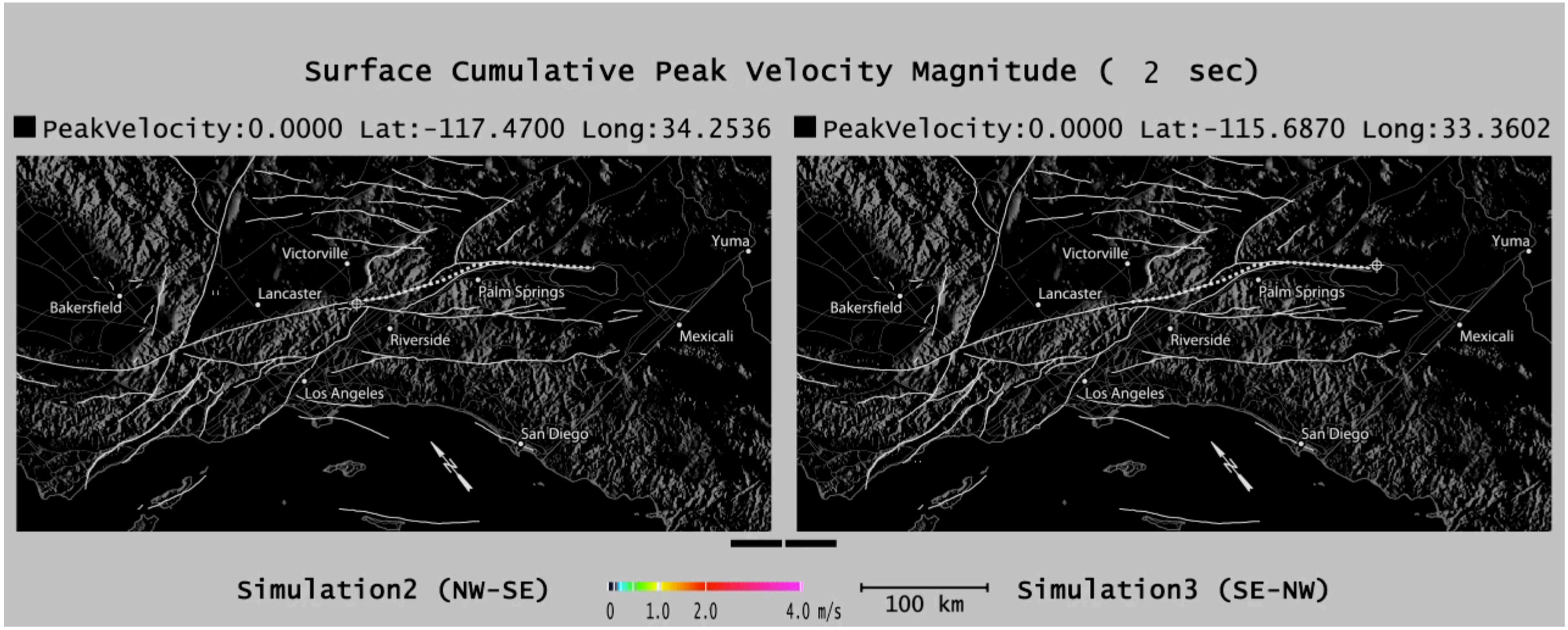

The two views in this movie show the cumulative velocities for a San Andreas earthquake TeraShake simulation, rupturing south to north and north to south. The crosshairs pinpoint the peak velocity magnitude as the simulation progresses.

www.scec.org

Source spectrum

The displacement pulse, corrected for the geometrical spreading and the radiation pattern can be written as:

$$u(t) = M_0 \left[B\left(t;\tau\right) * B\left(t;T_R\right) \right]$$

and in the frequency domain:

$$\left|U\left(\omega\right)\right| = M_0 \left|F\left(\omega\right)\right| = M_0 \left| \frac{\sin\left(\frac{\omega\tau}{2}\right)}{\left(\frac{\omega\tau}{2}\right)} \right| \left| \frac{\sin\left(\frac{\omega L}{v_r 2}\right)}{\left(\frac{\omega L}{v_r 2}\right)} \right| \approx \begin{cases} M_0 & \omega < \frac{2}{T_r} \\ \frac{2M_0}{\omega T_R} & \frac{2}{T_r} < \omega < \frac{2}{\tau} \\ \frac{4M_0}{\omega^2 \tau T_R} & \omega > \frac{2}{\tau} \end{cases}$$

Source spectrum

$$U(\omega) \approx \begin{cases} M_0 & \omega < \dfrac{2}{T_r} \\ \dfrac{2M_0}{\omega T_R} & \dfrac{2}{T_r} < \omega < \dfrac{2}{\tau} \\ \dfrac{4M_0}{\omega^2 \tau T_R} & \omega > \dfrac{2}{\tau} \end{cases}$$

Figure 4.6-4: Approximation of the (sin *x*)/*x* function, and derivation of corner frequencies.

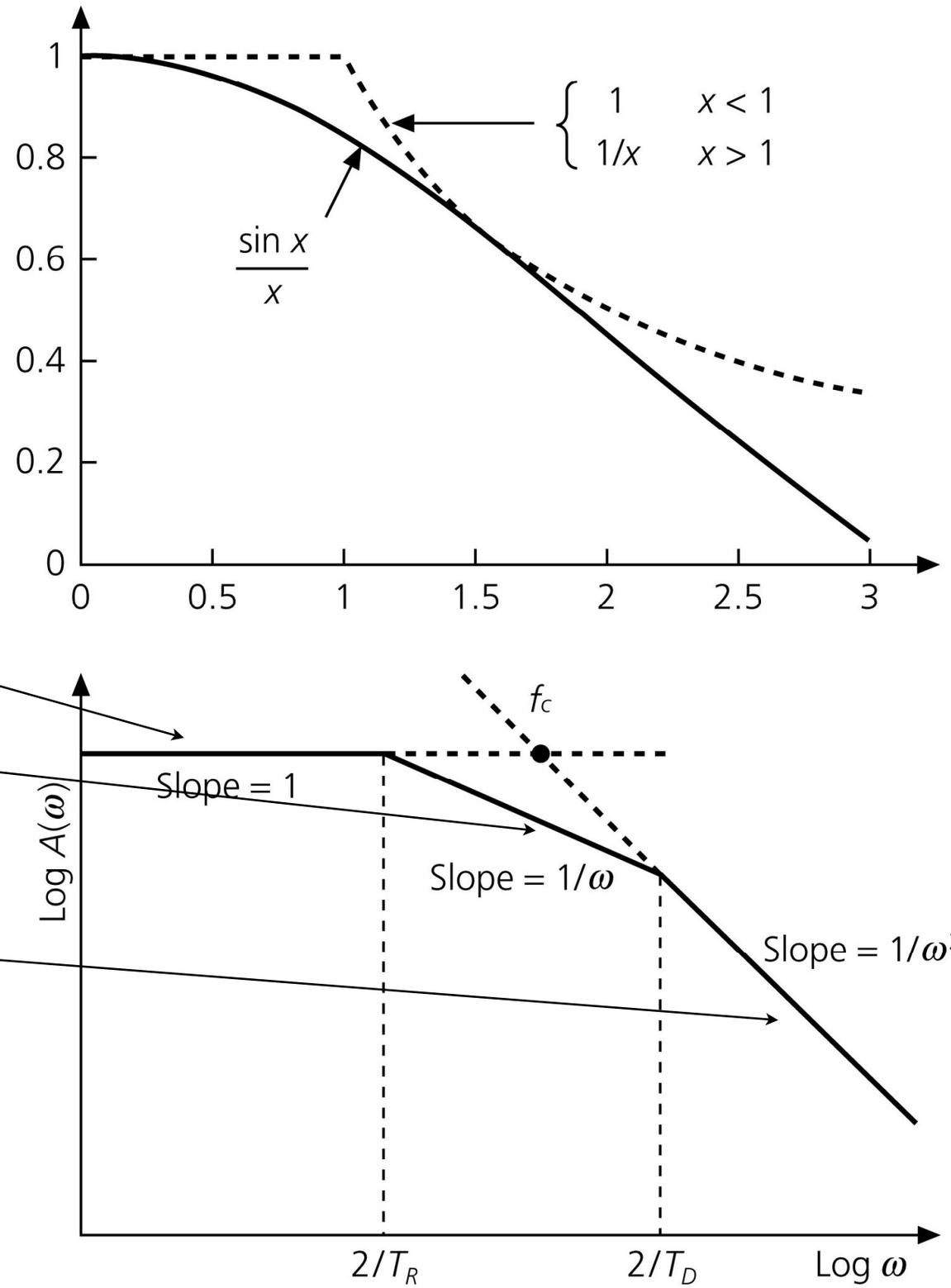

Magnitude saturation

Nature limits the maximum size of tectonic earthquakes which is controlled by the maximum size of a brittle fracture in the lithosphere. A simple seismic shear source with linear rupture propagation has a typical "source spectrum".

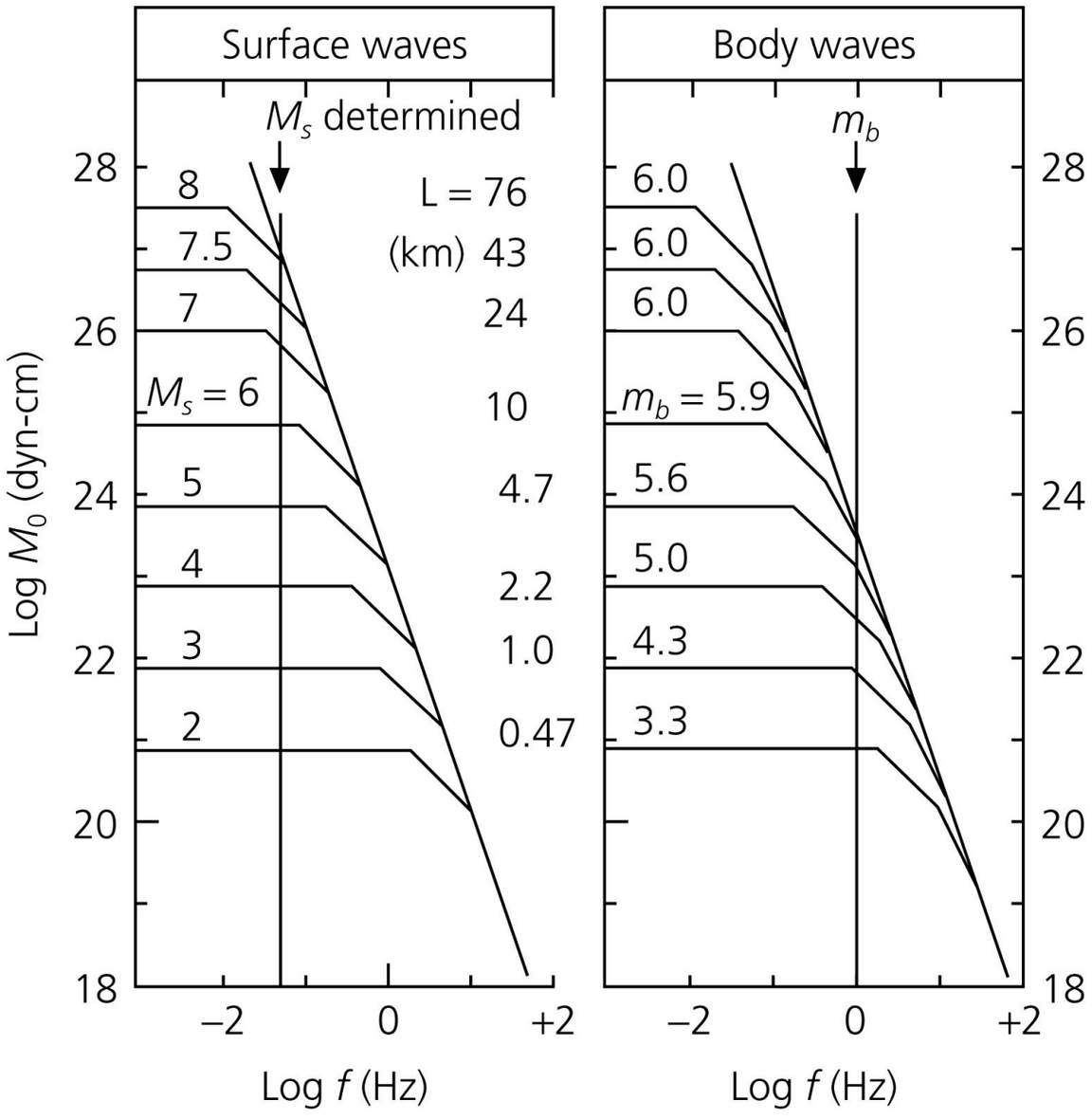

Ms is not linearly scaled with M_0 for $M_s > 6$ due to the beginning of the so-called saturation effect for spectral amplitudes with frequencies $f > f_c$. This saturation occurs already much earlier for m_b which are determined from amplitude measurements around 1 Hz.

Moment magnitude

Empirical studies (Gutenberg & Richter, 1956; Kanamori & Anderson, 1975) lead to a formula for the released seismic energy (in Joule), and for moment, with magnitude:

$\log E = 4.8 + 1.5 M_s \quad \log M_0 = 9.1 + 1.5 M_s$

resulting in

$$u(x,t) = A\cos\left(\frac{2\pi t}{T}\right) \Rightarrow v(x,t) \propto \frac{A}{T}u$$

$$\Rightarrow e \propto v^2 \propto \left(\frac{A}{T}\right)^2 \Rightarrow \log E = C + 2\log\left(\frac{A}{T}\right)$$

$$M_w = 2/3 \log M_0 - 6.07$$

when the Moment is measured in N·m (otherwise the intercept becomes 10.73); it is related to the final static displacement after an earthquake and consequently to the tectonic effects of an earthquake.

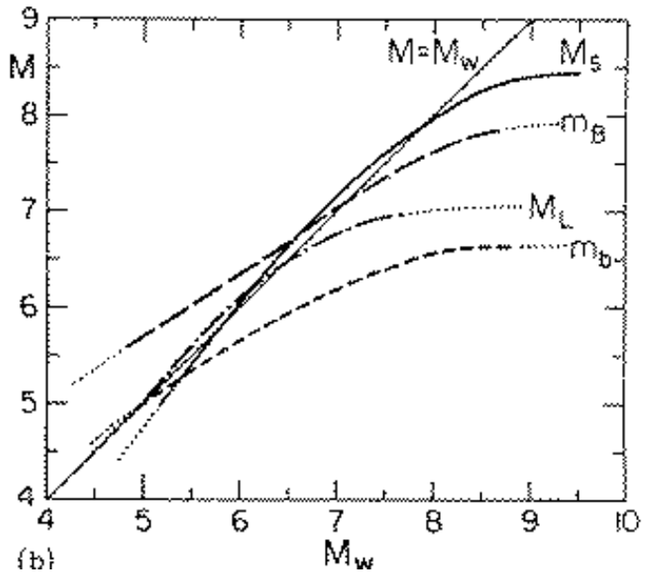

Earthquake	Body wave magnitude m_b	Surface wave magnitude M_s	Fault area (km^2) length × width	Average dislocation (m)	Moment (dyn-cm) M_0	Moment magnitude M_w
Truckee, 1966	5.4	5.9	10×10	0.3	8.3×10^{24}	5.8
San Fernando, 1971	6.2	6.6	20×14	1.4	1.2×10^{26}	6.7
Loma Prieta, 1989	6.2	7.1	40×15	1.7	3.0×10^{26}	6.9
San Francisco, 1906		8.2	320×15	4	6.0×10^{27}	7.8
Alaska, 1964	6.2	8.4	500×300	7	5.2×10^{29}	9.1
Chile, 1960		8.3	800×200	21	2.4×10^{30}	9.5

Moment, Magnitude and area

San Fernando, 1971

$M_0 = 1.2 \times 10^{26}$

$M_S = 6.6$

Slip = 1.4 m

San Francisco, 1906

$M_0 = 5.4 \times 10^{27}$

$M_S = 7.8$

Slip = 4 m

Alaska,1964

$M_0 = 5.2 \times 10^{29}$

$M_S = 8.4$

Slip = 7 m

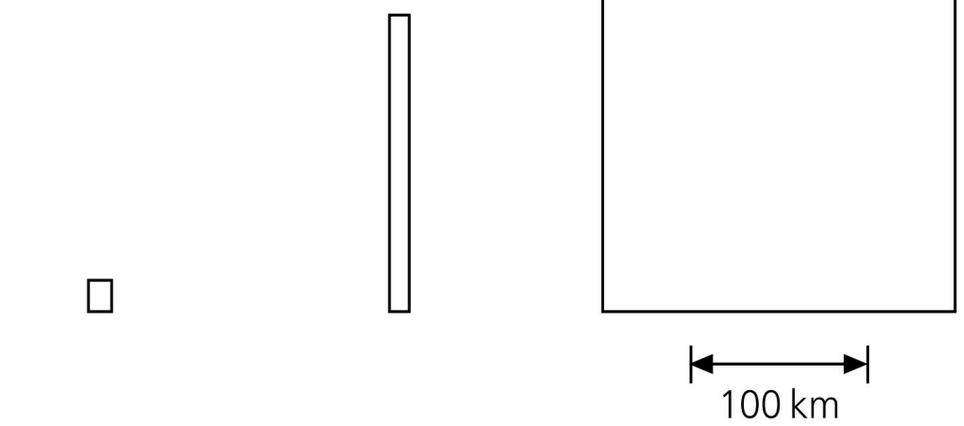

SEISMIC MOMENT Mo = fault area * slip * rigidity (dyn-cm)

MOMENT MAGNITUDE Mw = log Mo /1.5 - 10.73

NORTHRIDGE 1994

Mo 1 x10 ^{26}
Mw 6.7
slip 1 m

LOMA PRIETA 1989

Mo 5.4 x10 ^{26}
Mw 6.9
slip 2 m

SAN FRANCISCO 1906

Mo 5 x10 ^{27}
Mw 7.8
slip 4 m

SUMATRA 2004

Mo 1 x10 ^{30}
Mw 9.3
slip 11 m

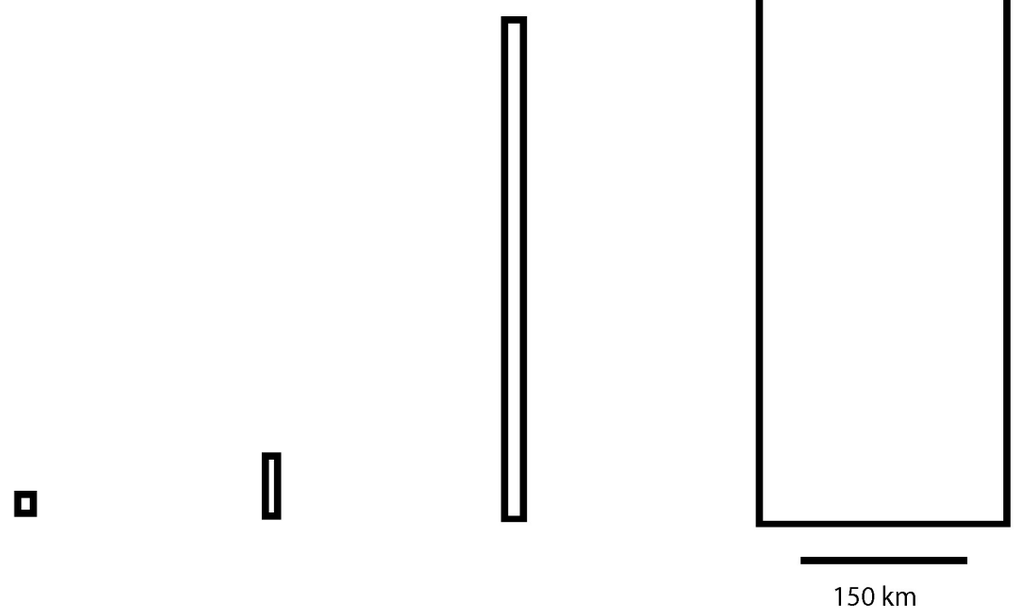

Energia (magnitudo)

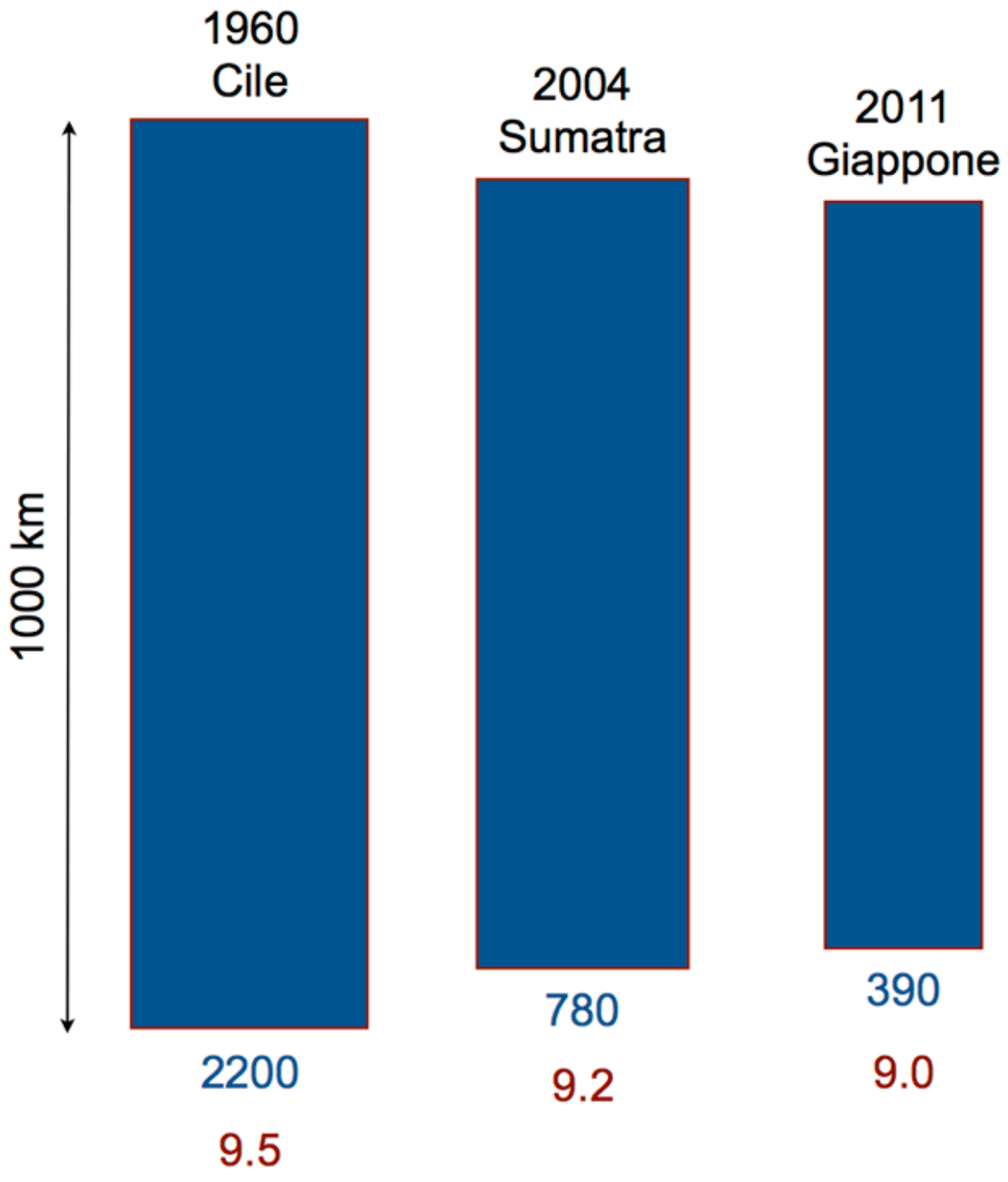

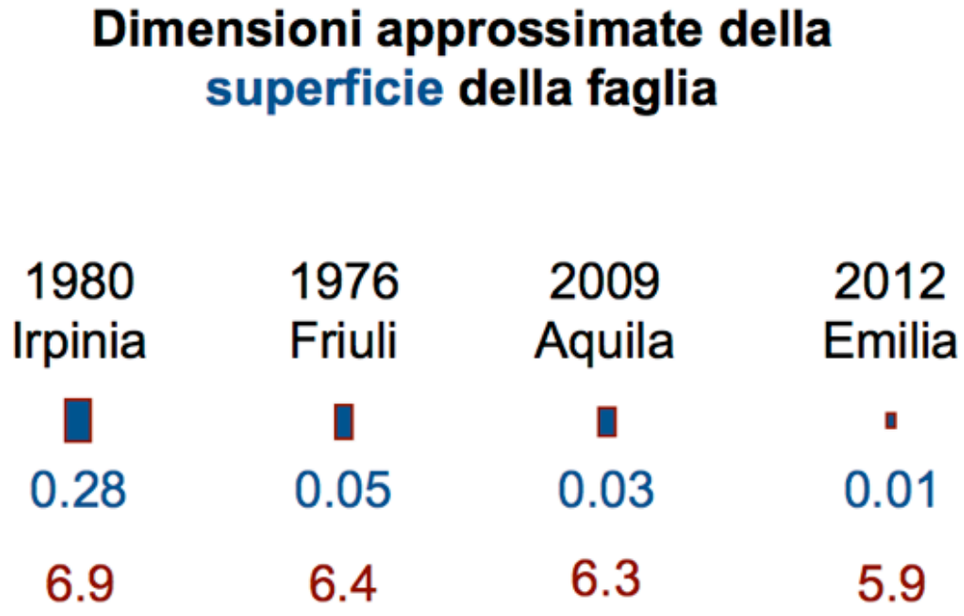

Slip, length and moment

Figure 4.6-7: Empirical relations between slip, fault length, and moment.

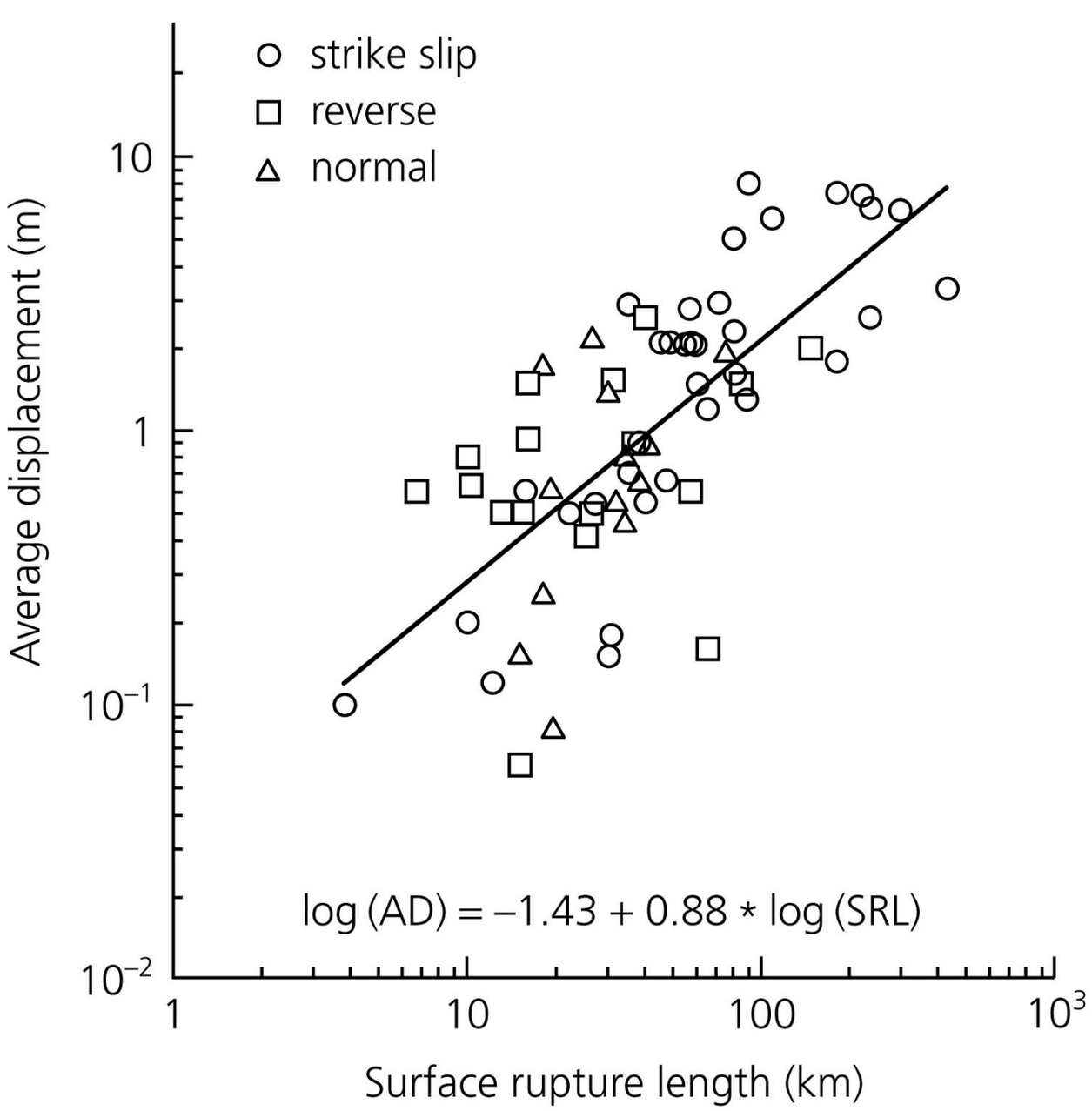

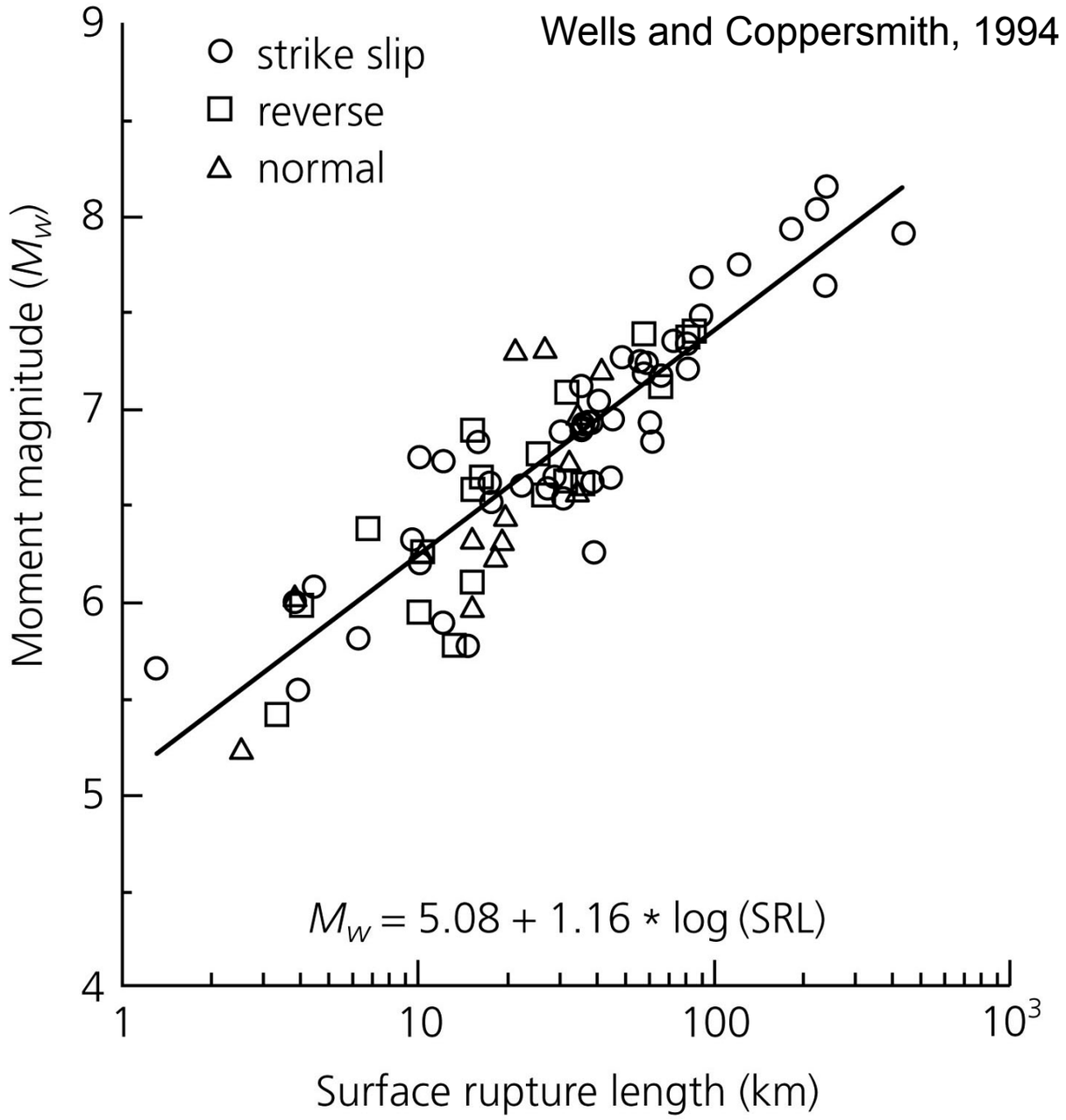

M7, ~ 100 km long, 1 m slip; M6, ~ 10 km long, ~ 20 cm slip

Important for tectonics, earthquake source physics, hazard estimation

Wells D.L. e **Coppersmith** K.J.; **1994**: New empirical relationships among magnitude, rupture length, rupture width, rupture area, and surface displacement. Bull. Seism. Soc. Am., **84**, 974-1002.

Gutenberg-Richter law

They proposed that in a given region and for a given period of time, the frequency of occurrence can be represented by: $\log N = A - bM_s$, where N is the number of earthquakes with magnitudes in a fixed range around M_s. It can be written also as a power-law for moment, distribution that arises from the self-similarity of earthquakes. While the a-value is a measure of earthquake productivity, the b-value is indicative of the ratio between large and small quakes. Both a and b are, therefore, important parameters in hazard analysis. Usually b is close to a unity.

Figure 4.7-1: Frequency-magnitude plot for earthquakes during 1968-1997.

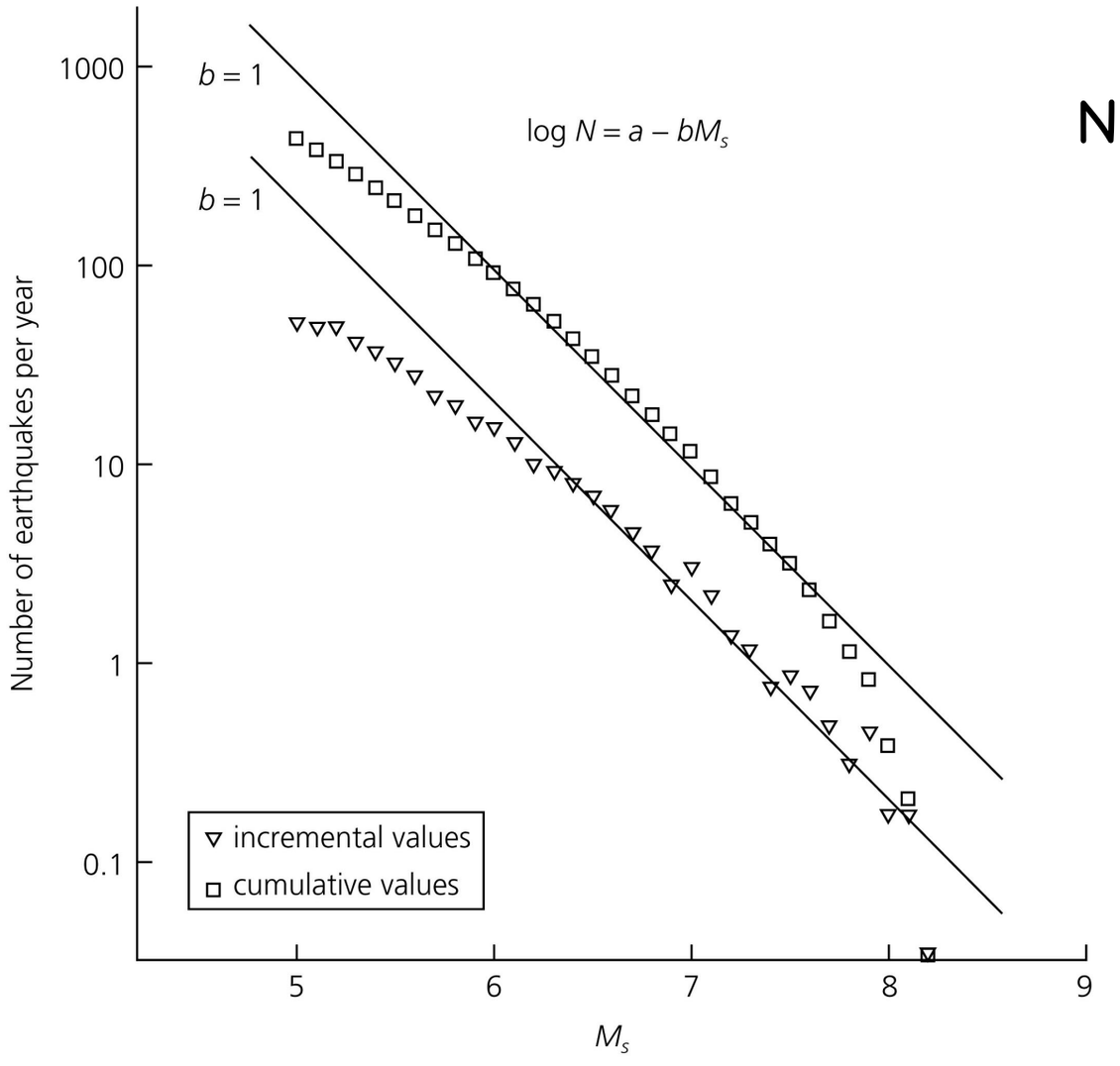

$$N = \frac{10^A}{\left(10^{M_s}\right)^b} = \frac{C}{\left(M_0\right)^{2b/3}} = CM_0^{-2b/3} \approx CM_0^{-2/3}$$

Figure 4.7-2: Frequency-moment plot for earthquakes during 1976-1998.

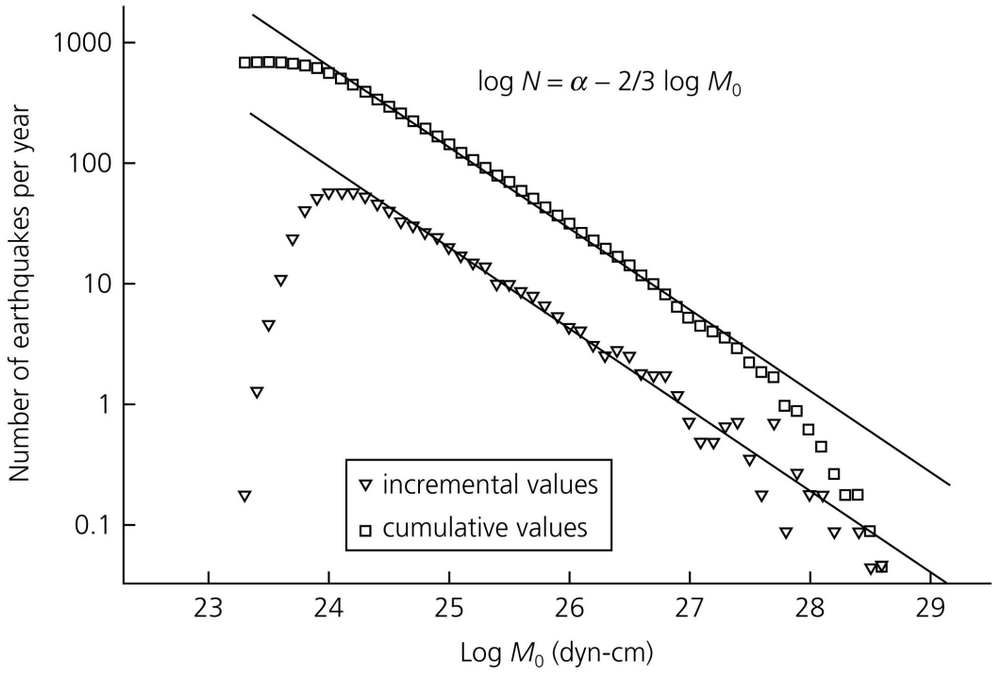

GR & Characteristic

Two end-member models can explain the G-R statistics:

• Each fault exhibits its own G-R distribution of earthquakes.

• There is a power-law distribution of fault lengths, with each fault exhibiting a characteristic distribution.

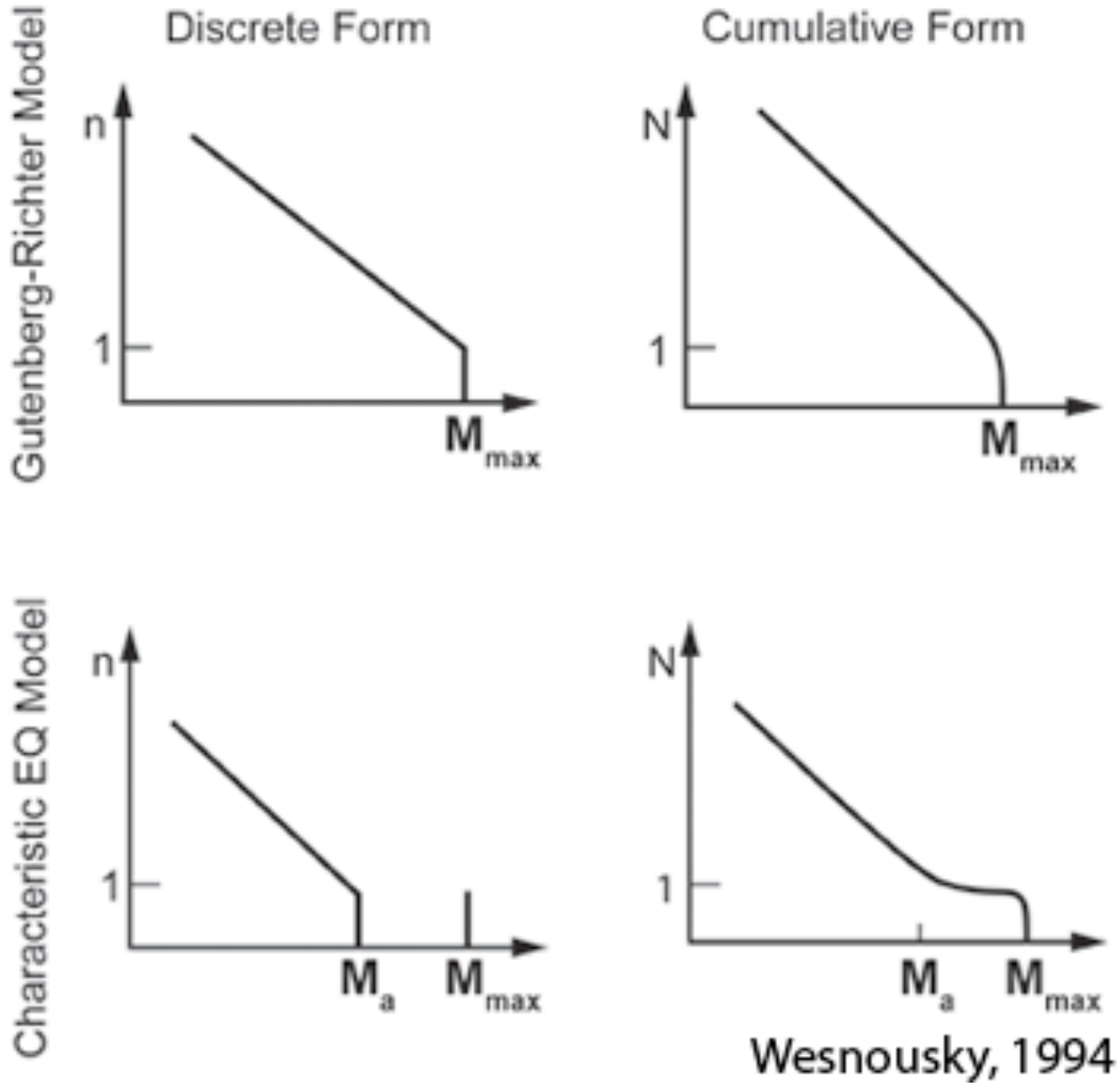

• For a statistically meaningful population of faults, the distribution is often consistent with the G-R relation.

• For a single fault, on the other hand, the size distribution is often characteristic.

• Note that the extrapolation of the b-value inferred for small earthquakes may result in under-estimation of the actual hazard, if earthquake size-distribution is characteristic rather than power-law.

Strong motion seismology

- Strong ground motion is an event in which an earthquake cause the ground to shake at least strongly enough for people to feel the motion or to damage or destroy man-made structures.

- The goal of strong motion seismology is to be able to understand and predict seismic motions sufficiently well that the predictions can be used for engineering applications

- The field of strong-motion seismology could initially be identified with a type of instrument, designed to remain on-scale and record the ground motion with fidelity under the conditions of the strongest ground motions experienced in earthquakes.

Anderson J.G Physical Processes That Control Strong Ground Motion. In: Gerald Schubert (editor-in-chief) Treatise on Geophysics, 2nd edition, Vol 4. Oxford: Elsevier; 2015. p. 505-557.

Strong motion seismology

- Early instruments were typically designed so that ground motions up to the acceleration of gravity (1g) would be on-scale.

- The lower limit of ground motion considered by the early strong motion seismology studies was roughly defined by the thickness of the light beam read until the edge of a recorded film. The minimum acceleration resolved is somewhat less than 0.01g, that approximately coincided with minimum ground motions that humans are able to feel.

- Since much smaller ground motions can be recorded on modern instruments, the distinction between strong-motion seismology and traditional seismology is blurred.

Example of Recordings

Ground acceleration, velocity and displacement, recorded at a strong-motion seismometer that was located directly above the part of a fault that ruptured during the 1985 Mw = 8.1, Michaocan, Mexico earthquake.

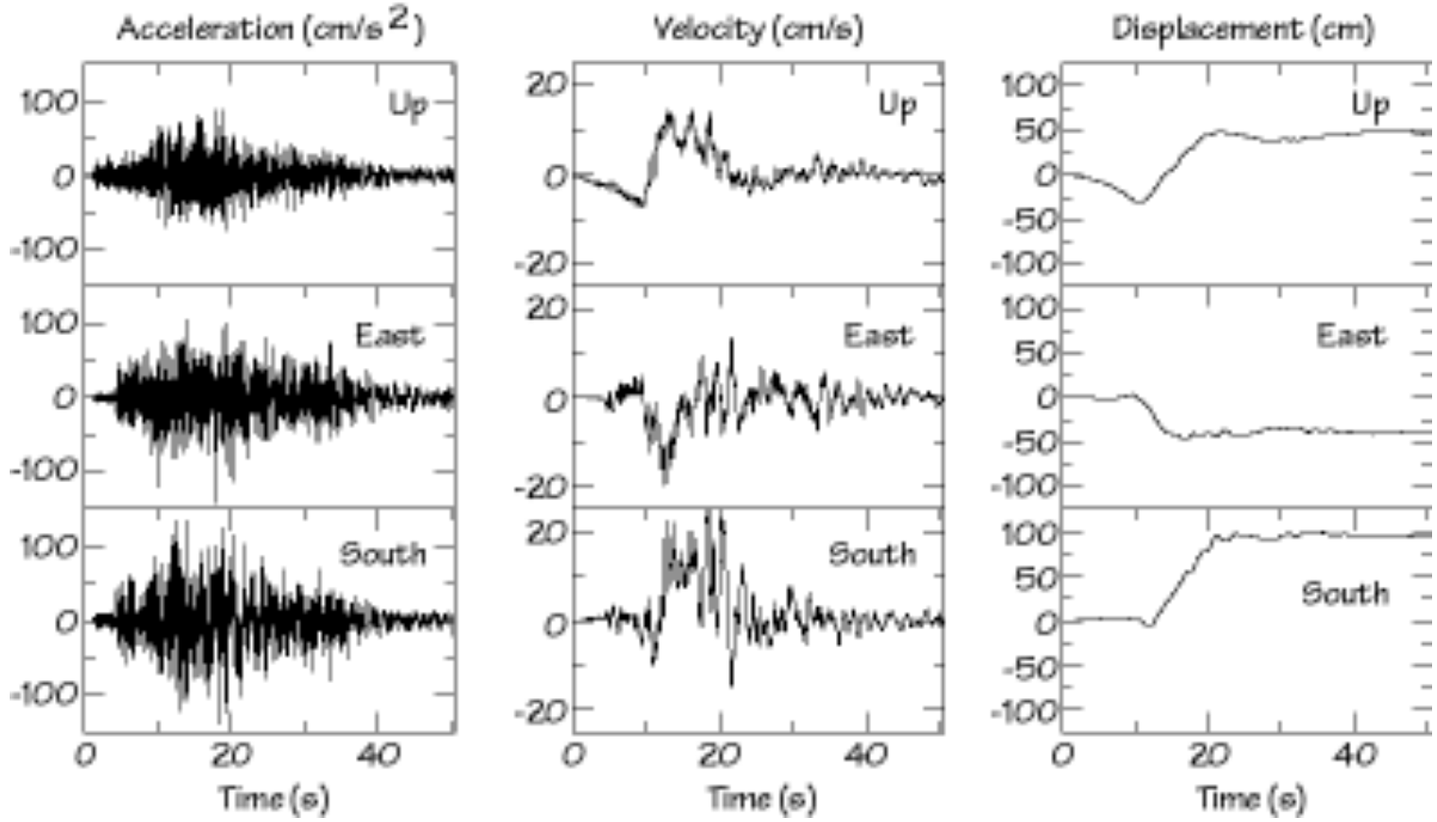

The left panel is a plot of the three components of acceleration: strong, high-frequency shaking lasted almost a minute and the peak acceleration was about 150 cm/s^2 (or about 0.15g). The middle panel shows the velocity of ground movement: the peak velocity for this site during that earthquake was about 20-25 cm/sec. Integrating the velocity, we can compute the displacement, which is shown in the right-most panel: the permanent offsets near the seismometer were up, west, and south, for a total distance of about 125 centimeters.